DMG OPEN-FILE REPORT 91-20

Turkey Flat, USA

Site Effects Test Area

REPORT 6

Weak-Motion Test: Observations and Modeling

September 1991

TECHNICAL REPORT NO. 91-1

CALIFORNIA DEPARTMENT OF CONSERVATION

DIVISION OF MINES AND GEOLOGY

EARTHQUAKE SHAKING ASSESSMENT PROJECT

CALIFORNIA DEPARTMENT OF CONSERVATION
Division of Mines and Geology

THE RESOURCES AGENCY
DOUGLAS P. WHEELER
SECRETARY FOR RESOURCES

STATE OF CALIFORNIA
PETE WILSON
GOVERNOR

DEPARTMENT OF CONSERVATION
EDWARD G. HEIDIG
DIRECTOR

The Turkey Flat site effects test area is one of a series of international test areas endorsed by the International Association of Physics of the Earth's Interior and the International Association of Earthquake Engineers.

Members of the Turkey Flat Site Effects Prediction Committee:

Dr. J. Carl Stepp (Chairman)
Electric Power Research Institute

Dr. C.Y. Chang
Geomatrix Consultants, USA

Dr. Neville C. Donovan
Dames & Moore, USA

Mr. James E. Gates
California Department of Transportation, USA

Dr. I.M. Idriss
University of California, Davis, USA

Dr. William B. Joyner
U.S. Geological Survey, USA

Dr. Marshall Lew
LeRoy Crandall and Associates, USA

Mr. Maurice S. Power
Geomatrix Consultants, USA

Mr. Charles R. Real
California Department of Conservation, USA

Mr. Bruce Redpath
Redpath Geophysics, USA

Dr. Michael Reichle
California Department of Conservation, USA

Dr. Wolfgang Roth
Dames & Moore, USA

Dr. Anthony F. Shakal
California Department of Conservation, USA

Dr. Jogeshwar P. Singh
Geospectra, USA

Mr. John Vrymoed
California Department of Transportation, USA

This report contains contributions in draft form and has not been edited to the standards of a formal publication. The views and conclusions contained in this document are those of the authors, and should not be interpreted as representing the official policies, either expressed or implied, of the State of California.

TURKEY FLAT, USA
SITE EFFECTS TEST AREA

Report 6

Weak-Motion Test: Observations and Modeling

Prepared by

Chris H. Cramer

SEPTEMBER 1991

TECHNICAL REPORT NO. 91-1
CALIFORNIA DEPARTMENT OF CONSERVATION
DIVISION OF MINES AND GEOLOGY
EARTHQUAKE SHAKING ASSESSMENT UNIT

Turkey Flat, USA
Site Effects Test Area

OVERVIEW

NEEDS The 1985 Mexico City and 1989 Loma Prieta earthquakes are our most recent reminders that local ground conditions can have a strong influence on where damage will occur in urbanized areas during an earthquake, and underscore the need to incorporate seismic shaking potential in land-use decisions. Although several different methods for making such assessments are currently in use, their accuracy and costs are not well known. Reliability and cost of methods must be known before they can be routinely used to provide a sound basis for safer land-use and construction practices.

GOALS The principal goals of the Turkey Flat Site Effects Test Area are to systematically compare and determine the reliability of contemporary methods used to estimate the effect of local geology on earthquake shaking, and to test the linearity of shallow stiff-soil site response.

OBJECTIVES Principal objectives are to collect high quality weak- and strong-motion data produced by local and regional earthquakes at several locations in the test area, to quantify the site geology in terms of its geotechnical properties, and to distribute the information to experts around the world.

APPROACH Using the acquired data, a series of "blind" predictions will be made by ground motion experts for test area locations where the response will be known, but not be available until all predictions have been received. Results of each prediction will be compared with one another and with actual observed ground motion.

PRODUCTS A series of reports describing each principal phase of the project will be available as the work progresses. An evaluation of all site response estimation methods will be prepared with recommendations as to suitability and cost of routine application for urban earthquake shaking hazard assessment.

Acknowledgments

Special recognition is due to Lawrence Livermore National Laboratory (LLNL) for the loan of field recording equipment and for assistance in setting up and maintaining some of the recording equipment in the field. I wish to acknowledge and thank Brian Tucker of DMG for his help in designing and laying out the profile array, Steve Jarpe of LLNL for his help with data acquisition for the profile study presented in this report, Lalliana Mualchin of DMG for his help is setting up the site-specific array, and Charles Real of DMG for his assistance and support during the field recording and his encouragement to perform the modeling study. I would also like to thank Bob Darragh, Steve McNutt, and Michael Reichle for helpful discussions about aspects of this report.

Most of all, I am grateful for the cooperation of Donald and Nila McCornack, owners of the land on which the Turkey Flat strong-motion array is located.

TABLE OF CONTENTS

ILLUSTRATIONS

Figures

Figures

Tables

FOREWORD

IASPEI/IAEE Joint Working Group

At the 1985 meeting of the International Association of Seismology and Physics of the Earth's Interior (IASPEI), held jointly with the International Association of Earthquake Engineering (IAEE) in Tokyo, Japan, a resolution was passed forming the IASPEI/IAEE Joint Working Group on The Effects of Local Geology on Seismic Motion. The purpose of this group is to coordinate the establishment of an international series of test areas designed to provide a data base for comparing and testing contemporary methods, and developing new methods, to predict the effects of local geology on ground motion caused by earthquakes. The 1985 Michoacan and 1989 Loma Prieta earthquakes are only the most recent reminders that local ground conditions can have a major influence on where damage will occur in major earthquakes. Although methods for assessing site effects are being used to construct critical facilities around the world, the reliability of these methods has not been rigorously tested. It is the goal of this international program to fulfill this need. An international program provides a forum for experts around the world to exchange ideas, and significantly increases the prospects of acquiring the necessary data in a short time period.

Turkey Flat Experiment

The California Department of Conservation's Division of Mines and Geology (DMG) has, among other mandates, the responsibility to look after the interests of the state and its people with regard to seismic and geologic hazards, and to promote safe utilization of the state's terrain. Safety analyses of critical facilities such as nuclear power plants, liquid natural gas repositories, and hospitals, as well as provision of hazard information to local governments for planning and development, require application of state-of-the-art techniques in predicting ground motion expected from future earthquakes; however, contemporary methods have not been thoroughly validated. When asked why microzonation has not been implemented in the U.S., the answer is often: "if you ask ten different experts how the ground might shake at a specific site during an earthquake, you will get ten different answers." We see a strong need to identify those methods that are reliable and those that are not, and to establish guidelines and procedures that insure repeatability, in order to effectively carry out our mandates. As a consequence, we have established a test area at Turkey Flat, California, where a series of experiments will help answer this need.

Our general perceptions and experiment objectives echo those of IASPEI/IAEE's Joint Working Group. In their first work-

shop, held during the XIX Assembly of the International Union of Geodesy and Geophysics in Vancouver, British Columbia, Canada in August of 1987, a resolution was passed incorporating the experiment at Turkey Flat into the international program.

The principal objectives of the Turkey Flat Experiment are to systematically test and compare all methods of estimating the influence of local geology on ground motion during earthquakes, in order to determine the reliability and cost-effectiveness of each. Secondary objectives are to generate a data base for the improvement of these methods, or the development of new methods, and to address the long-standing debate on the linearity of site response. The approach is to collect high quality weak and strong ground motion data, and geotechnical data, and to carry out a series of "blind predictions." Experts from around the world are invited to use their preferred method and the acquired data to predict ground motion at locations where the actual response will be known but held in confidence until all predictions have been submitted.

The experiment is being conducted in a number of phases. This report presents the weak-motion observations made by DMG and the simple modeling done by DMG as part of phase IV, Weak-Motion Blind Prediction Test. A more detailed

description of the overall experiment is provided in Report 1, Turkey Flat, USA, Site Effects Test Area: Needs, Goals and Objectives. A detailed description of the local site geology and geotechnical properties of the site is provided in Report 2, Turkey Flat, USA, Site Effects Test Area: Site Characterization. A detailed description of the site effects blind prediction test phases at Turkey Flat is provided in Report 3, Turkey Flat, USA, Site Effects Test Area: Weak-Motion Test: Prediction Criteria and Input Rock Motions. The weak-motion test event's observed seismic response at all sites is provided in Report 4, Turkey Flat, USA, Site Effects Test Area: Weak-Motion Test: Observed Seismic Response. An initial summary of results for the weak-motion blind prediction test at Turkey Flat is provided in Report 5, Turkey Flat, USA, Site Effects Test Area: Weak-Motion Test: Statistical Analysis of Submitted Predictions and Comparisons to Observations.

This report covers three subjects: 1) two weak-motion data sets recorded at Turkey Flat and the observed site response (empirical transfer functions) in terms of Fourier spectral ratios; 2) simple modeling of the observed spectral ratios with site amplification functions from SHAKE (Schnabel, et al., 1972); and 3) an examination of the character of the Weak-Motion Test Event.

SYNOPSIS

Empirical transfer functions and theoretical site amplification functions are compared at several sites across Turkey Flat Site-Effects Test Area near Parkfield, CA. Observed site response relative to a bedrock reference site has been determined for a given site by using the Fourier amplitude spectral ratio method as applied to 14 local and regional earthquakes in a profile study and to 33 local and regional earthquakes in a site-specific study. Surface bedrock site response between two stations separated by two kilometers agrees to within a factor of 1.3 (30%). At several stations, surface stiff-soil site response over a sensor separation of 10m is reproducible to within a factor of 1.3 (30%). For sensor separations of 20m there are occasional significant variations in stiff-soil site response by a factor of 2-3 in the 10-20 Hz band. For sensor separations of 100m there are systematic variations in the 5-20 Hz band stiff-soil site response by a factor of 3-10 related to variations in soil thickness.

Observed transfer functions are modeled using relative amplification functions from the computer program SHAKE. Better fits are obtained by using damping values close to those measured *in situ* as opposed to damping values determined by laboratory tests. Modeling of observed transfer functions

indicates that the model fit is sensitive to 5% changes in S-wave velocity. Errors of 10-20% in field measurements of S-wave velocity at Turkey Flat suggest accurate and consistent prediction of weak motion may not be possible when based on field geotechnical measurements alone.

The character of the Weak-Motion Test Event (WMTE) is examined and compared with other weak-motion events recorded at Turkey Flat. Magnitude, epicentral distance, azimuth from source to array, and hypocentral depth are typical for the weak-motion events recorded at Turkey Flat. Variations of up to a factor of four in Fourier spectral ratios between East and North components appear to be normal random variations, typical for weak-motion spectral ratios at Turkey Flat and similar to another site located 30 km to the north in the town of Coalinga. There are no systematic variations between East and North components or between Radial and Transverse components as large as a factor of two. P-wave arrivals for the WMTE propagate across the Turkey Flat array at 6.0 km/sec but S-waves arrive simultaneously across the array. Waveform coherence is poor (<.75) between the four sites of the Turkey Flat array (>500m separations) but good (>.75 in the 1-10 Hz band) between seismometers at the same site (<25m separations). This coherence pattern is not unexpected for the Parkfield area.

INTRODUCTION

This report briefly describes the data acquisition and processing methods used to obtain weak-motion transfer functions at Turkey Flat, and presents Fourier spectral ratio observations from two weak-motion site response studies at the Turkey Flat, USA, Site Effects Test Area. It also presents the simple modeling of these observations based on the geotechnical site characterization of the test area, and examines the spectral and waveform characteristics of the Weak-Motion Test Event. The two weak-motion site response studies are 1) a profile across the valley at Turkey Flat and 2) a site-specific study of the four strong-motion instrument sites comprising the strong-motion test array at Turkey Flat. The objectives of the weak-motion site response studies and modeling are to check on the repeatability and spacial variation of site response to weak motion (<.001g) at the Turkey Flat test area, to determine if weak-motion transfer functions can be modeled from the geotechnical measurements given the assumption of linear, one-dimensional behavior, and to determine if the Weak-Motion Test Event is representative of weak-motion response at the Turkey Flat recording sites.

Turkey Flat is located halfway between Los Angeles and San Francisco in the central California coast ranges and near the San Andreas Fault just east of the town of Parkfield (Figure

1). The test area is located on a shallow, stiff-soil valley that is two kilometers in width and has a maximum soil thickness of twenty meters. The valley lies in a small syncline of Upper Cretaceous and Tertiary marine sedimentary rocks and is filled with late Pleistocene and Holocene sedimentary deposits. Figure 2 shows the location of the twelve recording sites that form a profile extending from bedrock onto the valley surface. Figure 2 also shows the location of four strong-motion array sites where weak-motion recordings were made, two on rock and two in the valley. There are seven surface and downhole strong-motion sensor locations at the four recording sites: a surface and a downhole sensor at Rock South, a surface and two downhole sensors at Valley Center, a surface sensor at Valley North, and a surface sensor at Rock North. Detailed geotechnical information is provided in Real (1988).

Figure 1

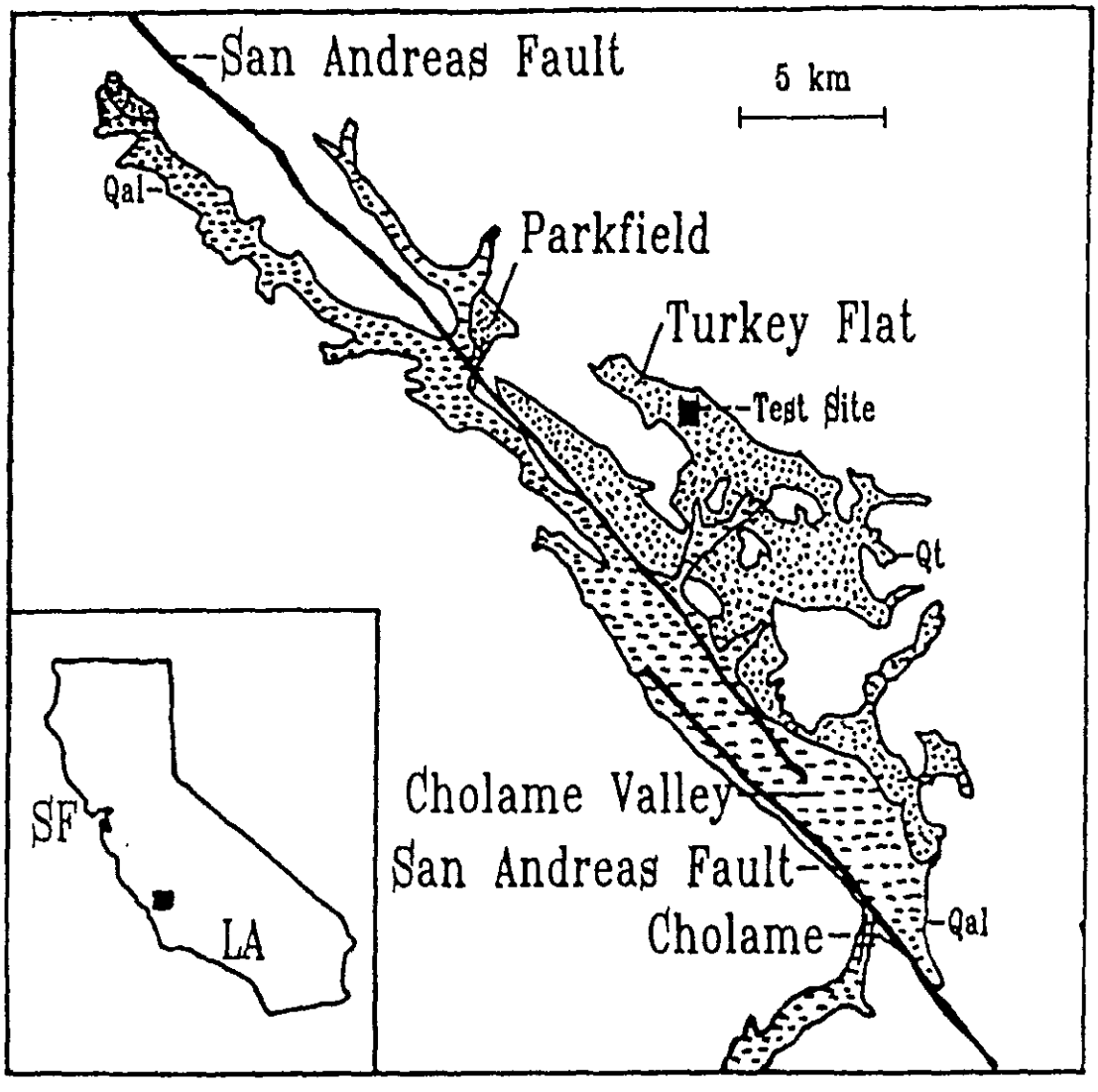

Location map for Turkey Flat Site Effects Test. Inset shows the location of the test area in Central California and relative to San Francisco (SF) and Los Angeles (LA). The main map shows the location relative to Parkfield and the San Andreas Fault. Qal (dashed area) represents Quaternary alluvial deposits and Qt (dotted areas) represent Quaternary terrace deposits.

Figure 2

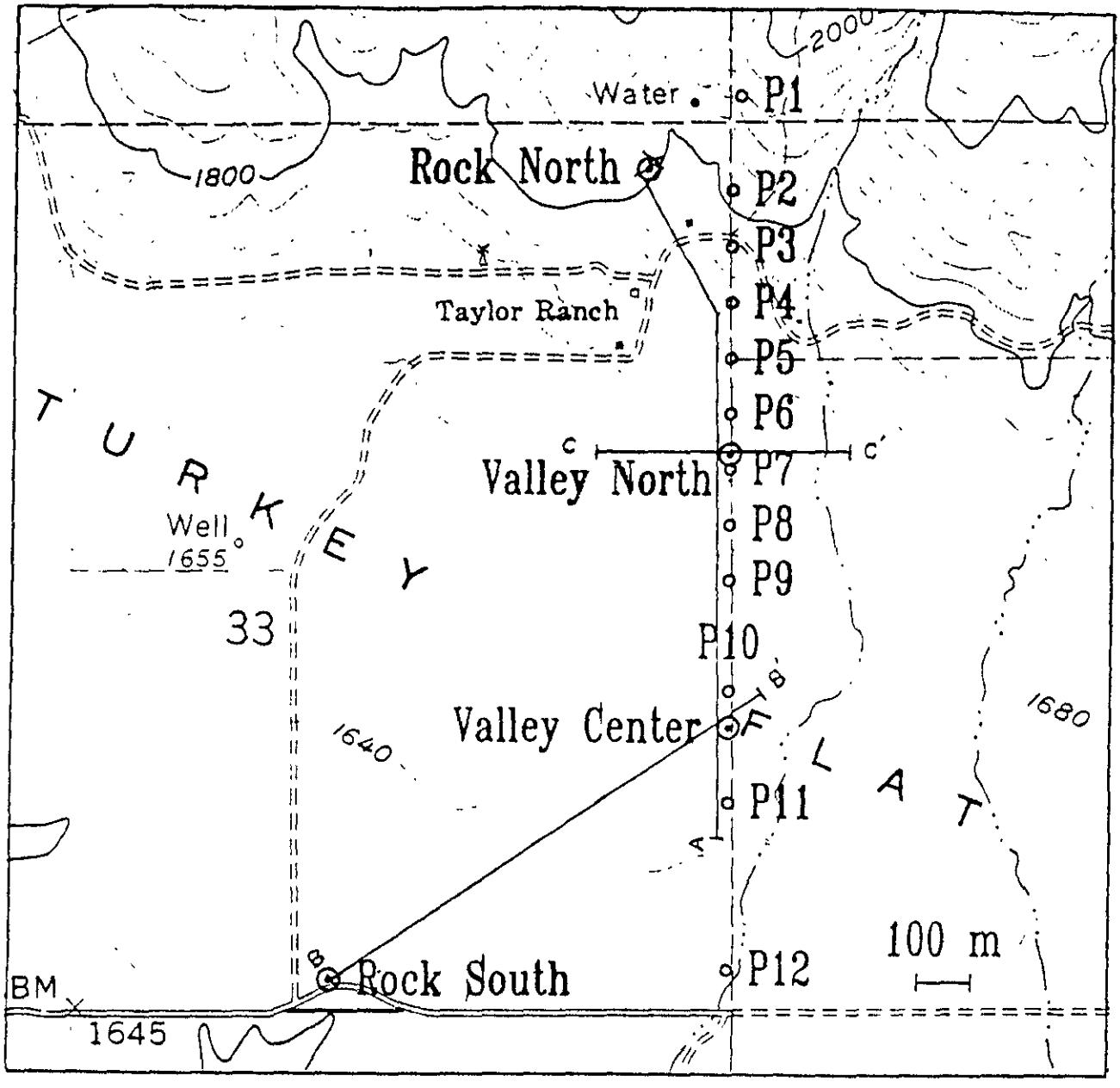
2000
Water
P1
Rock North
1800
P2
P3
P4
Taylor Ranch
P5
P6
C
C'
Valley North
P7
T U R K E Y
Well
1655
P8
P9
33
P10
B
Valley Center
1640
1680
L A T
P11
A
100 m
B
Rock South
P12
BM
1645

DATA RECORDING AND PROCESSING

As part of the process of selecting Turkey Flat as a site effects test area and as a component of the Turkey Flat Test Area ground motion prediction test, two weak-motion site amplification studies were conducted at Turkey Flat. The first study consisted of a twelve-station profile extending from bedrock to beyond the middle of the valley. The study was done for the purpose of confirming a site effect and for testing the stability (or variability) of spectral ratio determinations of site transfer functions on the scale of 100m and 10-20m. The second study consisted of collocating weak motion sensors at the selected surface and downhole strong motion sensor locations in order to determine low strain level empirical transfer functions for the instrumentation sites, and to provide data for a low strain ground motion prediction test (see Real and Cramer, 1989, for details on the prediction tests at Turkey Flat). Data from the profile were recorded during the spring of 1986 and data from the strong motion sites were recorded during the spring of 1988.

Figure 2 shows the locations of twelve temporary recording sites composing the profile (labelled small circles), and the four principal sites of the Turkey Flat Site Effects strong motion array (circled dots). Each profile site consisted of three Teledyne Geotech S-13 1-Hz Seismometers all oriented

east-west (approximately parallel to the axis of the valley so as to detect any two-dimensional resonance): one seismometer at the site, one seismometer 10m north (or south) of the site, and one seismometer 20m west of the site. The only exception to this layout was the rock site (profile site P1) which had a north-south oriented seismometer and an east-west oriented seismometer at the site and an east-west oriented seismometer 7.6m north of the site.

Instrument sensor locations for the site-specific study are shown in Figures 3 and 4. Figure 3 shows cross sections A-A', B-B', and C-C' indicated on Figure 2. The locations of the four surface and three downhole strong-motion three-component sensors are indicated in Figure 3 (R1, R2, V1, V2, D1, D2, & D3). Three-component weak-motion sensor locations (CTF1-9) relative to the strong-motion sensors are shown in Figure 4. The surface weak-motion sensors were Sprengnether S-6000 2-Hz triaxial seismometer packages and the downhole weak-motion sensors were Mark Products L10-3D-SWC 4.5-Hz triaxial seismometer packages. Note that for part of the site-specific study an extra weak-motion downhole sensor was placed first at the surface of the D1 sensor hole at the Rock South site and then at the bottom of the test hole at the Valley North site.

Local and regional earthquakes in the magnitude 1-4 range were recorded on a Lawrence Livermore National Laboratory

Figure 3

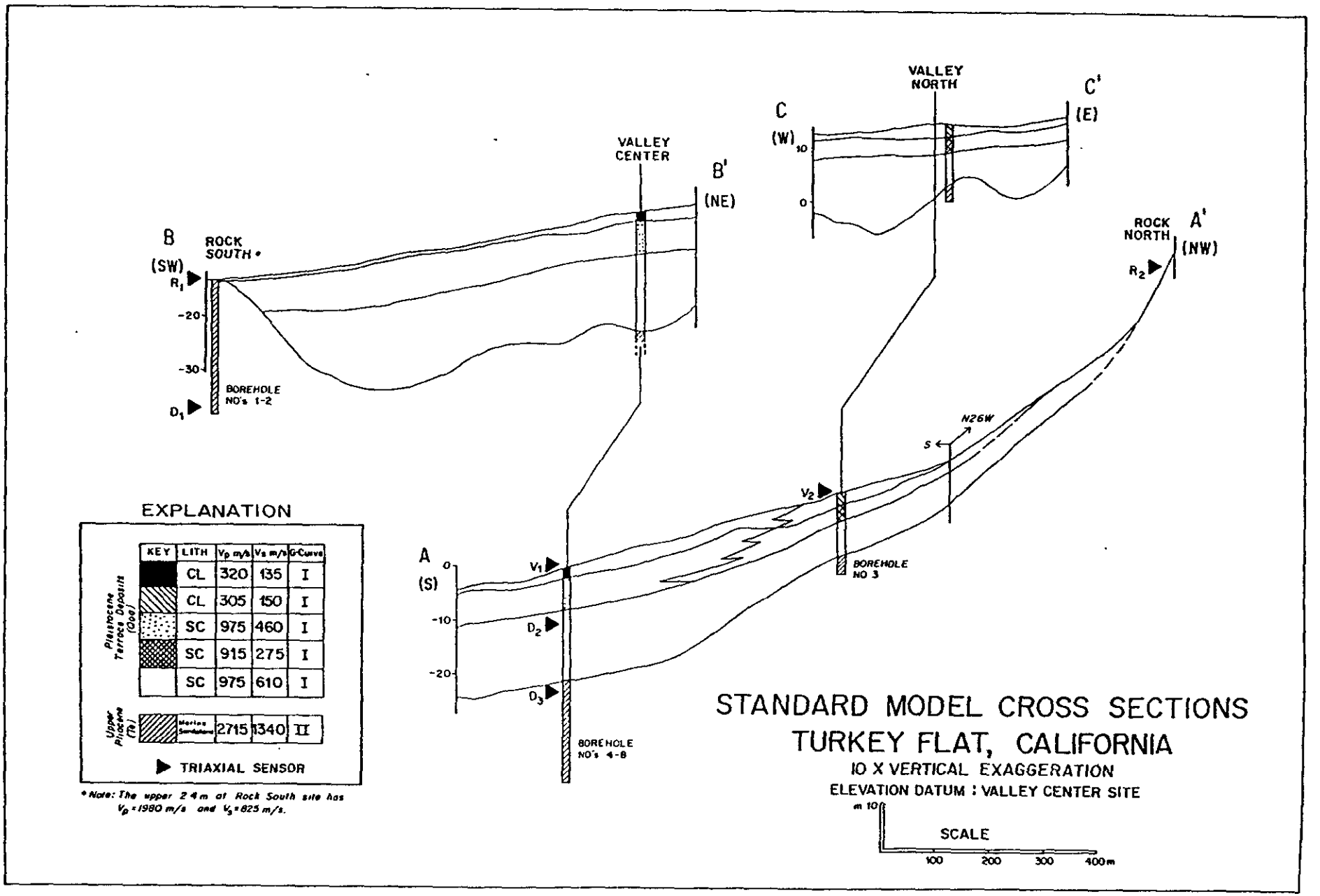
VALLEY NORTH
C'
(E)
C
(W)
10
0
VALLEY CENTER
B'
(NE)
B
ROCK SOUTH *
(SW)
R1
-20
-30
D1
BOREHOLE NO's 1-2
ROCK NORTH
A'
(NW)
R2
N26W
S
V2
BOREHOLE NO 3
A
0
(S)
V1
-10
D2
-20
D3
BOREHOLE NO's 4-8
EXPLANATION
KEY
LITH
Vp m/s
Vs m/s
G-Curve
Pleistocene Terrace Deposits (Qae)
CL 320 135 I
CL 305 150 I
SC 975 460 I
SC 915 275 I
SC 975 610 I
Upper Pliocene (Tu)
Marine Sandstone
2715 1340 II
TRIAXIAL SENSOR
* Note: The upper 2.4 m at Rock South site has Vp = 1980 m/s and Vs = 825 m/s.
STANDARD MODEL CROSS SECTIONS
TURKEY FLAT, CALIFORNIA
10 X VERTICAL EXAGGERATION
ELEVATION DATUM : VALLEY CENTER SITE
m 10
SCALE
100
200
300
400m

Figure 4: Site Maps Showing Weak- & Strong-Motion Sensors

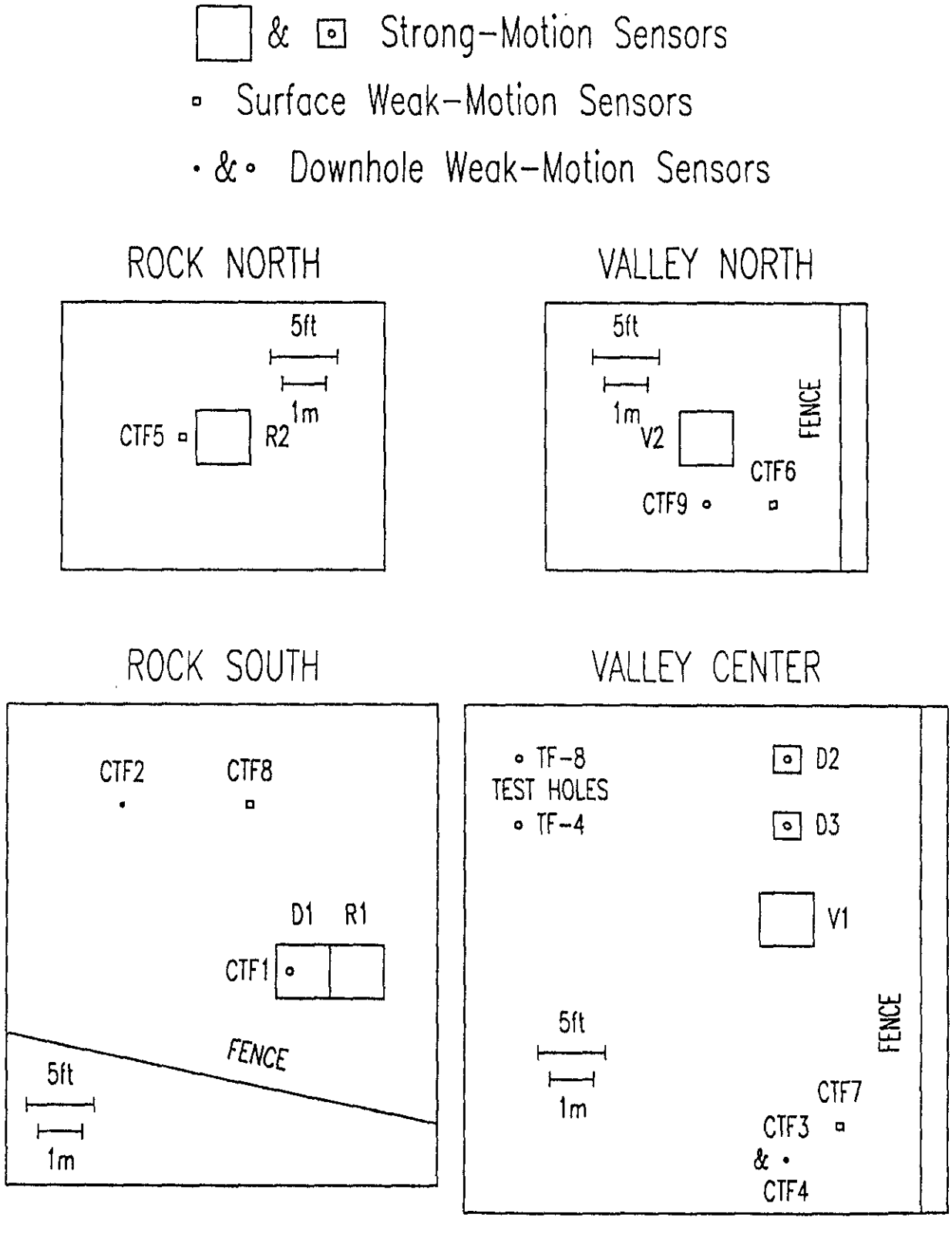

(LLNL) central recording, digital telemetry system during the profile study and on an array of Sprengnether DR-100 event-recorders hardwired to an array control box during the site-specific study. The LLNL system used in the profile study has a dynamic range of 90dB (10 bit sample plus 2 bits for gain ranging), a sample rate of 120 samples per second, and is described in Jarpe, et al. (1988). The event recorder array used in the site-specific study has a dynamic range of 66dB (12 bit sample, no gain ranging), a sample rate of 100 samples per second, and is described by Real and Cramer (1989). Fourteen (14) local and regional earthquakes were used in the profile study and thirty-three (33) in the site-specific study (Table 1). Figure 5 presents histograms showing the distance, azimuth, magnitude, and depth distributions of these two sets of earthquakes.

Data processing for both studies follows the spectral ratio method outlined in Jarpe, et al. (1988), with some exceptions. Because of the small size of the arrays at Turkey Flat (less than 2 km across), no correction has been made for geometric spreading and attenuation in either study. For the profile study, average horizontal amplitude spectra were not calculated for each site because the seismometers were oriented in the same direction (E-W). Instead, each component at each site was treated as a separate station and only mean spectral ratios for the east-west direction of motion have

Table 1:

Table of earthquakes used in weak-motion spectral ratio studies at Turkey Flat (From USGS Central California Network)

Event No.	Date	Time GMT	Latitude (N)	Longitude (W)	Depth (km)	Mag (M_L)	Dist (km)	Az (°)
Profile Study:								
1	860516	0601 48.50	36-12.31	120-23.31	5.60	1.39	35	355
2	860516	0737 31.33	36-12.64	120-20.16	7.15	1.96	36	2
3	860518	2334 18.99	36- 3.17	120- 7.26	2.45	1.70	28	49
4	860519	1758 15.66	35-59.34	120-36.58	0.00	1.97	26	295
5	860519	1801 9.38	36- 0.17	120-35.42	4.71	1.84	25	300
6	860520	0223 25.03	35-46.43	121-17.13	0.00	2.16	85	261
7	860520	0337 3.23	36-11.14	120-47.57	10.17	2.62	51	309
8	860520	0819 44.43	35-59.27	120-35.34	4.59	1.91	24	297
9	860520	1236 6.08	36- 8.16	120-13.85	1.75	1.09	29	22
10	860521	1507 7.87	36-11.94	120-19.73	9.67	2.36	34	4
11	860523	0041 13.14	36-11.44	120-17.79	4.23	1.95	34	9
12	860523	1141 54.17	35-47.45	118- 1.93	0.01	3.88	210	94
13	860523	1811 55.75	36-16.80	120-21.21	15.52	1.46	43	0
14	860525	0346 2.44	36-45.29	121-15.33	12.49	2.72	125	320
Site-Specific Study:								
1	880313	1921 5.16	36-42.52	120-45.90	2.05	2.64	98	338
2	880316	0618 50.56	36-33.28	121-12.26	5.02	2.98	106	314
3	880316	0808 3.83	35-59.82	120- 9.75	13.26	1.88	21	56
4	880326	2120 45.64	35-59.72	120- 9.49	14.06	3.03	21	57
5	880331	0847 33.13	35-55.57	120-30.57	12.06	1.73	15	285
6	880410	0511 41.49	36- 7.02	120- 7.98	1.72	2.05	32	38
7	880411	2006 23.76	36- 6.44	120- 3.60	6.07	1.86	36	48
8	880411	2021 54.06	36- 7.92	120- 2.52	5.55	1.83	39	46
9	880419	0642 47.03	36-43.30	120-45.44	1.85	2.99	99	339
10	880420	1423 51.62	36-30.55	121- 8.90	6.00	2.84	99	314
11	880423	1657 31.25	36-10.39	120-15.95	11.35	2.69	32	14
12	880427	0229 25.29	36-10.96	120-19.76	4.10	1.98	32	4
13	880501	0110 18.76	36- 6.29	120-14.75	1.75	2.48	26	22
14	880502	0007 7.00	35-45.00	120-17.26	11.36	1.00	17	159
15	880502	1923 27.54	36-39.46	121-20.26	1.89	2.83	122	314
16	880504	0021 27.57	36-43.30	120-45.60	1.75	3.14	99	338
17	880504	0028 32.87	35-57.81	120-34.06	3.80	1.30	21	292
18	880504	2339	Small Local Eqk (2 sec S-P)			Not Located by USGS		
19	880507	0907 51.32	36-40.26	121-21.85	1.53	2.71	125	314
20	880507	1415 36.79	36-40.18	121-21.70	1.67	3.01	125	314
21	880508	2051 24.42	36-31.67	121- 7.24	8.13	2.92	98	316
22	880517	1229 1.18	36- 8.17	120-14.12	9.63	2.22	29	21
23	880518	2235 44.41	36-15.73	120-24.66	7.94	2.12	42	353
24	880520	1503 33.17	36- 9.98	120-18.30	6.03	1.90	31	8
25	880523	0951 23.47	35-57.04	120-32.92	11.68	1.65	19	290
26	880524	2021 3.71	36-35.47	121-15.24	3.51	3.01	112	314
27	880525	2127 29.34	36- 7.19	120-11.71	5.04	1.86	29	29
28	880526	0356 52.98	37- 8.21	117-55.90	0.01	3.90	254	58
29	880526	1315 32.85	36-16.67	120-26.30	1.85	1.81	44	350
30	880527	2311 15.72	36- 0.19	120- 9.39	12.48	1.20	22	55
31	880528	1808 54.86	37-30.17	118-52.06	8.78	3.82	221	36
32	880530	1605 10.52	36-25.93	117-53.67	3.51	4.00	228	75
33	880530	1728 18.68	36-25.51	117-49.25	8.00	4.06	234	76

Figure 5a: Distribution of Profile Study Earthquakes with Distance, Azimuth, Magnitude, and Depth

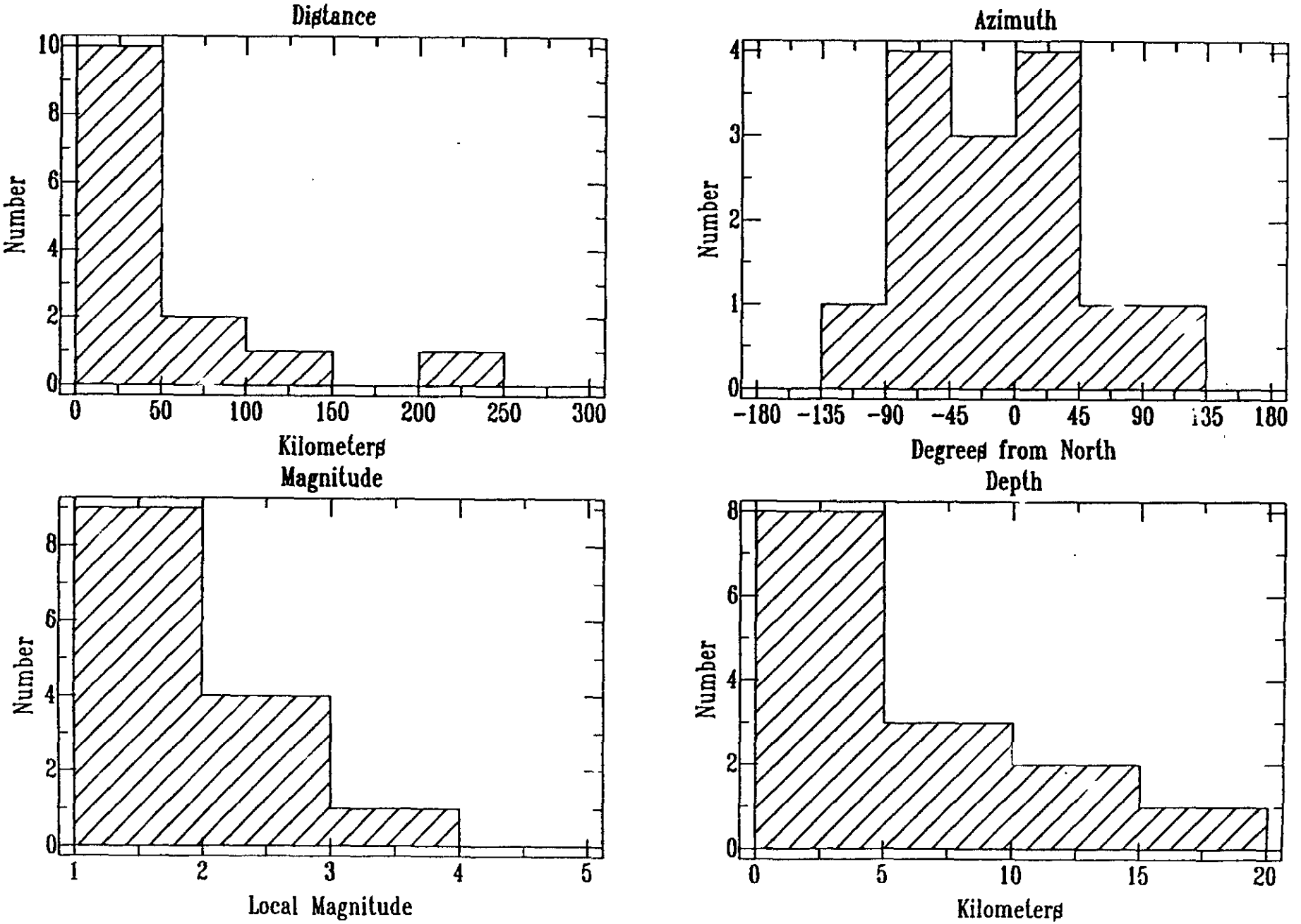

Figure 5b: Distribution of Site-Specific Study Earthquakes with Distance, Azimuth, Magnitude, and Depth

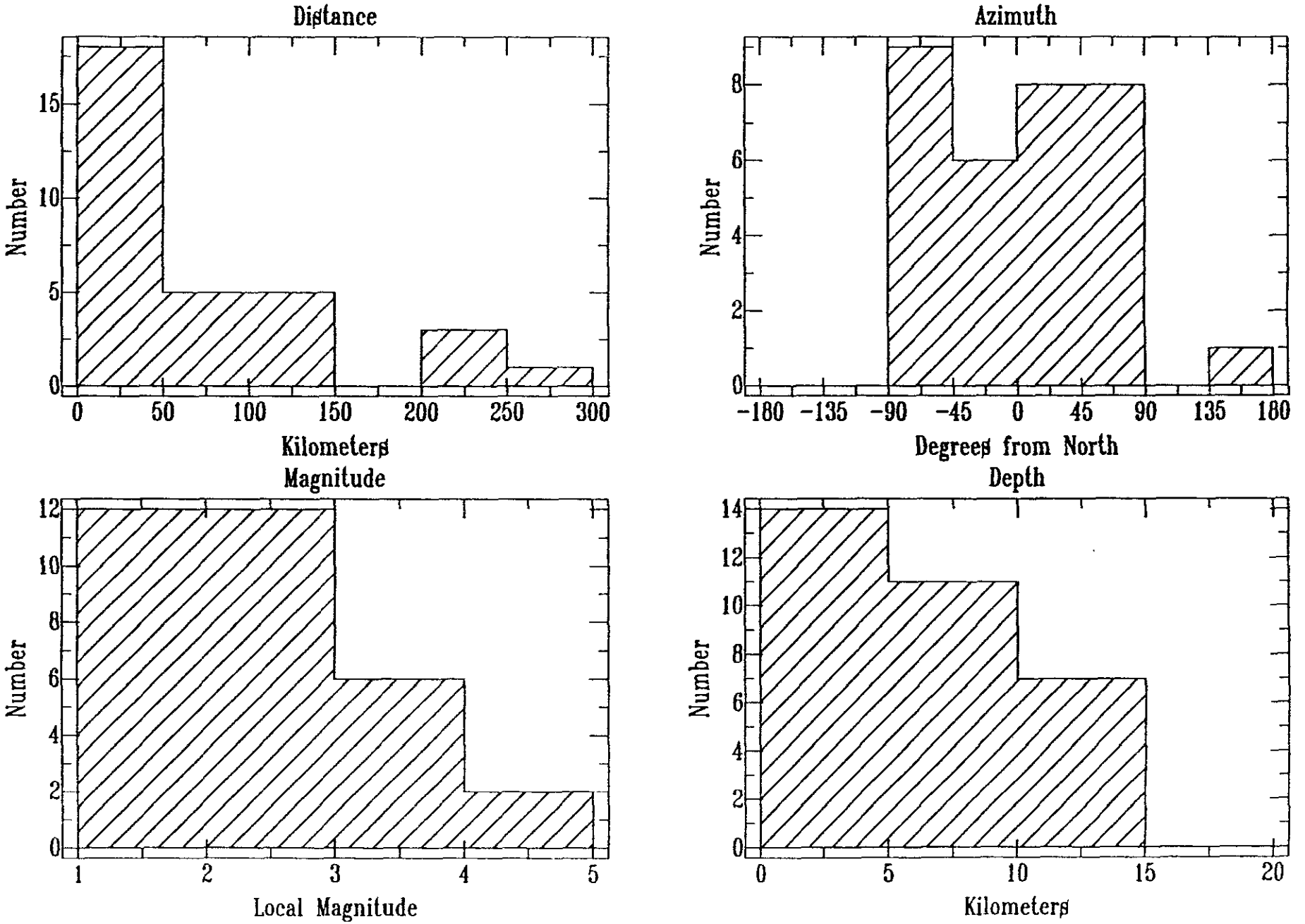

been computed according to the method used by Jarpe, et al. For the site-specific study, two different seismometer types were used so that the amplitude spectra had to be instrument-corrected prior to computing spectral ratios. The frequency-domain instrument-correction method used for this data set is described in Real and Cramer (1989). The spectral ratio method used by Jarpe, et al. was then applied to obtain average horizontal amplitude spectra, the spectral ratio of these average horizontal amplitude spectra with respect to a reference station, and finally a mean spectral ratio and its standard deviation for each triaxial sensor.

The instrumental error inherent in the spectral ratios has been determined from "huddle" tests. During a huddle test all seismometers are placed next to one another at one site. A local or regional earthquake is recorded and Fourier amplitude spectra of the S-wave are compared for all components with the same orientation. Jarpe et al. (1988) determined an instrumental error of 8% for the LLNL recording system using the same type seismometers used in the profile study. For the two seismometer types used in the site-specific study, Real and Cramer (1989) indicate an instrumental error of 10-20% after applying instrument corrections.

A basic assumption in this report is that Fourier amplitude spectral ratios for the first 8 seconds of the S-wave wave-

form provide an observational measure of site response relative to a bedrock reference site. The spectral ratio method tends to remove the effect of source and path from the observed ground motion leaving the relative site response as a function of frequency (transfer function). This is particularly true at Turkey Flat where the bedrock reference sites used in this study are no more than two kilometers from any observation site. Following the approach of Jarpe, et al. (1988), spectral ratios for several local and regional events have been averaged together to obtain a better estimate of the true relative site response for a given observation site. The resulting mean spectral ratio and its standard deviation is used in this report as the measure of "ground truth" for relative site response.

OBSERVATIONS

The observed mean spectral ratios and their standard deviations will be presented in four comparisons. The first comparison will be rock site to rock site. The second comparison will be along the profile of the profile study. The third comparison will be for the 10m and 20m subarray spacings of each of the profile sites. The fourth comparison will be among the strong-motion sensor sites. The reference bedrock site for the weak-motion profile array is site P1 and the reference site for the weak-motion site-specific array is the Rock South surface sensor CTF8.

Rock site to rock site comparison

Figure 6 shows the mean horizontal spectral ratio and the plus one and minus one standard deviation (sd) ratios for the Rock North surface weak-motion sensor (CTF5). Generally the mean spectral ratio is within a factor of 1.3 (30%) of unity (no amplification), except between 1 and 2 Hertz. **This is important for interpreting site transfer functions on valley sediments because it suggests that the site transfer functions agree within measurement error over the 1-20 Hz band for rock sites on both sides of the valley and over distances of two kilometers.**

Figure 6: Rock Site to Rock Site Comparison (2 km separation)

Solid - mean Dotted - one standard deviation

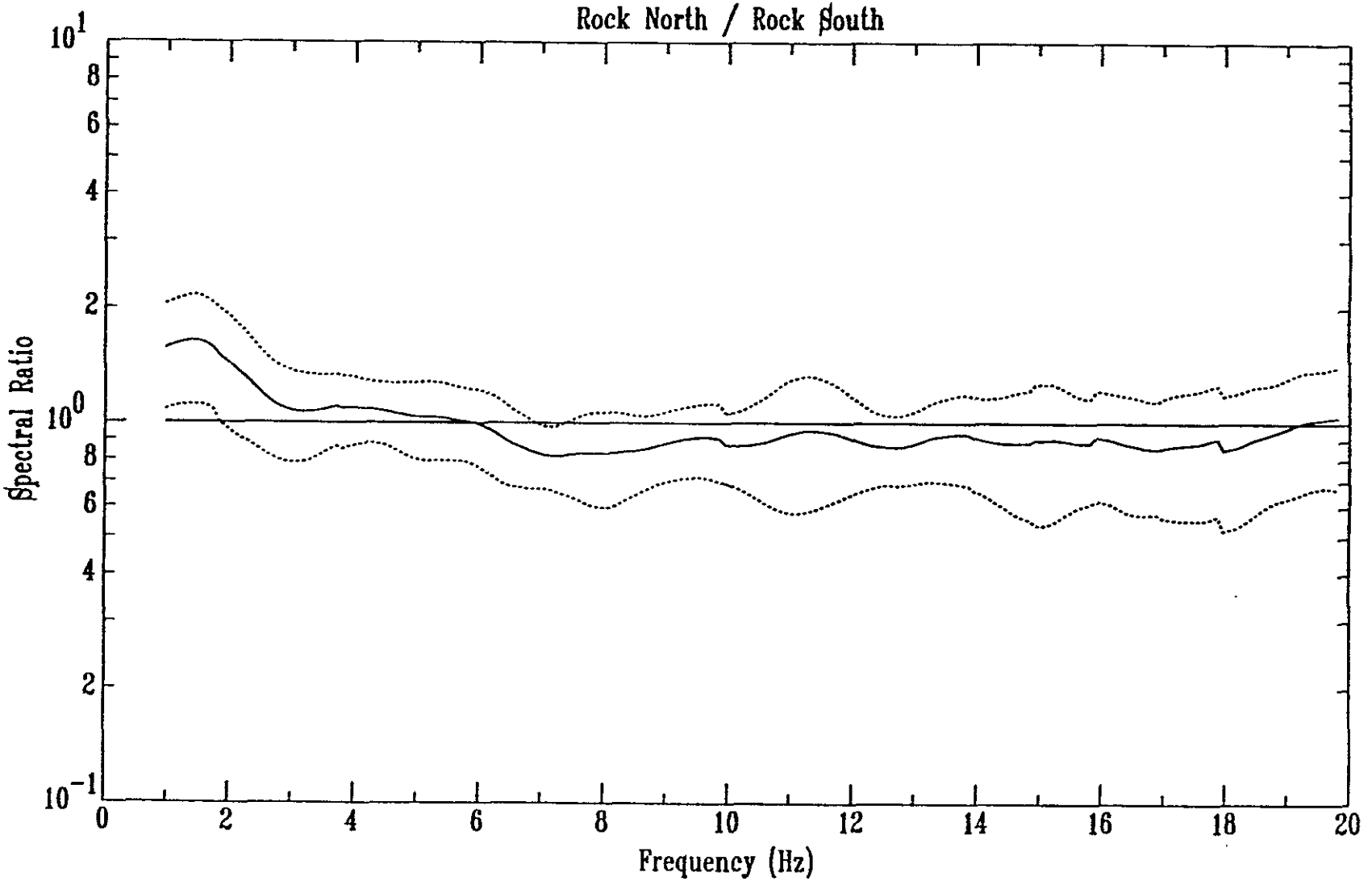

Comparison along the profile

Figure 7 shows the east-west mean and +/- 1 sd spectral ratios for sites along the profile. DMG's P-wave refraction section (Appendix H of Real, 1988) is shown next to the spectral ratio plots with the unity position of each site's ratio plot aligned to that site's location along the P-wave refraction section. Spacing between profile sites is generally 100m, except between P3 and P5 (200m), between P9 and P10 (200m), between P10 and P11 (200m), and between P11 and P12 (300m). Note the presence of a 5000 ft/sec velocity anomaly under the thinning valley sediments and the complicating effect it has on site transfer functions at sites P2 - P6. **There are no differences in the site response of profile sites for frequencies in the 1-3 Hz band; however, there are strong variations in mean spectral ratios in the 5-20 Hz band, probably due to variations in soil thickness and lateral variations in soil velocity.**

Comparison over 10m and 20m distances

Figure 8 presents the mean spectral ratio and its standard deviation for each seismometer in the profile array. The dashed lines represent the mean, the plus one standard deviation, and the minus one standard deviation (sd) spectral

Figure 7: Comparison Along Profile (100m spacing)

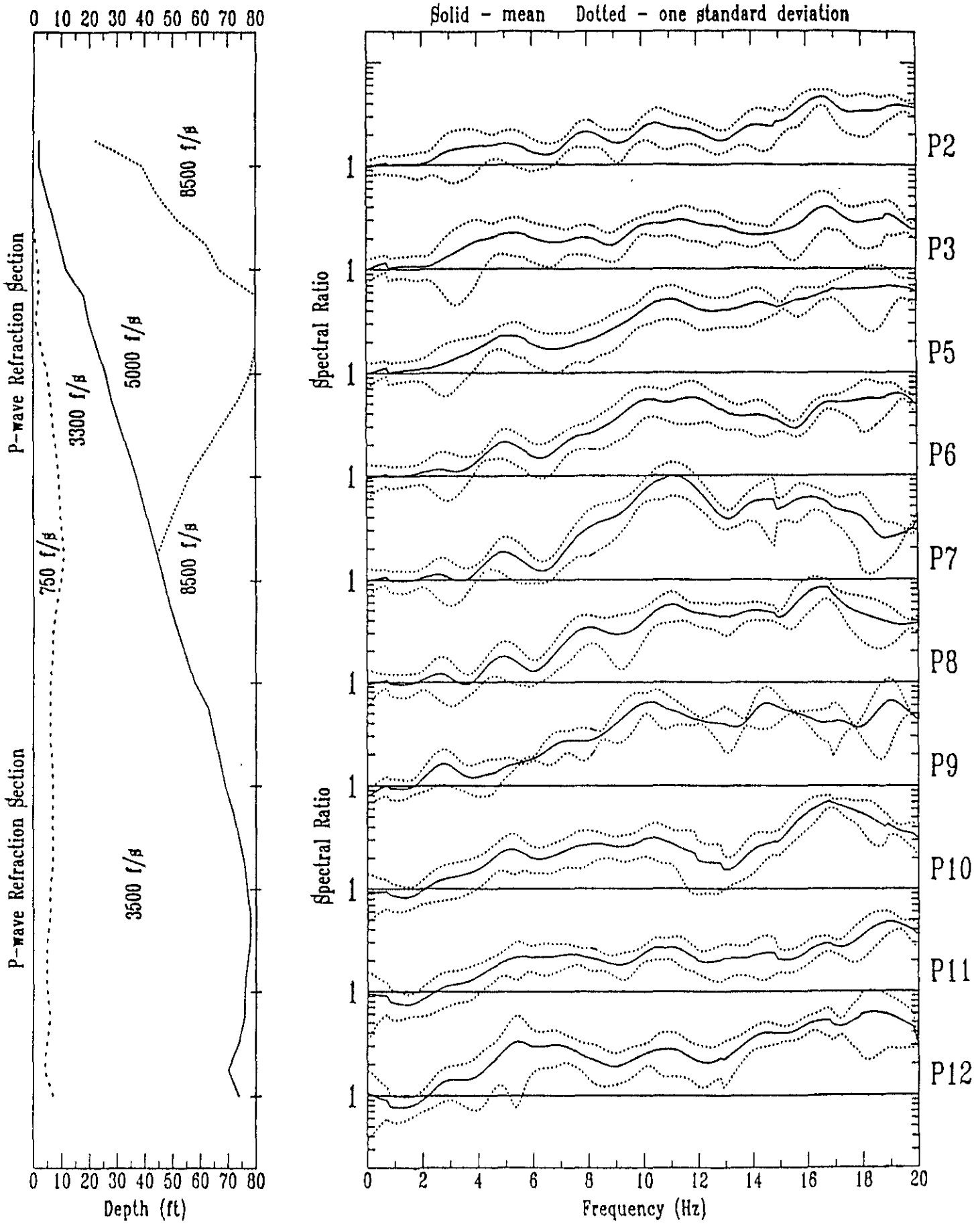

Figure 8a: Profile Spectral Ratios

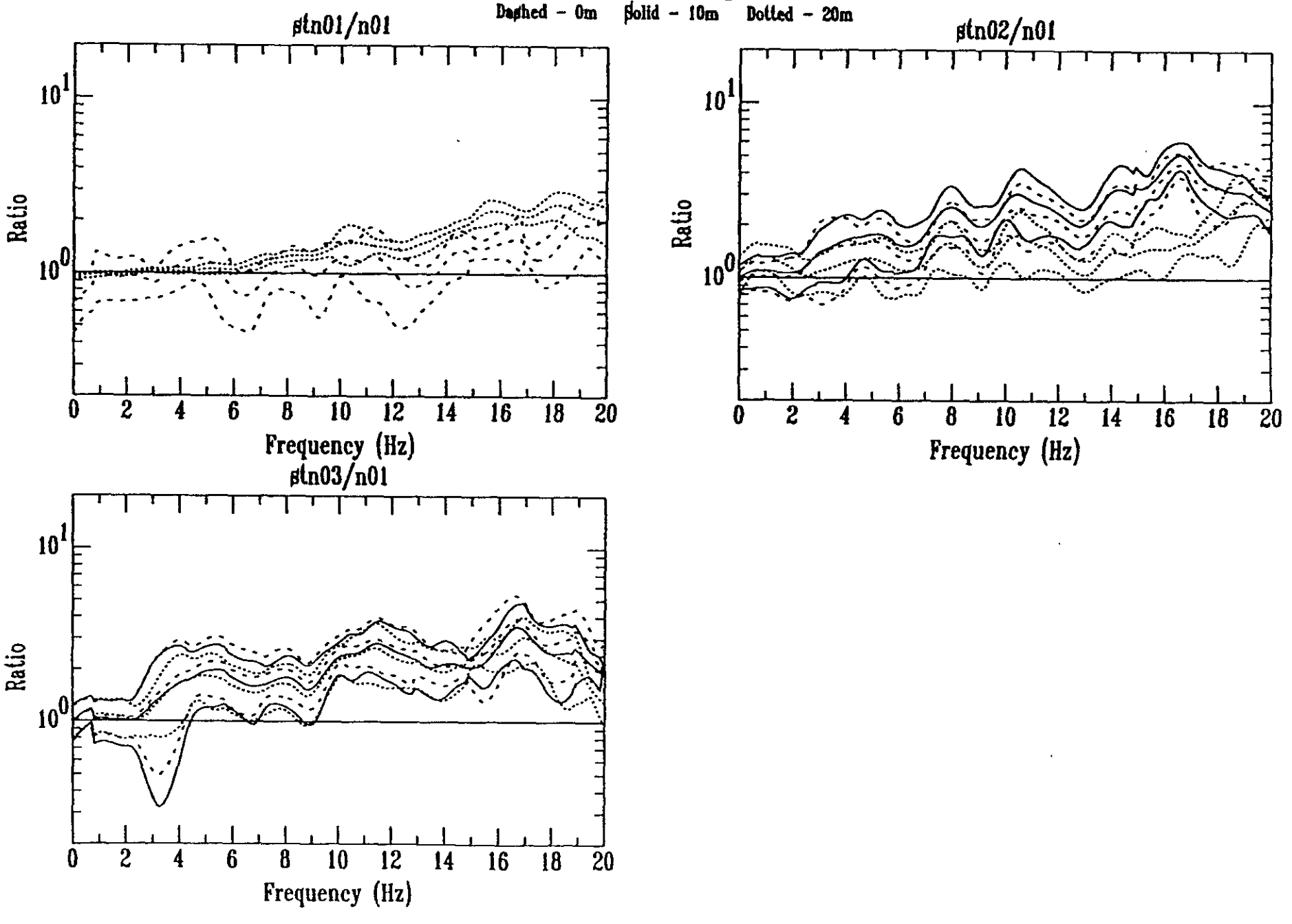

Figure 8b: Profile Spectral Ratios

Dashed - 0m Solid - 10m Dotted - 20m

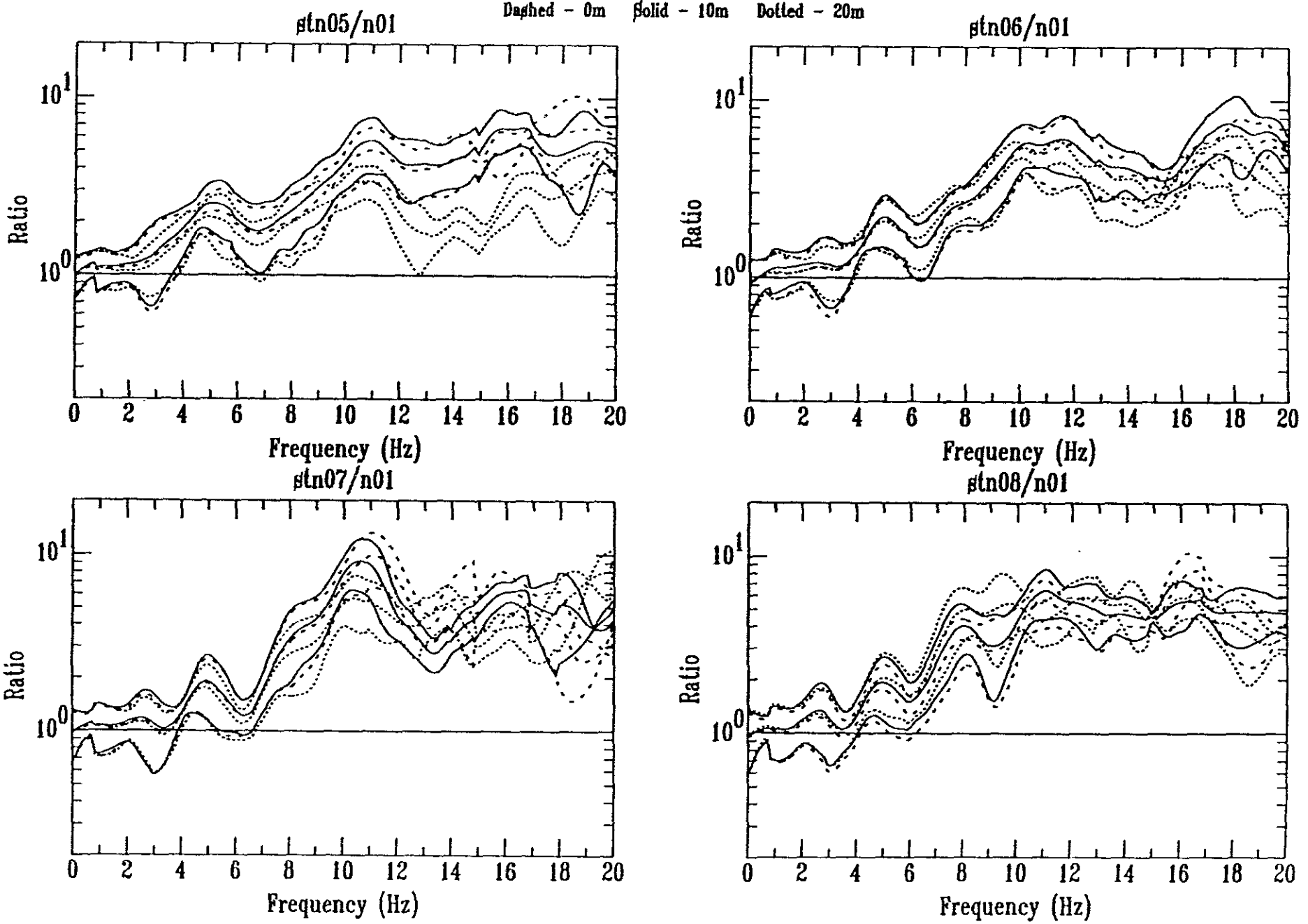

Figure 8c: Profile Spectral Ratios

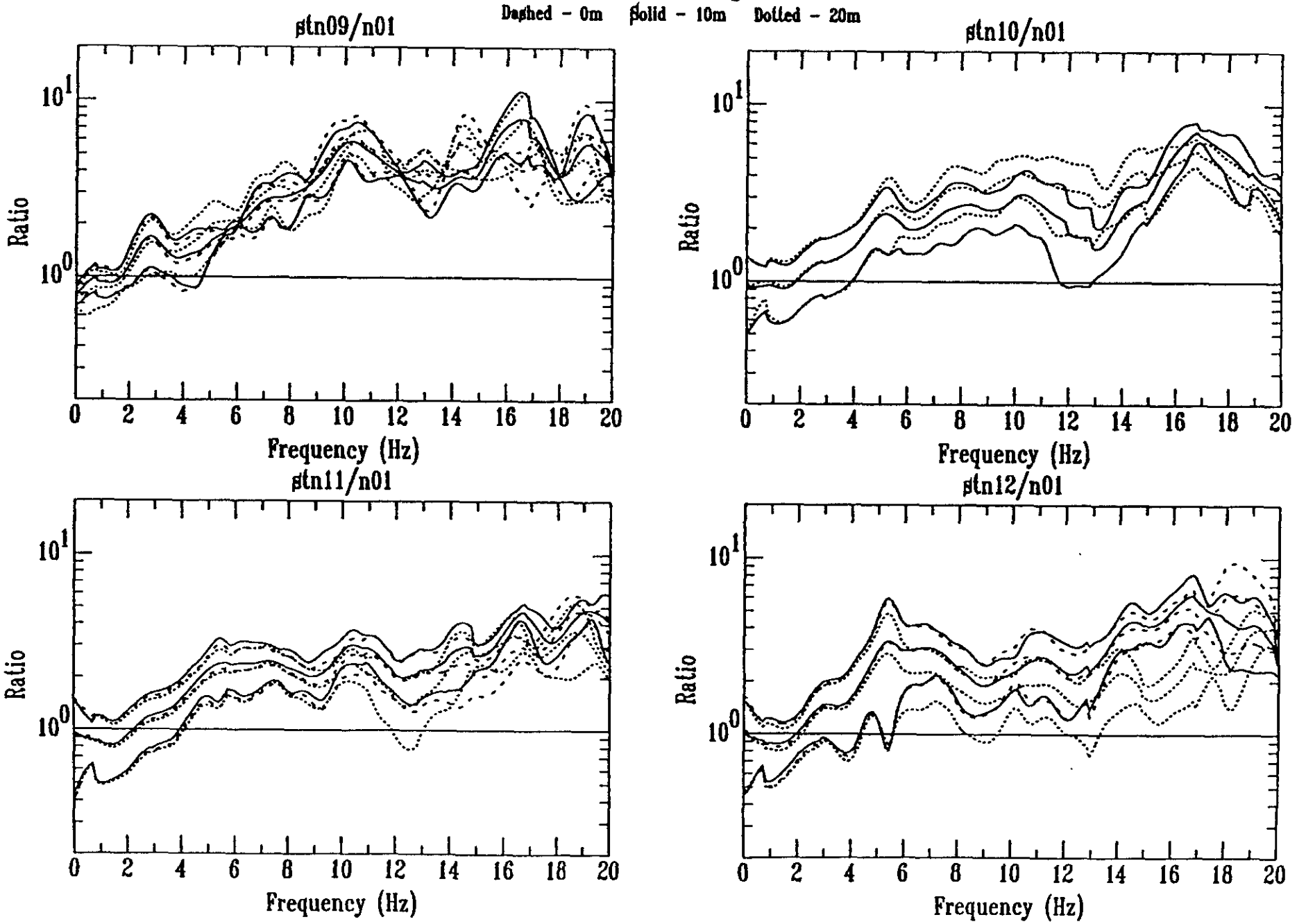

ratios for the seismometer at sites P2 - P12. The solid lines in Figure 8 represent the mean and +/- 1 sd spectral ratios for the seismometers 10m north (or south) of sites P2 - P12. The dotted lines in Figure 8 represent the mean and +/- 1 sd spectral ratios for the seismometers 20m west of sites P2 - P12. The bedrock reference seismometer for the profile study is the seismometer 7.6m north of site P1 (E-W orientation). The dotted lines for bedrock site P1 in Figure 8 are mean and +/- 1 sd spectral ratios for the east-west oriented seismometer at site P1, and the dashed lines are the same three spectral ratios for the north-south oriented seismometer at the site. Due to telemetry glitches, data were unusable for all three seismometers at site P4 and for the 0m (at site) seismometer at site P10. Hence the data plots for these four seismometers are missing from Figure 8.

Besides the general variations in mean spectral ratio among sites shown in Figure 7, which are over horizontal distances of 100m or more, there are also more localized variations in mean spectral ratio at some sites. A careful examination of the 0m and 10m mean spectral ratios for each site in Figure 8 (dashed and solid lines) reveals that mean spectral ratios over 10m distances tend to track one another, within a factor of 1.3, except at frequencies above 15 Hz at a few sites. However, over 20m distances mean spectral ratios do not track one another as well, particularly above 10 Hz. The

seismometers offset 20m to the west of the sites show significant variations in mean spectral ratios from the 0m and 10m seismometers by a factor of 2-3 at sites P2, P5, P10, and P12. **This suggests lateral variations in structure (soil layer thicknesses) or in S-wave velocity (soil composition) over 20m distances for some parts of Turkey Flat.**

Comparison among strong-motion sensor sites

Figure 9 presents the mean horizontal spectral ratio (solid line) and its plus one and minus one standard deviation (dotted lines) for the eight weak-motion seismometers of the site-specific study. All spectral ratios in Figure 9 are relative to a reference surface seismometer at the Rock South bedrock site (CTF8 - see Figure 4 for its location). Standard deviations are generally less than a factor of 2 and usually much less. As indicated in Figure 9, CTF1 and CTF2 are a second top-hole seismometer and a bottom-hole seismometer, respectively, at the Rock South site; CTF6 and CTF9 are top-hole and bottom-hole seismometers at the Valley North site; CTF7, CTF3, and CTF4 are top-hole, mid-hole, and bottom-hole seismometers at the Valley Center site; and CTF5 is a surface seismometer at the Rock North site.

Figure 9a: Strong-Motion Site Spectral Ratios

Solid - mean Dotted - one standard deviation

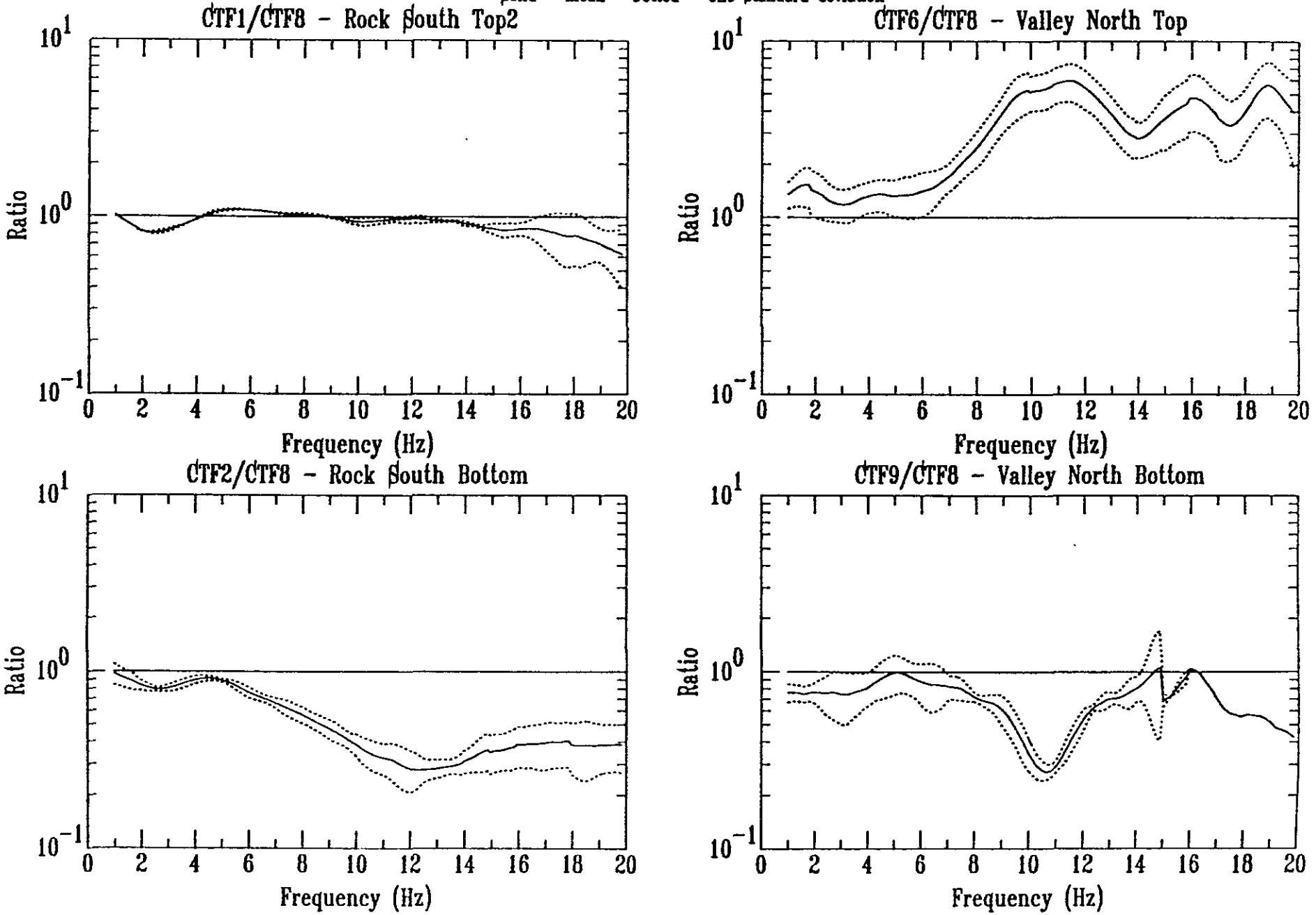

Figure 9b: Strong-Motion Site Spectral Ratios

Solid - mean Dotted - one standard deviation

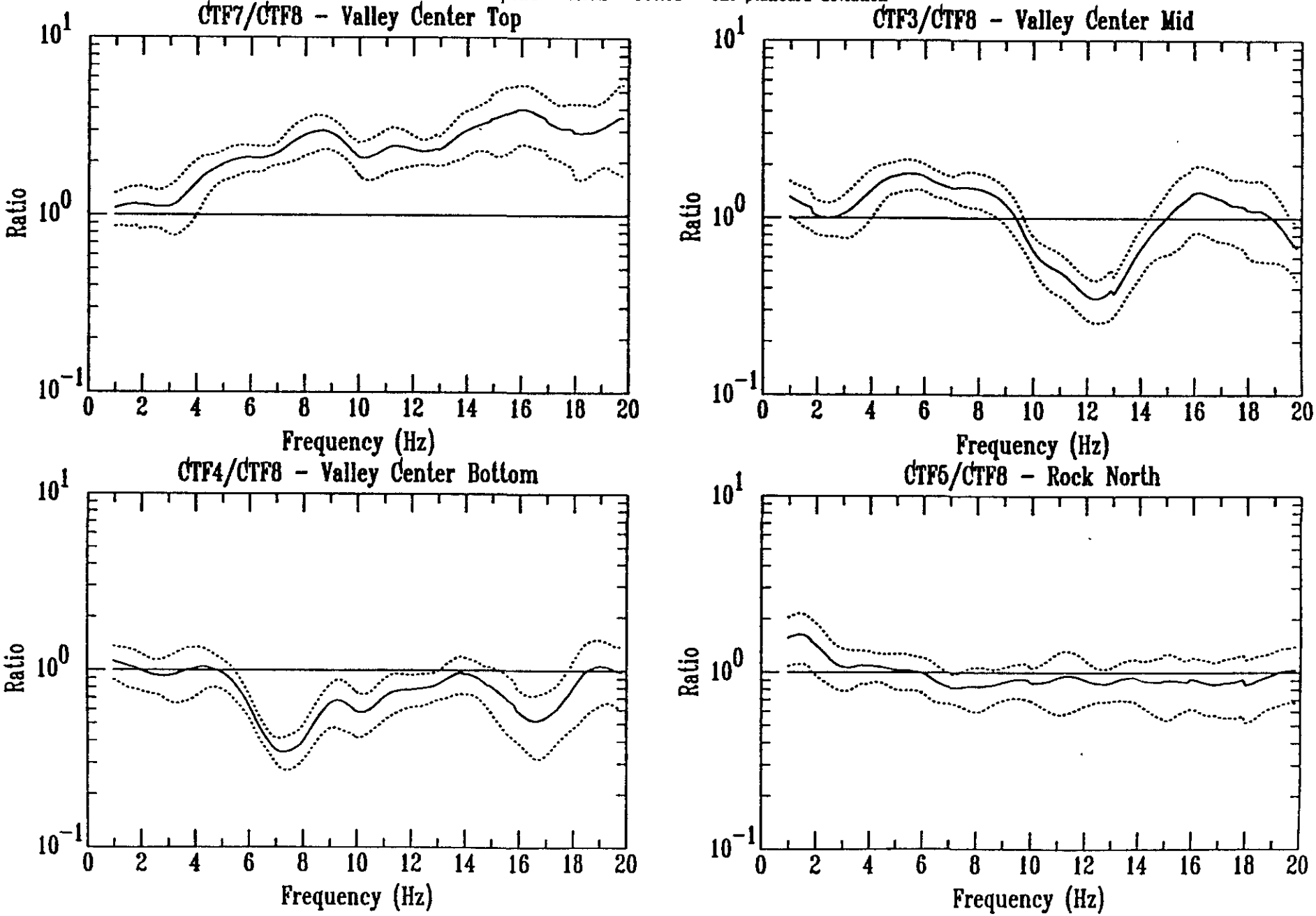

The surface bedrock sites CTF8, CTF1, and CTF5 have similar site transfer function characteristics suggesting stability of bedrock response over distances of 2 km. The adjacent surface bedrock seismometers at Rock South have a mean spectral ratio (CTF1/CTF8) near one, as expected. The observed variations in the high frequency response of CTF1 relative to CTF8 may be caused by looseness in the fill around the top of the plastic bore hole casing in which the seismometer at CTF1 was clamped. As discussed in the rock sites comparison above, the across-valley surface bedrock seismometer at Rock North also has a mean spectral ratio (CTF5/CTF8) within 30% of one.

The valley surface sites CTF6 and CTF7 have site transfer functions similar to neighboring profile sites while the downhole sensors CTF2, CTF3, CTF4, and CTF9 show site transfer functions dominated by resonant peaks and valleys. The Valley North site CTF6 falls between profile sites P6 and P7. These three sites have similar response characteristics, including similar amplitudes for their mean spectral ratios (Figures 7 and 9). A similar conclusion can be reached by comparing the mean spectral ratio for CTF7 in Figure 9 with the mean spectral ratios for profile sites P10 and P11 in Figure 7. The site transfer functions for the downhole sensors CTF2, CTF3, CTF4, and CTF9, although dominated by site resonant peaks, are difficult to interpret without modeling the observed transfer functions.

MODELING

This section of the report presents the results from a modeling study of the weak-motion observations for Turkey Flat. Empirically determined weak-motion transfer functions allow a comparison to theoretical transfer functions derived from geotechnical information. Theoretical transfer functions determined from different geotechnical models can be checked for accuracy in reproducing empirical transfer functions. Basic modeling assumptions concerning linearity at low strain levels, uncertainty in geotechnical measurements, and the nature of the valley response (one-, two-, or three-dimensional) can also be examined.

Modeling of site response is a non-unique process so assumptions must be made to simplify the modeling task and to model the form of the site response observed (relative transfer functions). Site response is dependent on density, damping, and S-wave velocities of sediments and rock, on layer thicknesses and shapes, and on the angle of incidence and mode of propagation of incoming S-waves. Because the incoming S-waves have peak accelerations less than .001g and are nearly vertically incident, and because the valley shape ratio (maximum depth to half-width) of about 0.02 indicates a strong potential for predominantly one-dimensional response (Bard and Bouchon, 1985), the modeling has been simplified by assuming

the site response to vertically propagating SH-waves is one-dimensional, linear, and viscoelastic. The medium is also assumed to be isotropic and plane-layered. Further, because mean spectral ratio is a relative site response observation, it is assumed that mean spectral ratios can be modeled by the relative site amplification function in the computer program SHAKE (1975 version) (Schnabel, et al., 1972). This latter assumption will hold true as long as the modeling results for the second surface bedrock seismometer at the Rock South site (CTF1) are near unity, within an experimental uncertainty of a factor of 1.3. As used in this report, site amplification as a function of frequency from SHAKE is the ratio of seismic response of the multilayered soil-rock structure of a given model to the seismic response of a simple half-space of rock with properties equivalent to the rock half-space at the bottom of that model.

Initial model parameters such as layer thickness, density, damping, and S-wave velocity structure must be chosen. Then these parameters are systematically varied to obtain a good fit to the observed mean spectral ratios. Geotechnical information for Turkey Flat is available in Real (1988). Two methods of *in situ* velocity structure determination are tested in this report: 1) downhole S-wave measurements and 2) P-wave refraction profiles with P-wave velocities converted by Vp/Vs ratio to S-wave velocities. Additionally, the Turkey Flat

Standard Geotechnical Model (a committee model) is also tested for the appropriateness of its velocity structure at weak-motions.

To obtain better model fits to the observed spectral ratios, damping and S-wave velocity were varied in a systematic manner. In SHAKE, the location of resonant peaks in the frequency domain are mainly dependent on S-wave velocity structure, while the amplitude of the amplification is dependent on damping. Thus to obtain the "best-fit" final model from an initial set of geotechnical information (downhole, refraction, or Standard Model), damping is varied to fit the amplitude of observed resonant peaks and S-wave velocity is systematically varied, as described below, to fit the position of resonant peaks in the frequency domain. The resulting final models are not unique results but only "best-fit" results for the modeling assumptions inherent in SHAKE and for the chosen geotechnical information and systematic manner in which the initial S-velocity model was varied.

As mentioned above, S-velocity was varied in a systematic manner to improve model fits to the observed spectral ratios. For downhole S-wave velocity measurements and for the Standard Geotechnical Model velocity structure, the model fit to observations has been improved by varying observed S-wave velocities in layers above the rock half-space by a uniform

percentage change in velocity (half-space S-wave velocity is never changed because it has a very small effect on the location of resonant peaks in the frequency domain). For P-wave refraction profiles, the model fit to observations has been improved by arbitrarily changing the Vp/Vs ratio of the layers above the rock half-space.

The presentation of the modeling results is divided into three parts. The first part is on modeling based on downhole S-wave measurements and discusses *in situ* properties, downhole-model results, and the effects of S-velocity and density changes on the modeling results. The second part is on modeling based on P-wave refraction profiles and discusses S-velocity estimates, refraction-model results, and a comparison to the results of modeling based on downhole measurements. The third part is on modeling using the Standard Geotechnical Model for Turkey Flat and discusses Standard-Model results.

Modeling based on downhole measurements

In situ properties

Table 2 lists the *in situ* properties determined from downhole measurements at three of the strong-motion array sites at Turkey Flat. Densities in Table 2 were taken from the Stan-

dard Geotechnical Model for Turkey Flat (Appendix D, Real and Cramer, 1989). *In situ* damping values in Table 2 are estimates from Appendices E and G of Real (1988). Layer thicknesses and S-wave velocities were taken from Cramer, 1987 (in Appendix H of Real, 1988). As noted in Table 2, errors in downhole velocity measurements are +/- 10-20 percent.

Initial and final models

Shown in Figure 10 are initial and final models based on the downhole measurements and improved by uniformly varying damping and S-velocities as indicated above. The final percent change to layer S-velocities (Vs) and the final damping value (Br for rock and Bs for soil) are indicated on each plot. Discussion of the initial and final models at Rock South, Valley North, and Valley Center follows.

The initial model from downhole measurements for the Rock South site (dashed line with squares) used a damping of .10 and does not fit the resonance peak and amplitude of the downhole sensor's mean spectral ratio. For the final model (dashed line with octagons), downhole determined S-velocities were reduced by 20% and damping was increased to .15 in order to fit the downhole resonant peak and its amplitude and spectral flattening above 10 Hertz. Summary plots of downhole velocity measurements (Figure 11) taken from Real (1988) show

Table 2

In Situ Properties from Downhole Measurements

Layer no.	Thickness m	Damping	Density g/cc	Velocity[1] m/s
		Rock South - Hole 2		
1	1.8	.10-.13	2.10	640.
2	7.0	.10-.13	2.20	1036.
3	8.8	.10-.13	2.20	1332.
4	-	.10-.13	2.20	1539.
		Valley Center - Hole 5		
1	1.8	.07-.09	1.50	130.
2	4.9	.07-.09	1.80	354.
3	14.0	.07-.09	1.90	622.
4	-	.10-.13[2]	2.20	1317.
		Valley North - Hole 3		
1	1.8	.07-.09[2]	1.55	131.
2	3.0	.07-.09[2]	1.75	283.
3	6.1	.07-.09[2]	1.90	543.
4	-	.10-.13[2]	2.20	1317.

[1]S-velocity errors are +/- 10-20 percent

[2]Estimate from measurements in other holes

Figure 10a: Models from Downhole Measurements

Observations: —— mean ····· 1 std deviation Models: ▫ - ▫ initial ○ - ○ final

Vs - S-wave velocity change; Br,Bs - rock, soil damping

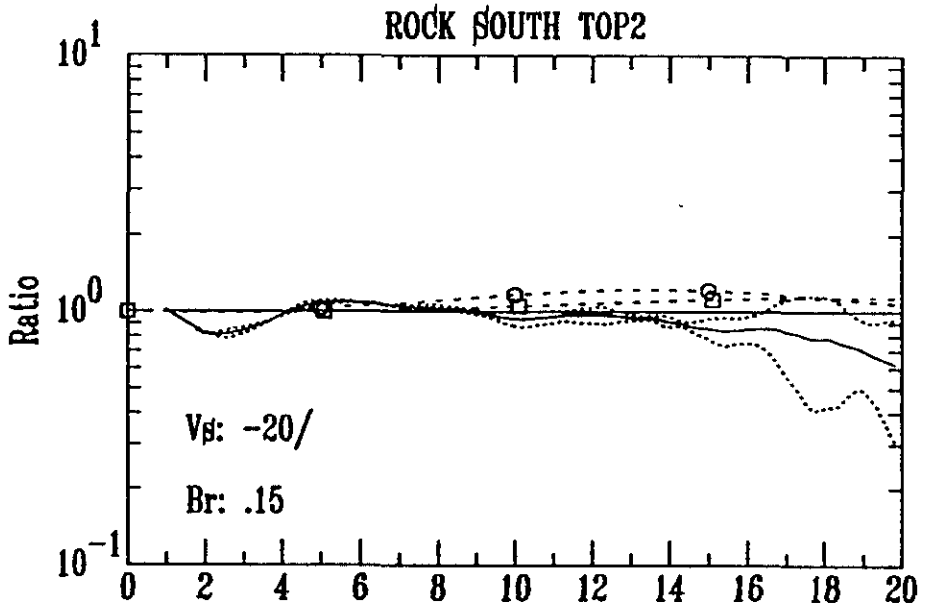

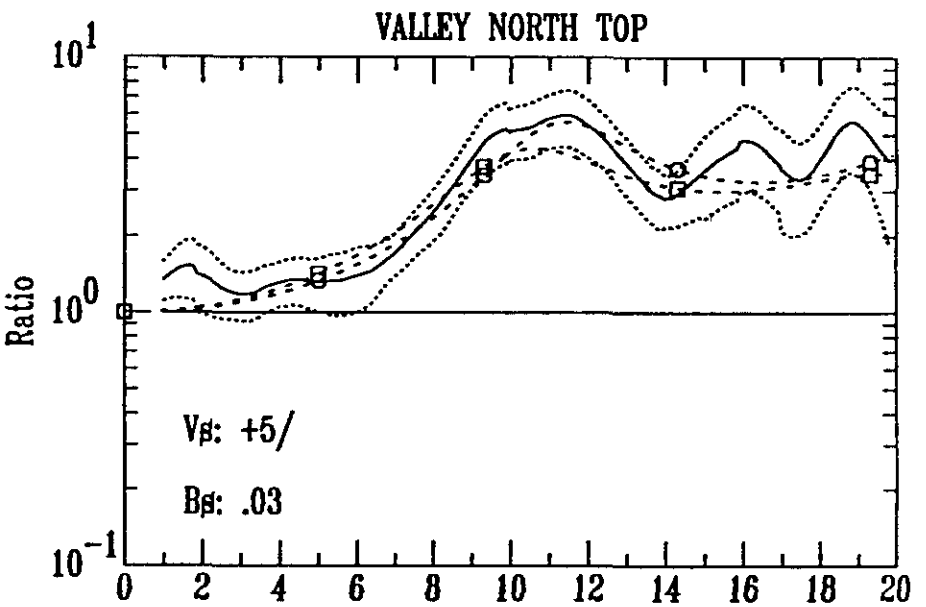

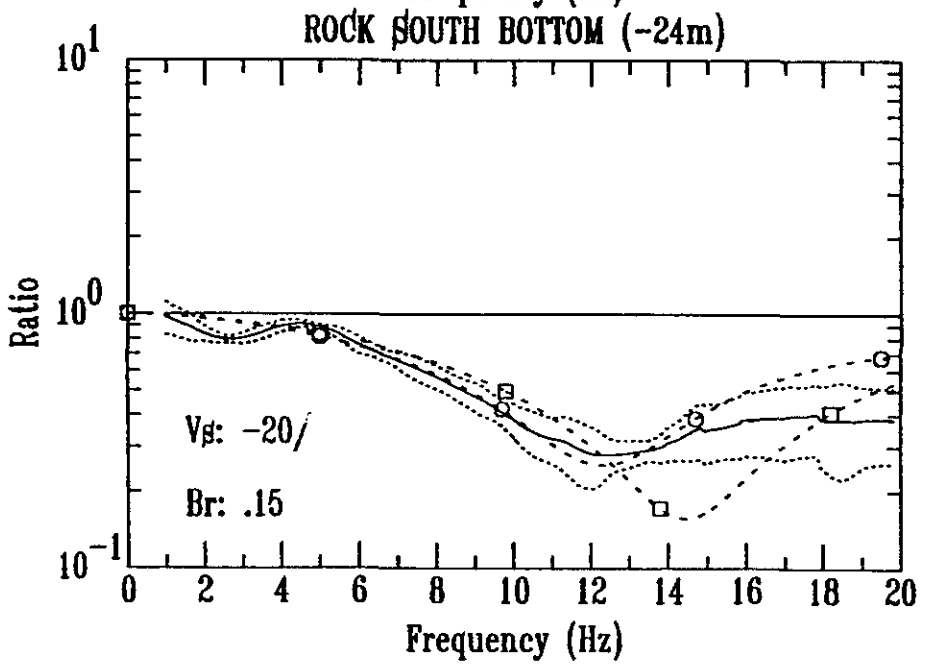

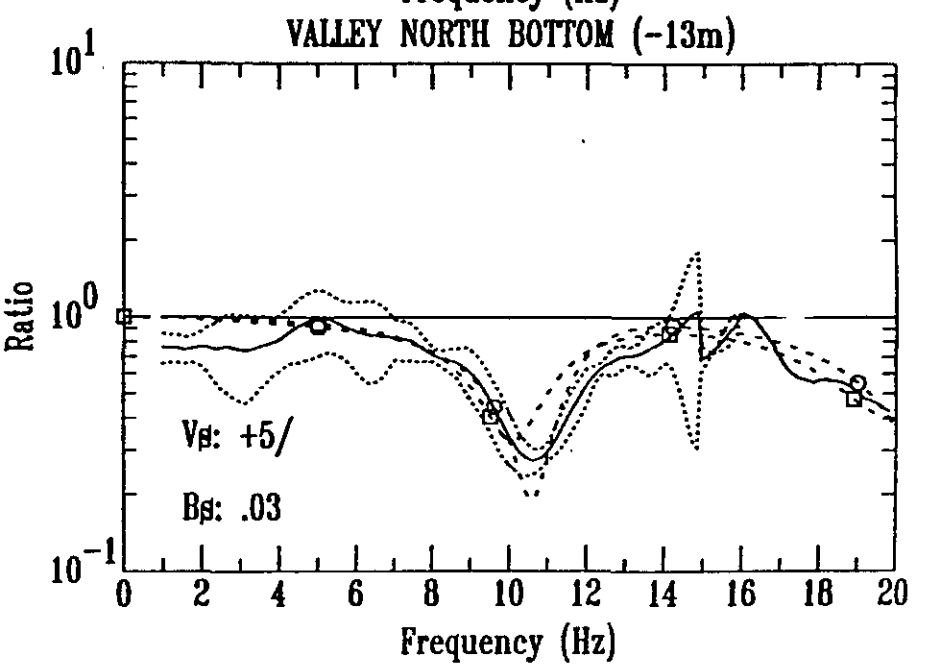

Figure 10b: Models from Downhole Measurements

Observations: —— mean ····· 1 σ/d deviation Models: ⊡ - ⊡ initial ⊙ - ⊙ final

Vβ - β-wave velocity change; Br,Bβ - rock, soil damping

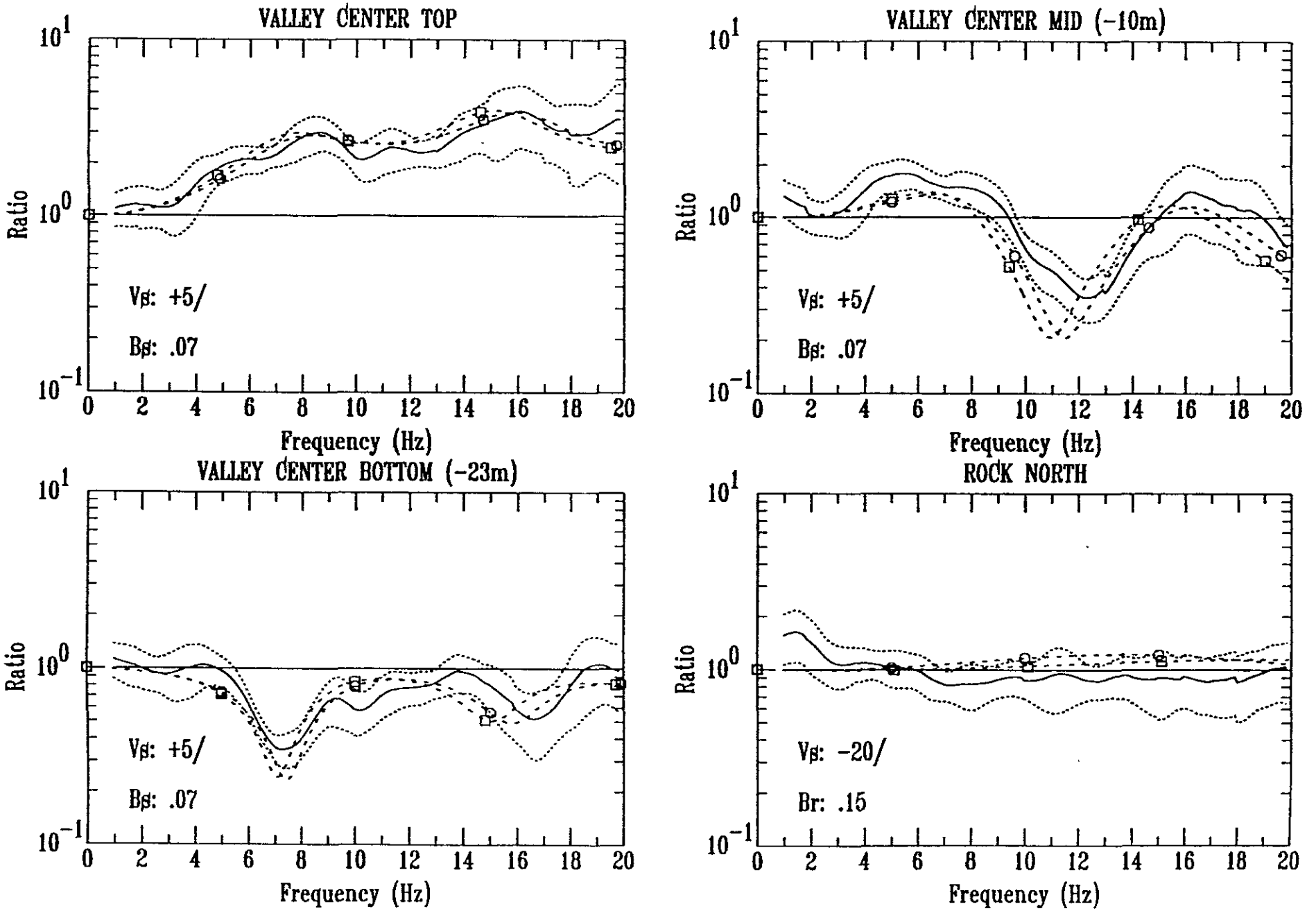

Figure 11: Summary of Downhole S-Velocity Measurements

Downhole: □ Dames-Moore; △ DMG; ○ Qest; ◇ Oyo; ▽ WCC

Cross-hole: × HardingLawsonAssoc.; Suspension: + Oyo

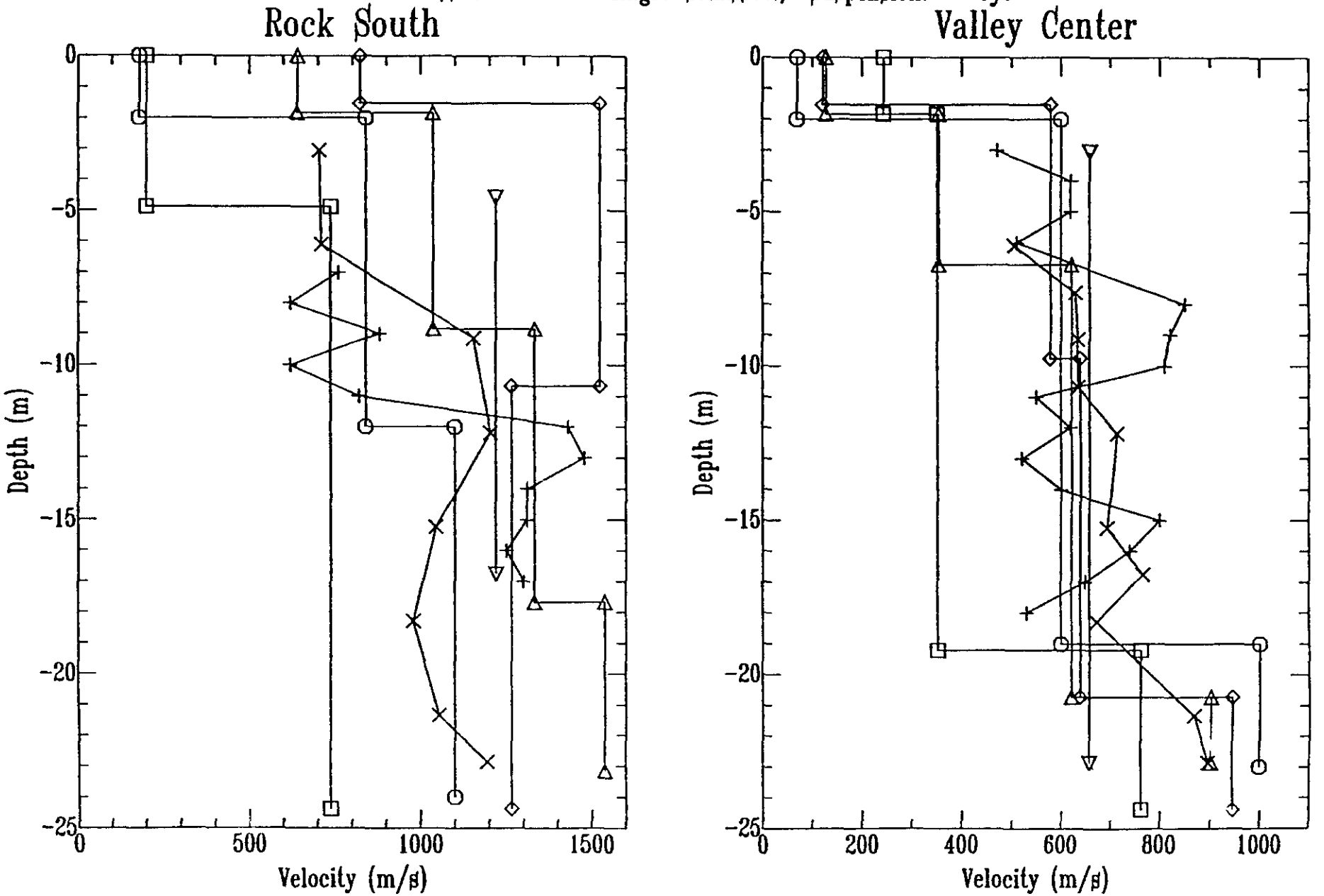

more scatter for the Rock South site (50%) than for the Valley Center site (20%). This increased scatter may indicate problems in generating S-waves at a stiff bedrock site and in picking S-wave arrivals due to P-wave contamination of S-wave arrivals. This may lead to systematically higher downhole S-velocity determinations at the Rock South site. Final S-velocities are different from downhole measured values but still within measurement error. **The final damping value of .15 is compatible with *in situ* determinations listed in Table 2 (.10-.13), but conflicts with laboratory determined values used in the Turkey Flat Standard Geotechnical Model (.01-.02).**

At the Valley North site, the initial model from downhole measurements (dashed line with squares) with .07 damping for soil underestimated the amplitude of the top and bottom hole mean spectral ratios. For the final model (dashed line with octagons), measured downhole S-velocities were increased by 5% to better match the location of the resonant peaks in top and bottom hole mean spectral ratios. This change in S-velocity is well within downhole measurement error. Final damping was reduced to .03 to better match the amplitudes of the mean spectral ratios, and is close to that of the Turkey Flat Standard Geotechnical Model although no *in situ* measurements are available for the Valley North site.

At the Valley Center site, the initial model from downhole measurements (dashed line with squares) provides a good estimate of the mean spectral ratio for all three spectral ratios. In order to better match the spectral ratio peaks in the frequency domain, the final model (dashed lines with octagons) adjusted the measured downhole S-velocities by +5%. Again the change in S-velocity is well within downhole measurement error. Final damping was unchanged from the initial value of .07. **For this site, damping is clearly compatible with the in situ measurements and incompatible with the laboratory measurements used in the Turkey Flat Standard Geotechnical Model (.01-.02).**

Sensitivity of models to S-velocity and damping

Figures 12 and 13 show the effects on the model fit of changes in S-velocity and damping, respectively. Generally plot symbols of squares, triangles, octagons, inverted triangles, and diamonds on dashed lines indicate the results for the first, second, third, fourth, and fifth parameter value listed in each plot. For S-velocity changes, this corresponds to percentage changes in S-velocity from the final models of Figure 10 of -10%, -5%, 0%, +5%, and +10%, respectively. For changes in damping, the symbols correspond to changes in damping from the final models of Figure 10 of -.04, -.02, .00, +.02, and +.04, respectively. In Figure 13, the Valley

Figure 12a: Effect of S-Velocity Changes

Observations: —— mean ····· 1 std deviation Models: - - -

Vs - S-wave velocity change; Br,Bs - rock, soil damping

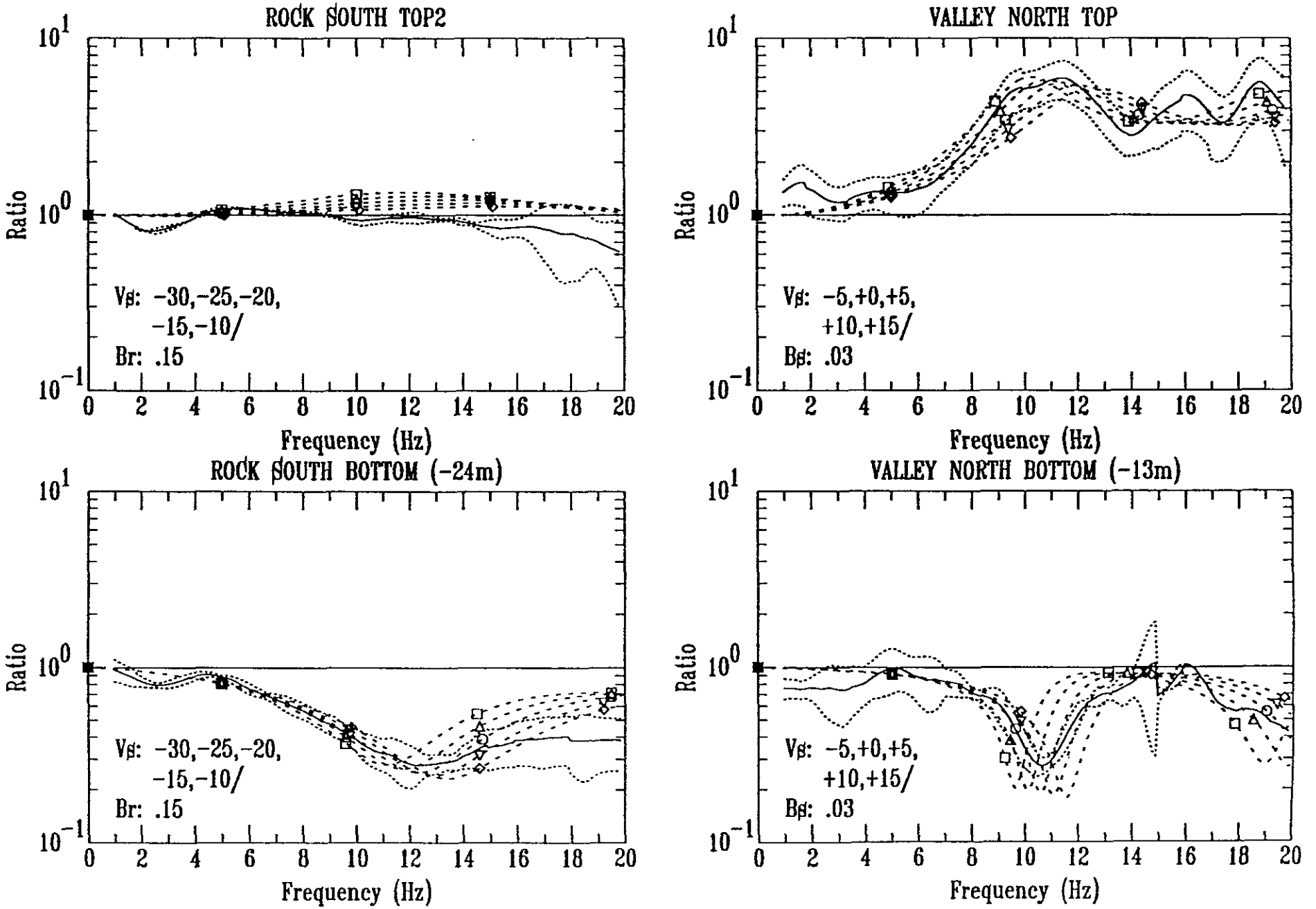

Figure 12b: Effect of S-Velocity Changes

Observations: —— mean ····· 1 std deviation Models: - - -
Vs - S-wave velocity change; Br,Bs - rock, soil damping

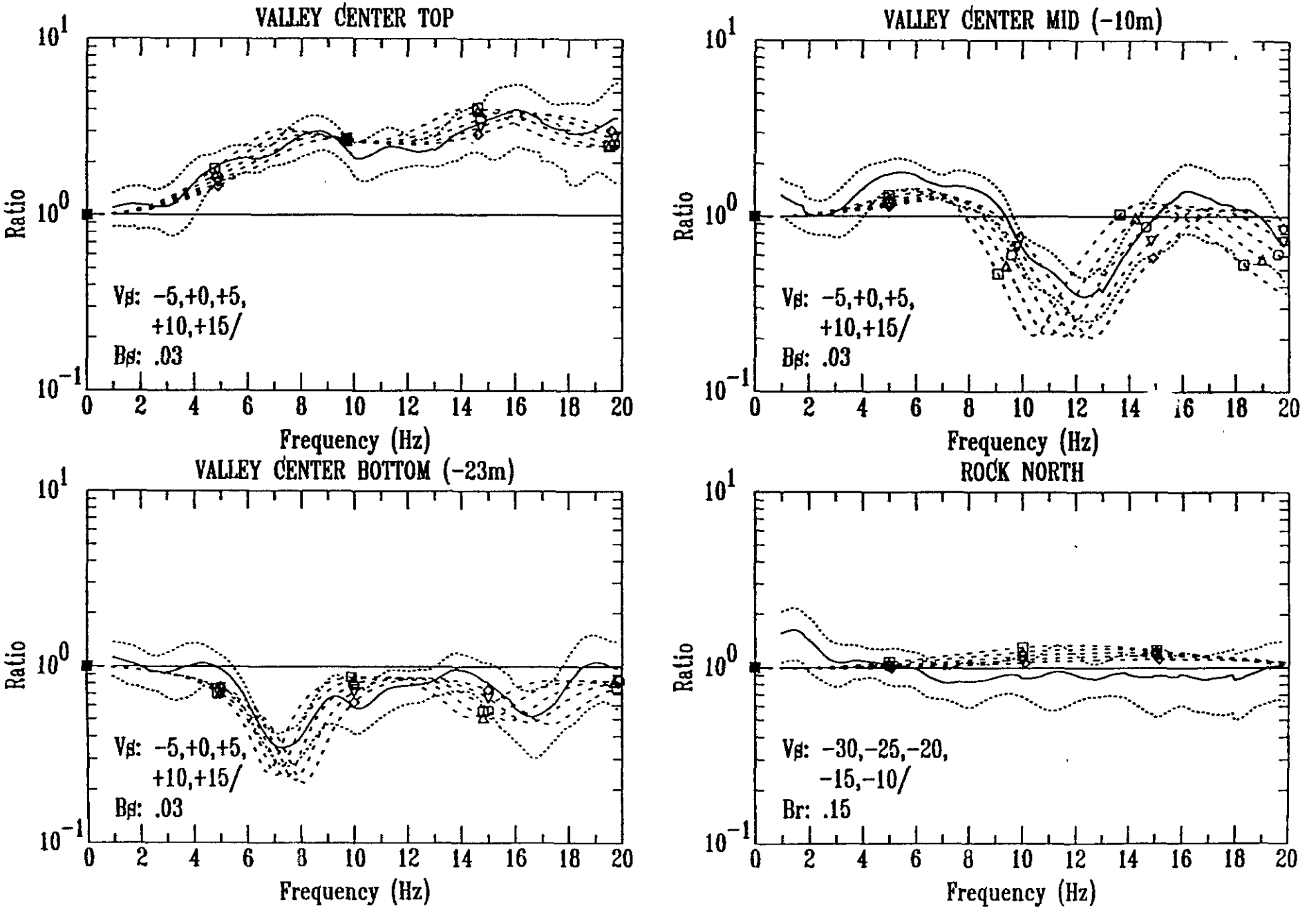

Figure 13a: Effect of Changes in Damping

Observations: —— mean ····· 1 std deviation Models: - - -

Vs - S-wave velocity change; Br,Bs - rock, soil damping

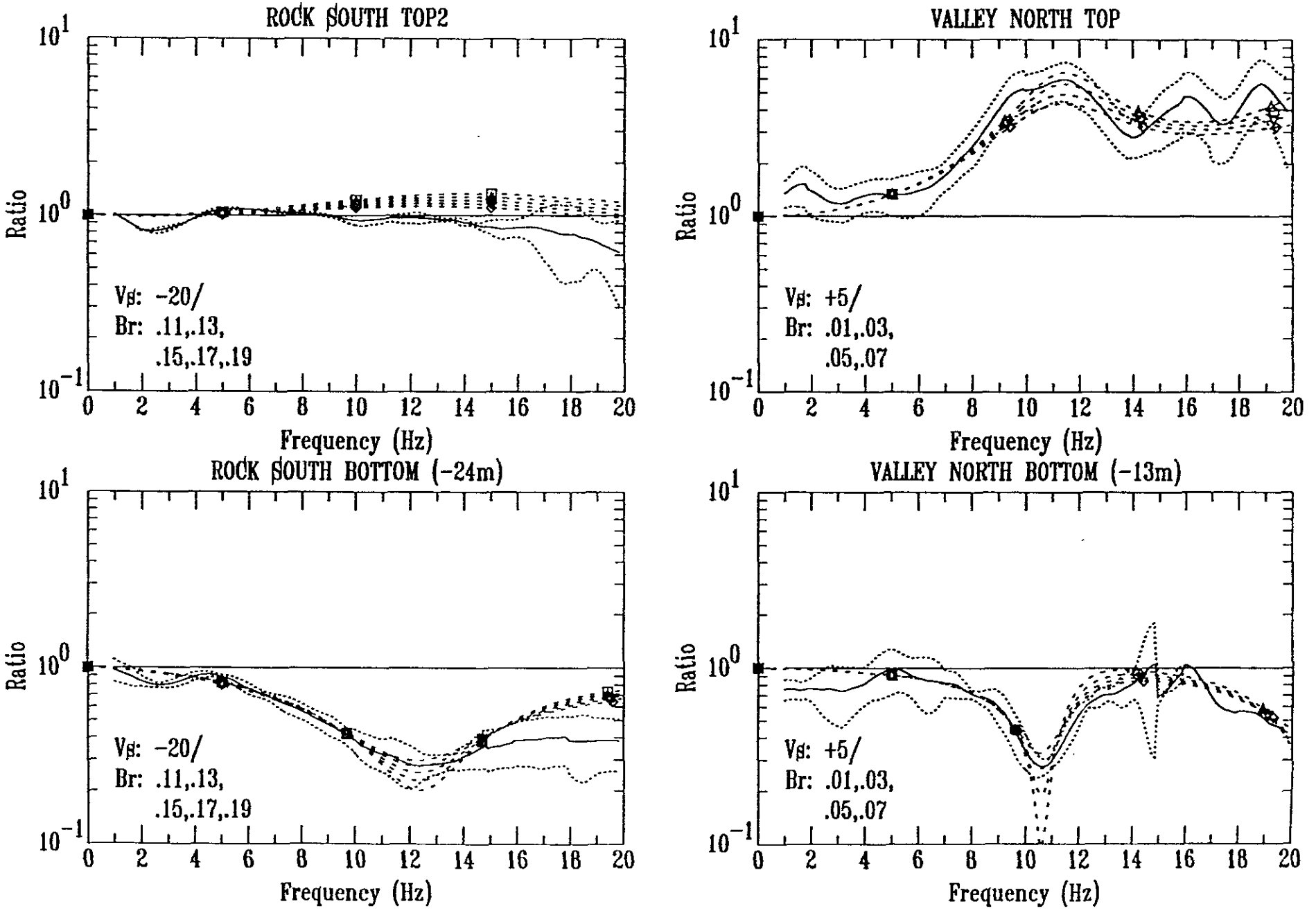

Figure 13b: Effect of Changes in Damping

Observations: —— mean ····· 1 std deviation Models: - - -

Vs - β-wave velocity change; Br,Bs - rock, soil damping

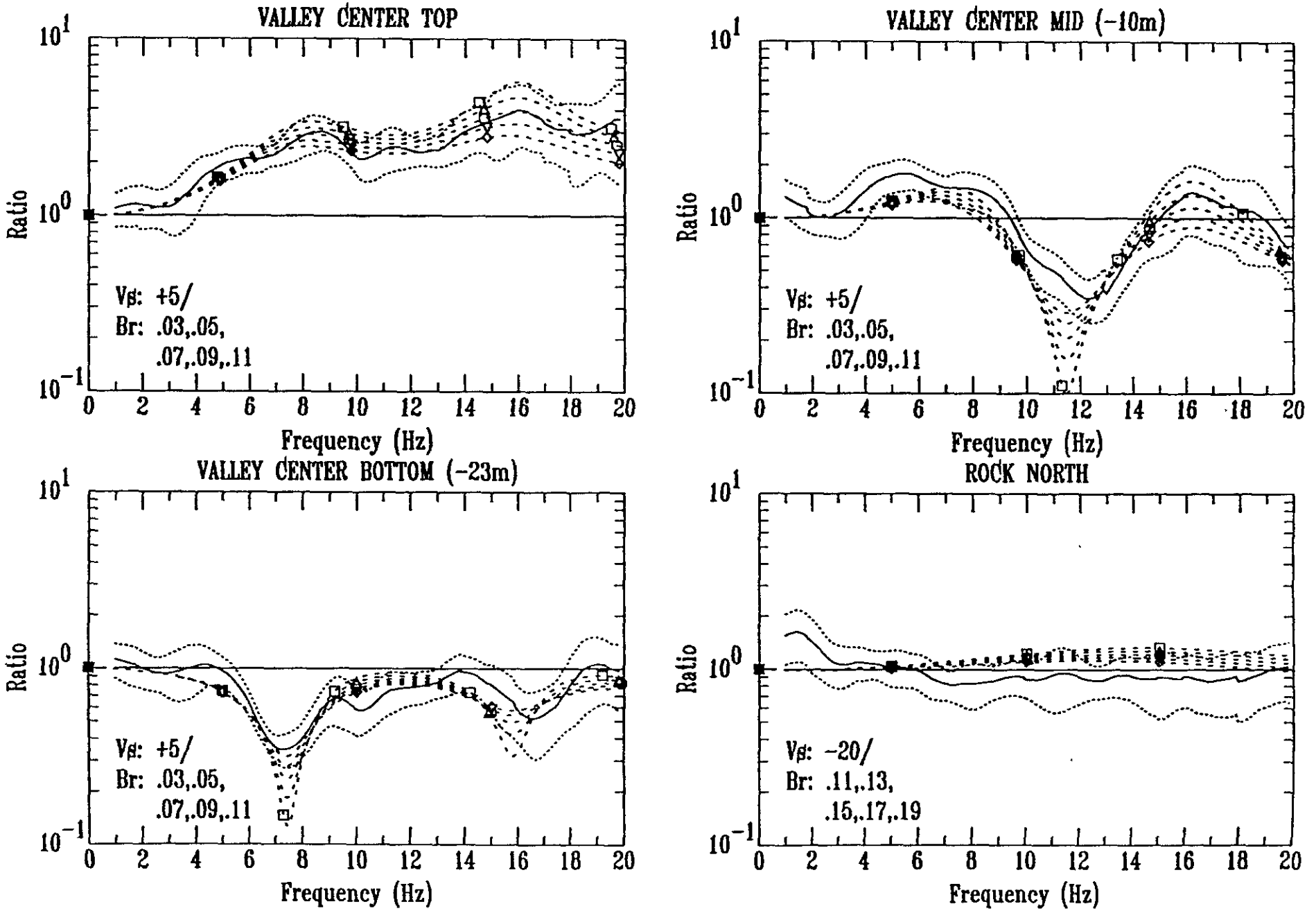

North plots show only four values of damping because the value corresponding to the square symbol is physically unreasonable and hence is absent.

From Figure 12, modeling fits to observed mean spectral ratios appear sensitive to S-velocity changes greater than 5%. Model fits to surface-sensor mean spectral ratios seem less sensitive to changes in S-velocity than model fits to downhole-sensor mean spectral ratios, which have clearer resonant peaks. Modeling sensitivity to greater than 5% changes in S-velocity is more precise than the current downhole S-velocity measurement error of 10-20%.

From Figure 13, modeling fits to observations are sensitive to changes in damping greater than plus or minus .02. Sensitivity of model fit appears to be more easily judged at resonant peaks in the frequency domain. Damping values determined from modeling pairs of surface and downhole sensors at Turkey Flat are still clearly compatible with *in situ* estimates of damping at Rock South and Valley Center. **The results from Figures 12 and 13 provide error estimates for the final models of Figure 10.**

Modeling based on P-wave refraction profiles

Velocity structure

Table 3 lists the P-wave velocity structure taken from two refraction profiles, one by OYO Corporation and one by DMG. Density values are taken from the *in situ* measurements listed in Table 2 and damping values are from the final results of the downhole modeling. Layer thicknesses and P-velocities for the OYO refraction profile are taken from Appendix F of Real (1988) and for the DMG refraction profile are taken from Appendix H of Real (1988). S-wave velocities have been estimated by dividing by a Vp/Vs ratio, initially an average value of 2.0 from downhole measurements (Appendix H of Real, 1988). Final models have been obtained by adjusting the Vp/Vs of the model layers to fit resonant peak frequencies and by adjusting damping values to fit amplitudes of the observed mean spectral ratios.

Initial and final models

Figure 14 shows the initial (dashed lines with squares) and final (dashed lines with octagons) model results for the OYO P-wave refraction profile. The initial models clearly do not match resonant peaks in the frequency domain. Final model Vp/Vs ratios range from 1.6 for the rock sites and the Valley

Table 3

P-wave Refraction Velocity Structures*

OYO Refraction Profile			DMG Refraction Profile		
Layer no.	Thickness m	Velocity m/s	Layer no.	Thickness m	Velocity m/s
Rock South:					
1	0.5	300.	1	16.8	1524.
2	2.0	1000.	2	-	3352.
3	27.5	1500.			
4	-	2600.			
Valley Center:					
1	2.5	300.	1	1.5	228.
2	19.5	1000.	2	22.5	1066.
3	-	2700.	3	-	2590.
Valley North:					
1	3.0	300.	1	3.0	228.
2	10.5	900.	2	9.8	1066.
3	1.5	1500.	3	-	2590.
4	-	2800.			

* Errors in refraction measurements are about 10%

Figure 14a: Models from OYO Refraction Data

Observations: —— mean ····· 1 std deviation Models: □ - □ initial ○ - ○ final

Vp/Vs - P to S velocity ratio; Br,Bs - rock, soil damping

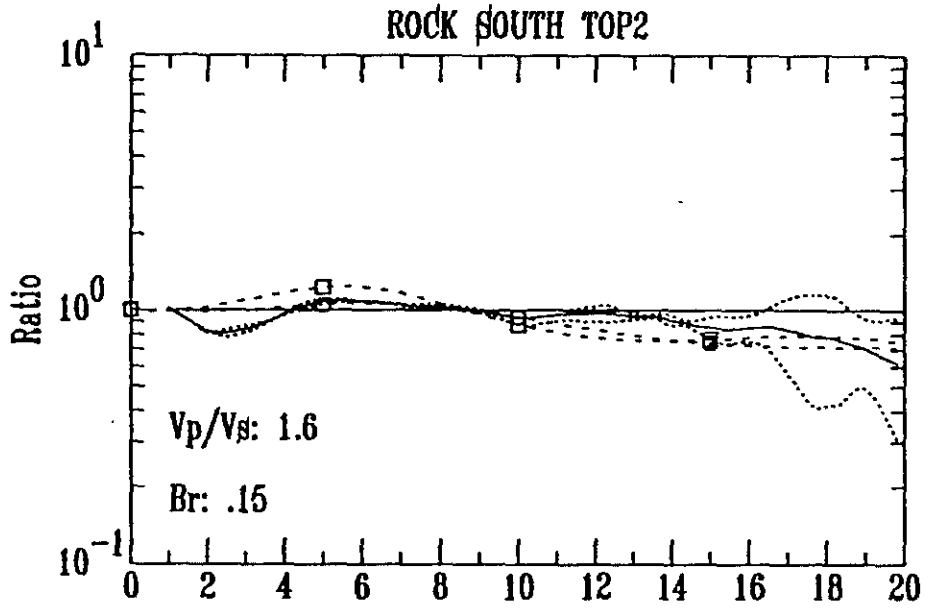

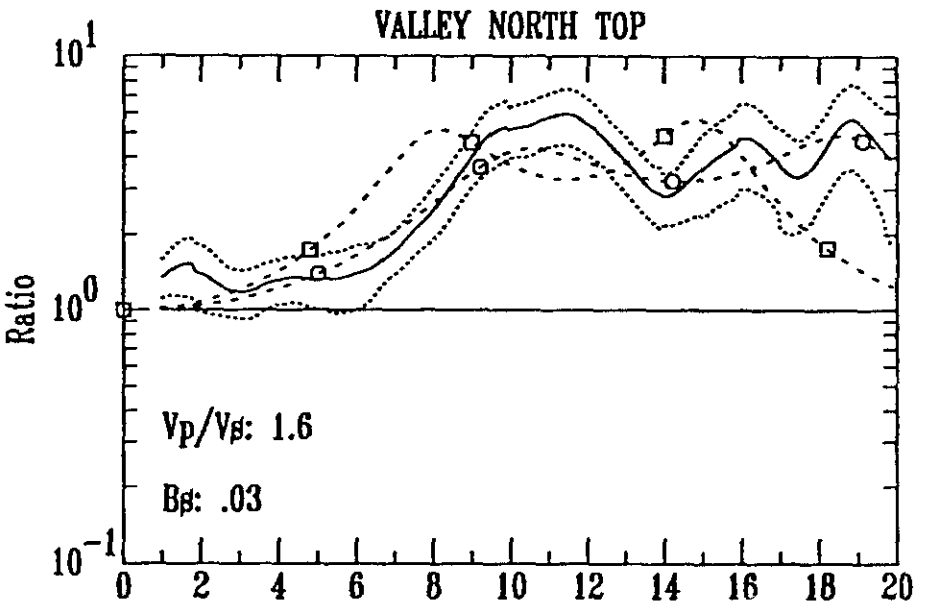

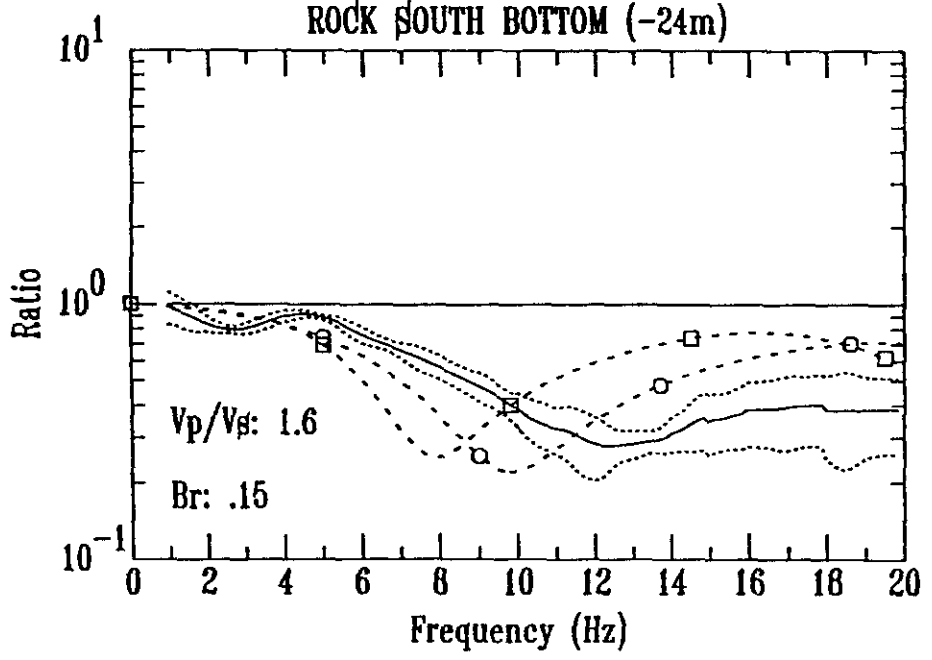

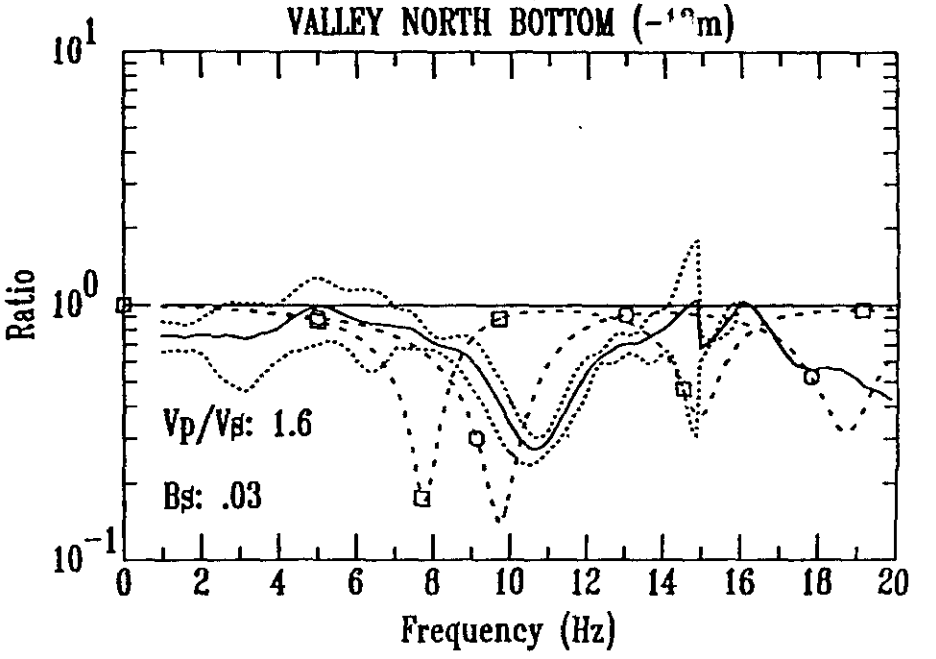

Figure 14b: Models from OYO Refraction Data

Observations: —— mean ····· 1 std deviation Models: ⊡ - ⊡ initial ⊖ - ⊖ final

Vp/Vs - P to S velocity ratio; Br,Bs - rock, soil damping

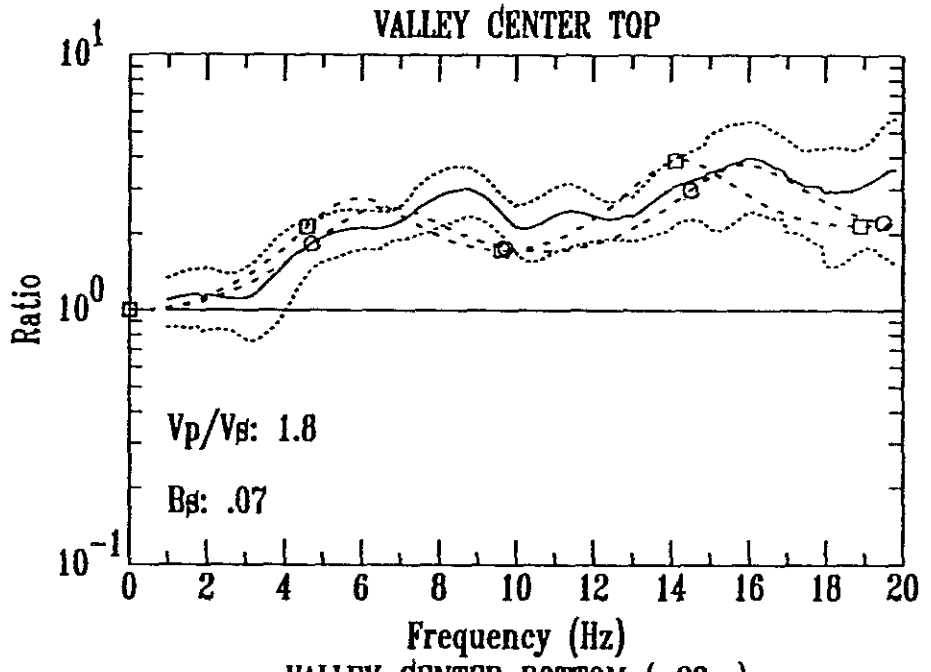

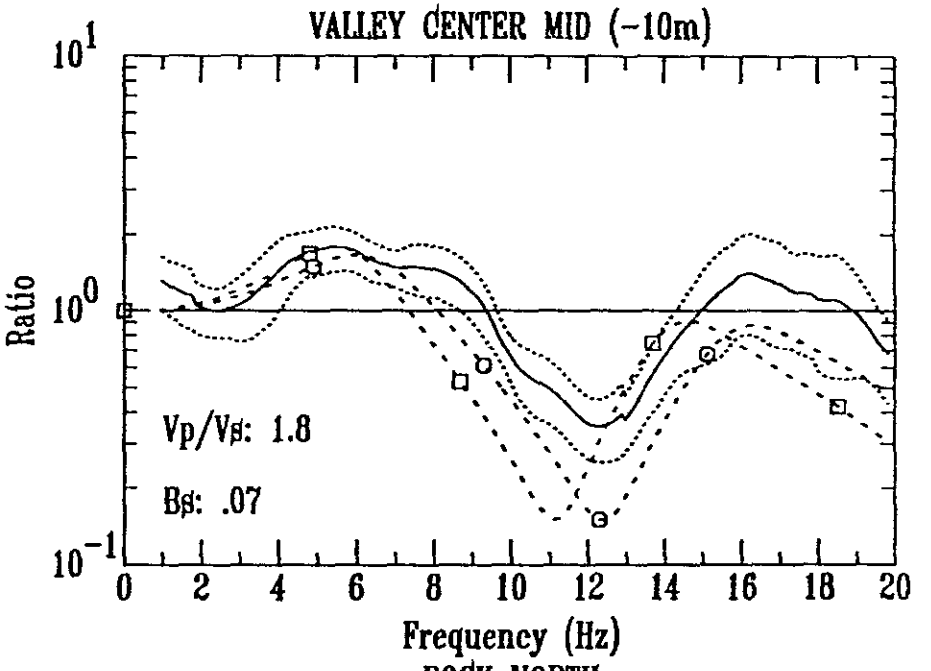

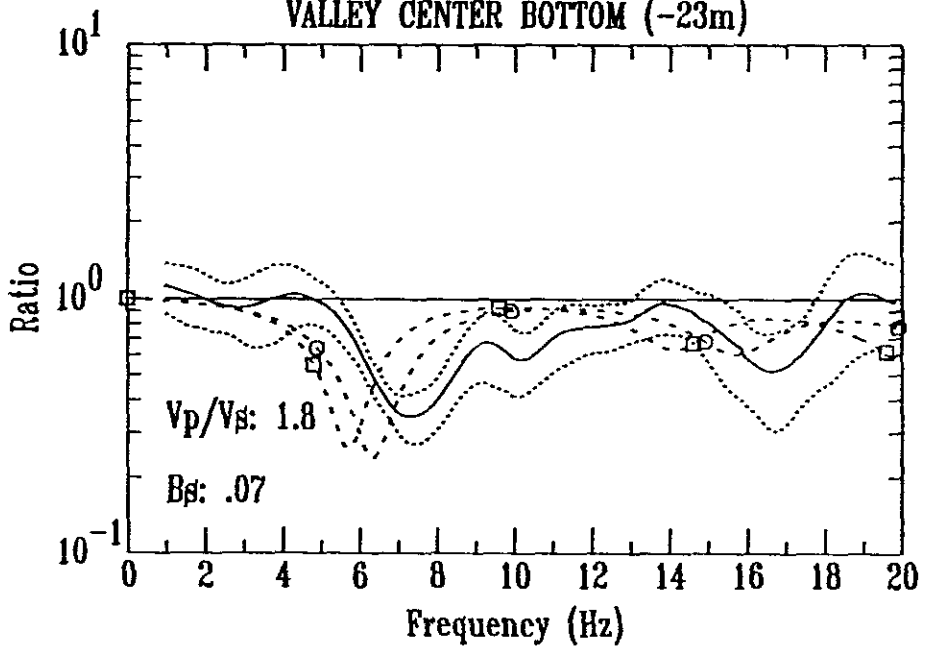

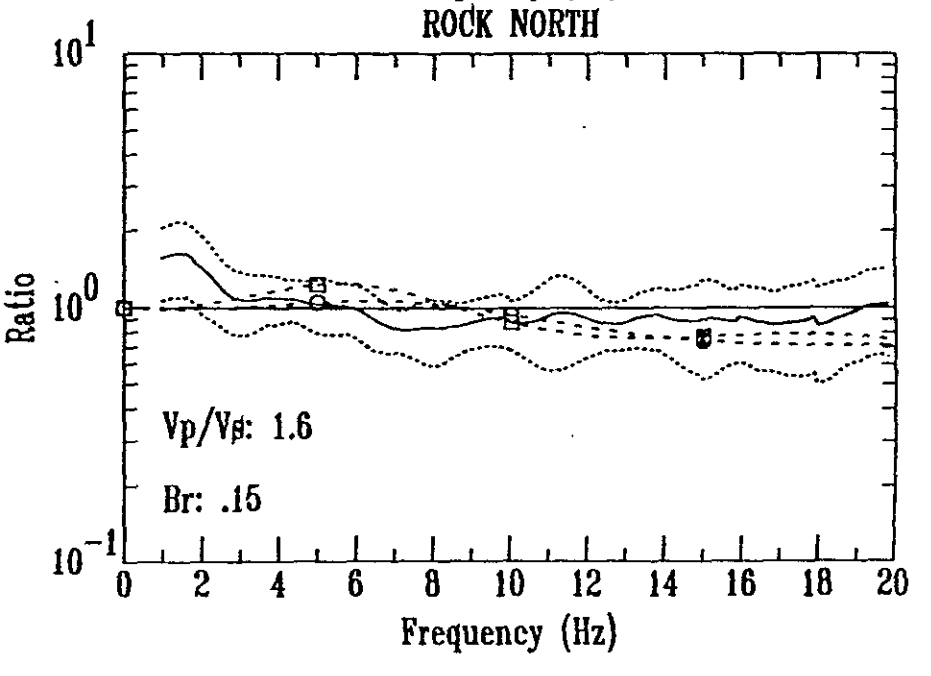

North site to 1.8 for the Valley Center site. Damping values (Br and Bs) are the same as for the final models based on downhole measurements (Figure 10).

Figure 15 shows the initial and final model results for the DMG P-wave refraction profile. The initial models do not match the observed mean spectral ratios. Final models used the same Vp/Vs ratios and damping values as the final OYO refraction profile models.

Final models is Figures 14 and 15 do not fit the observed means spectral ratios as well as the final models in Figure 10. The location and spacing of resonant peaks in the frequency domain from the P-velocity structure are not compatible with the observations, even when converted to equivalent S-velocity structure. **This suggests that site S-wave transfer functions can not be easily estimated from P-wave refraction profiles. It is not known whether S-wave refraction profiles would provide better results than P-wave refraction profiles at Turkey Flat.**

Modeling using the Standard Geotechnical Model

Velocity structure

Table 4 lists the S-wave velocity structure taken from the

Figure 15a: Models from DMG Refraction Data

Observations: —— mean ····· 1 std deviation Models: □ - □ initial ○ - ○ final

Vp/Vs - P to S velocity ratio; Br,Bs - rock, soil damping

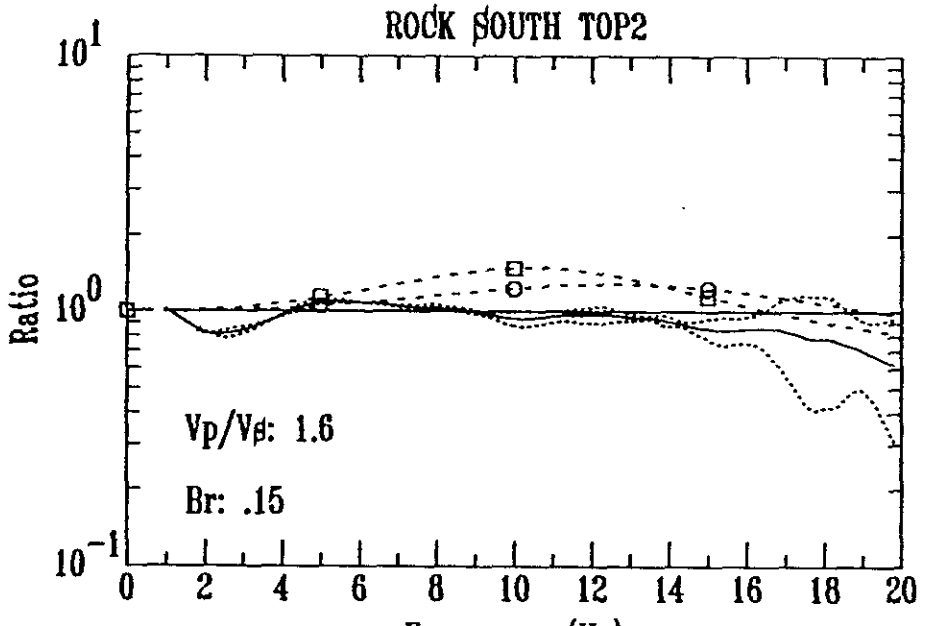

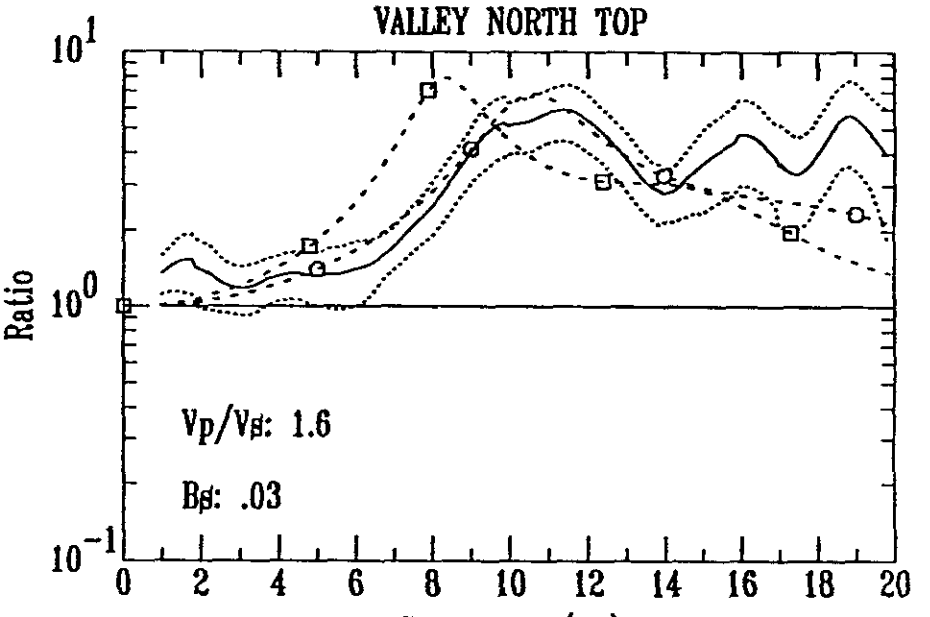

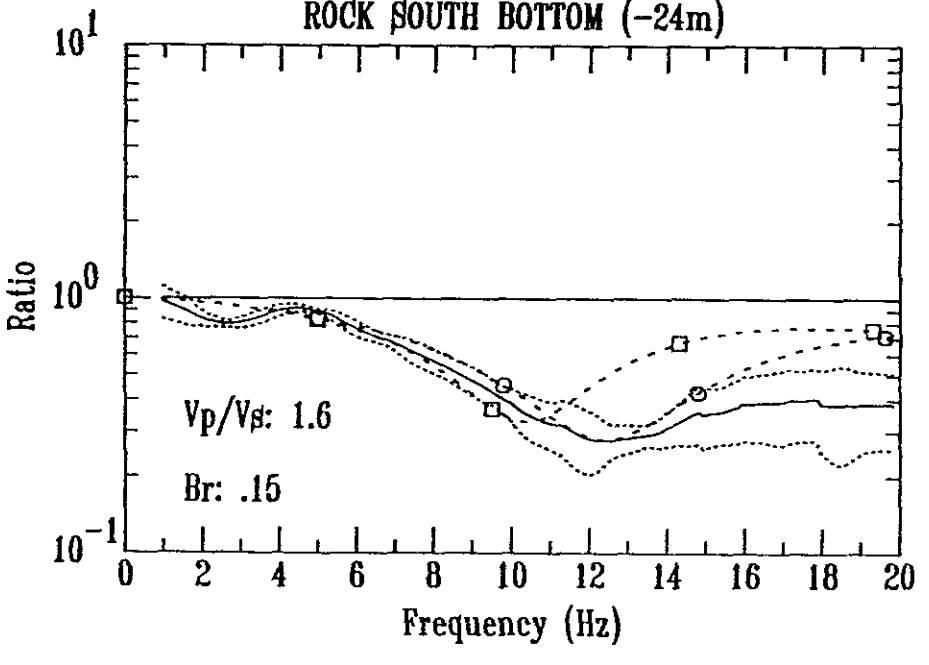

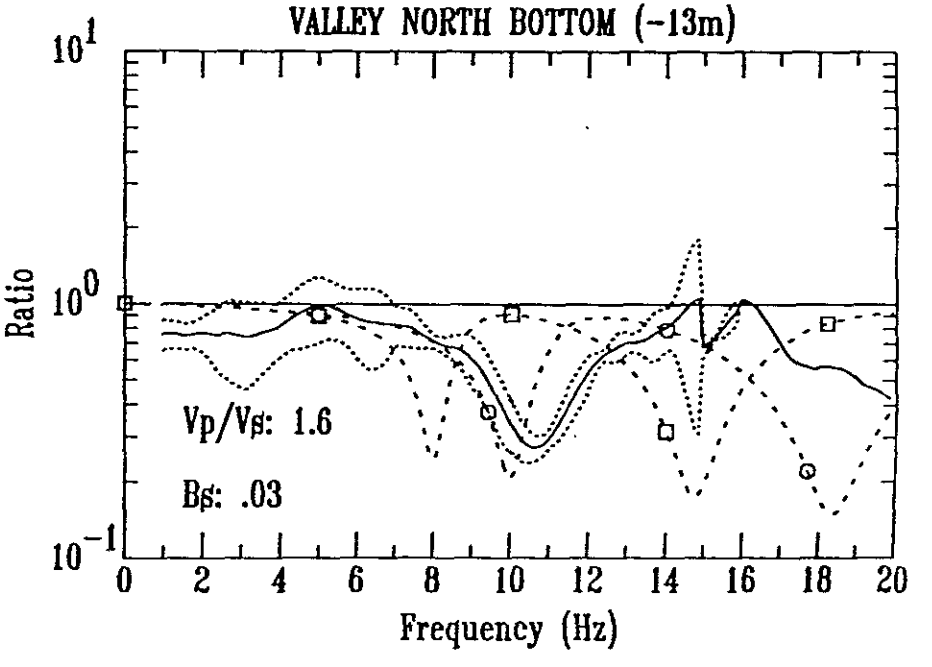

Figure 15b: Models from DMG Refraction Data

Observations: —— mean ····· 1 std deviation Models: □ - □ initial ○ - ○ final

Vp/Vβ - P to β velocity ratio; Br,Bβ - rock, soil damping

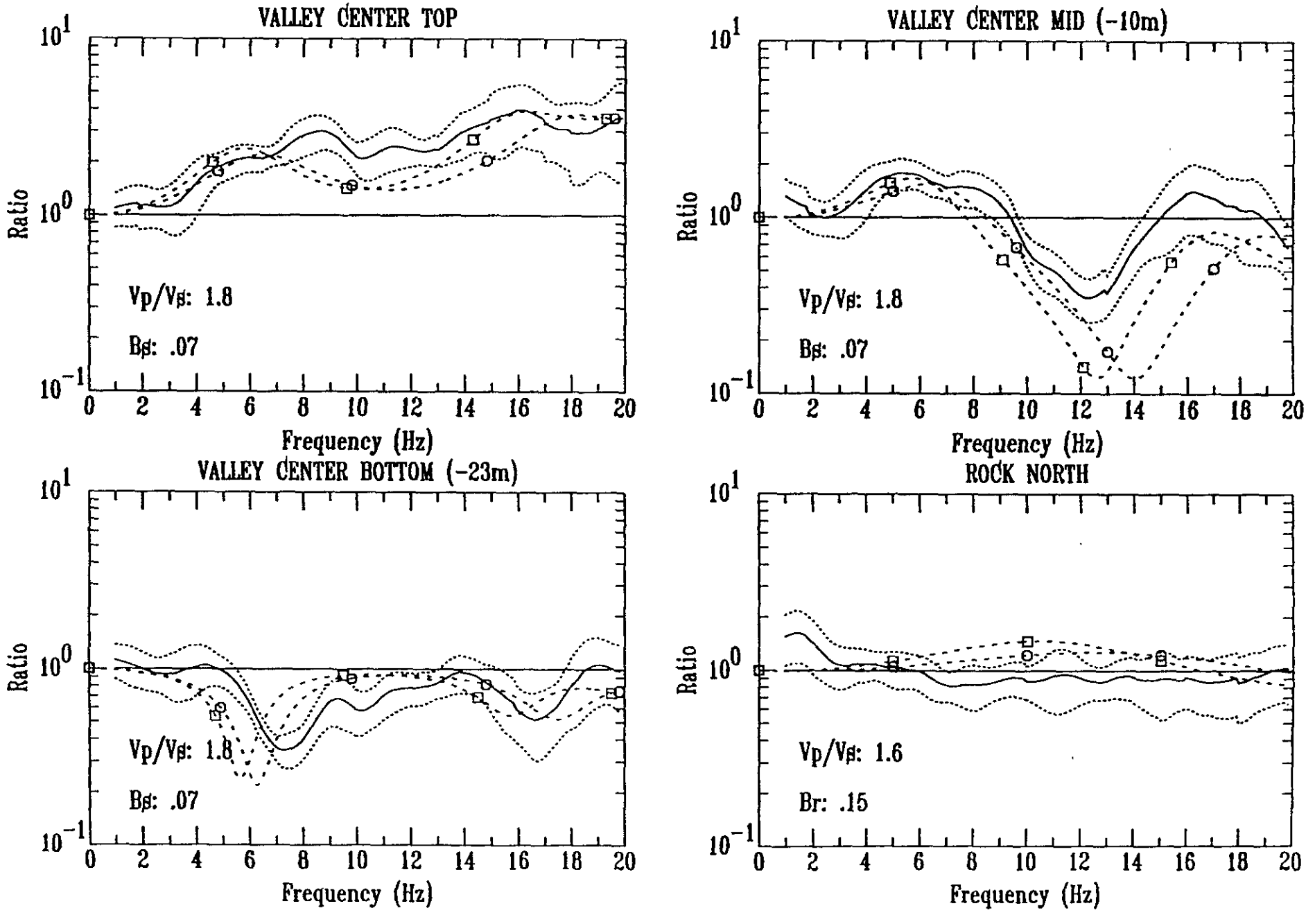

Standard Geotechnical Model for Turkey Flat. Real (1988) describes how this consensus model was derived from geotechnical measurements at Turkey Flat. Densities in Table 4 were taken from the Standard Geotechnical Model listed in Appendix D of Real and Cramer (1989). Final models have been obtained by adjusting S-velocities by a uniform percentage change in velocity to fit resonant peak frequencies and by adjusting damping values to fit amplitudes of the observed mean spectral ratios.

Initial and final models

Figure 16 shows the initial and final model results using the Standard Geotechnical Model for Turkey Flat. The initial models used damping values of .01 for rock and .015 for soil. Note that in Figure 16, initial models overestimate the amplitudes of resonant peaks, except at the surface sensor at Valley North. Locations of initial model resonant peaks in the frequency domain are close to observed resonant peaks except at the downhole sensor at Rock South. Final models in Figure 16 have the same damping values and percentage changes in S-velocity as the final models based on downhole measurements (Figure 10).

The final models shown in Figure 16 are almost as good in matching the observed mean spectral ratios as the final

Table 4

S-wave Velocity Structures from Standard Geotechnical Model

Layer no	Thickness m	Density g/cc	Velocity m/s
Rock South:			
1	2.4	2.10	825.
2		2.20	1340.
Valley Center:			
1	2.4	1.50	135.
2	5.2	1.80	460.
3	13.7	1.90	610.
4	-	2.20	1340.
Valley North:			
1	2.1	1.55	150.
2	3.4	1.75	275.
3	5.5	1.90	610.
4	-	2.20	1340.

Figure 16a: Models from Standard Geotechnical Model

Observations: —— mean ····· 1 std deviation Models: □ - □ initial ○ - ○ final

Vs - β-wave velocity change; Br,Bs - rock, soil damping

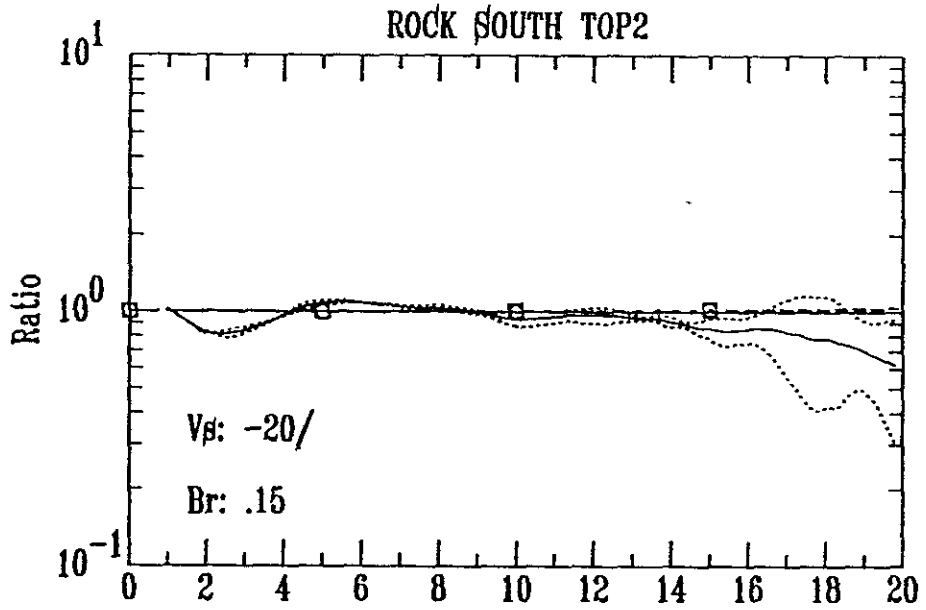

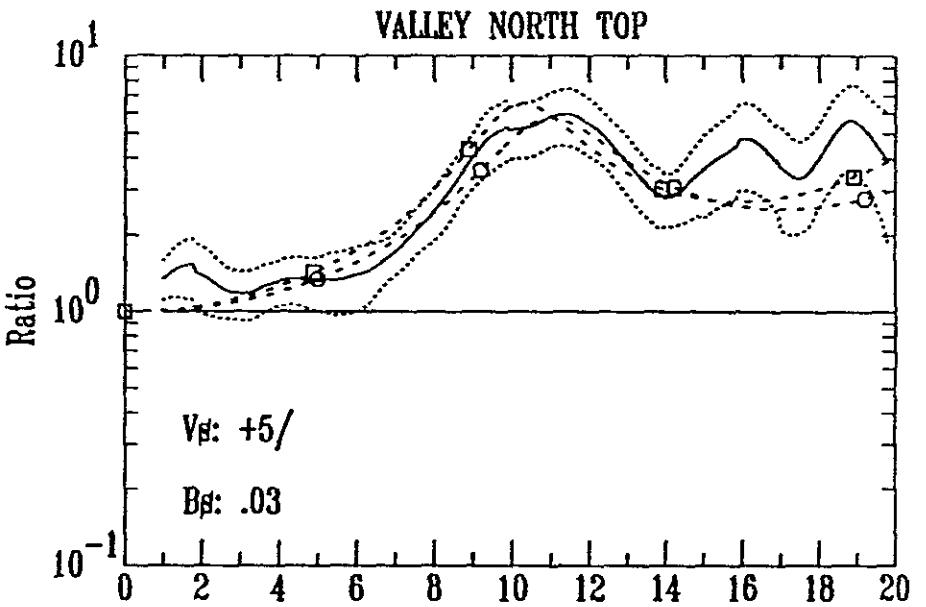

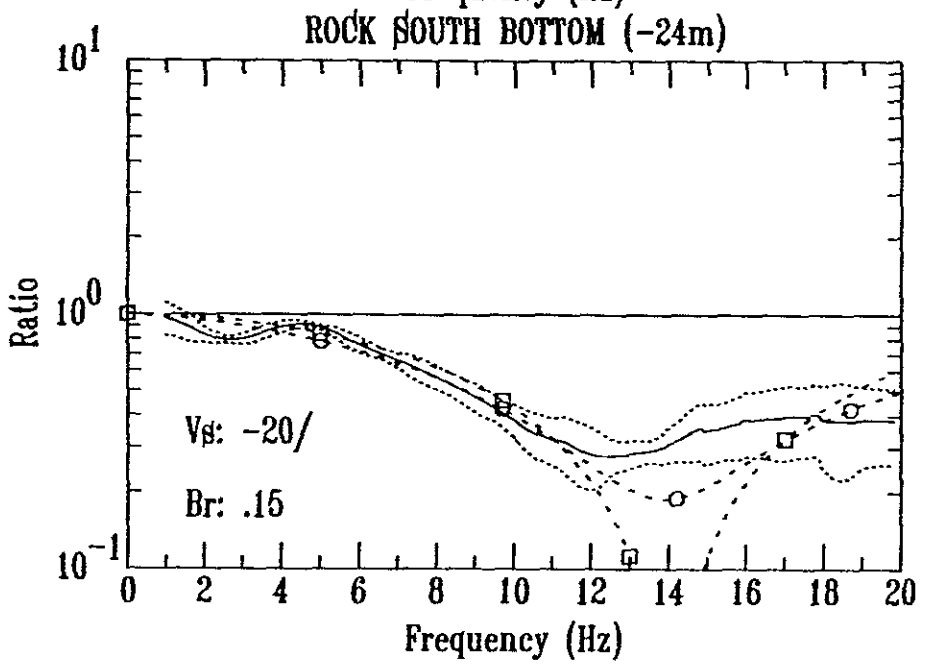

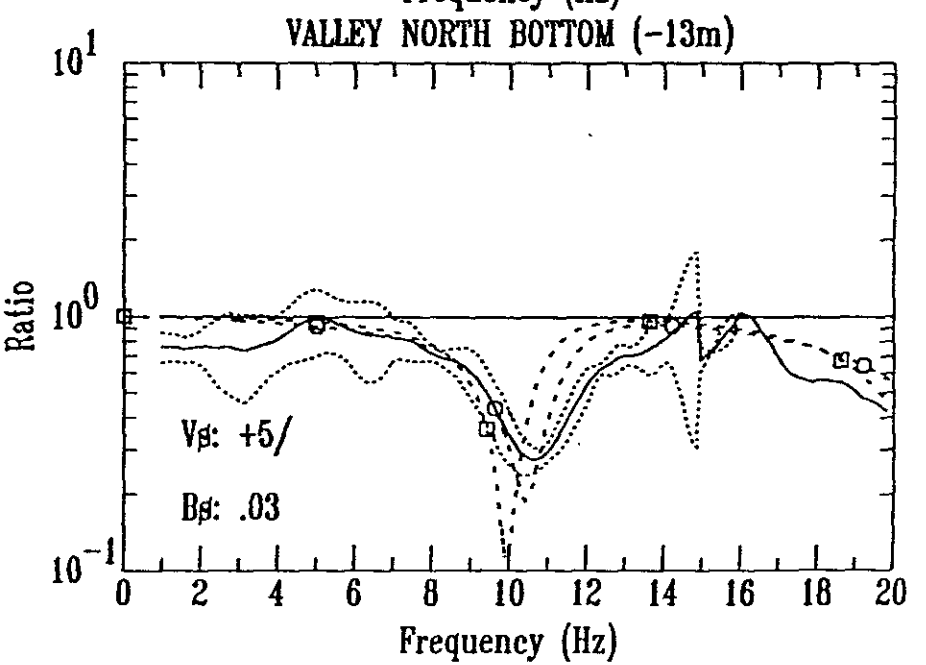

Figure 16b: Models from Standard Geotechnical Model

Observations: —— mean ····· 1 std deviation Models: □ - □ initial ○ - ○ final

Vβ - β-wave velocity change; Br,Bβ - rock, soil damping

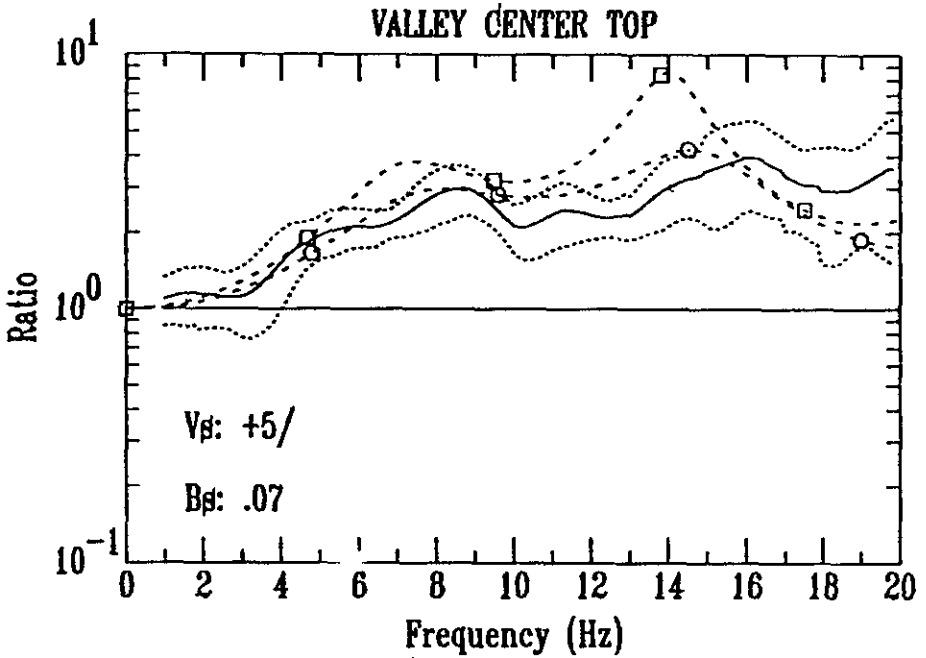

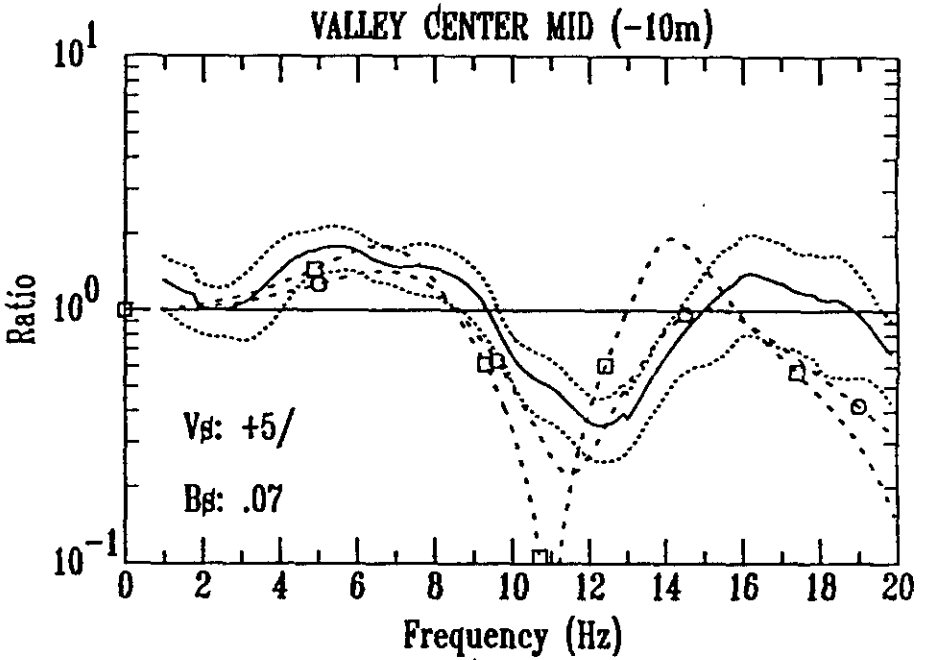

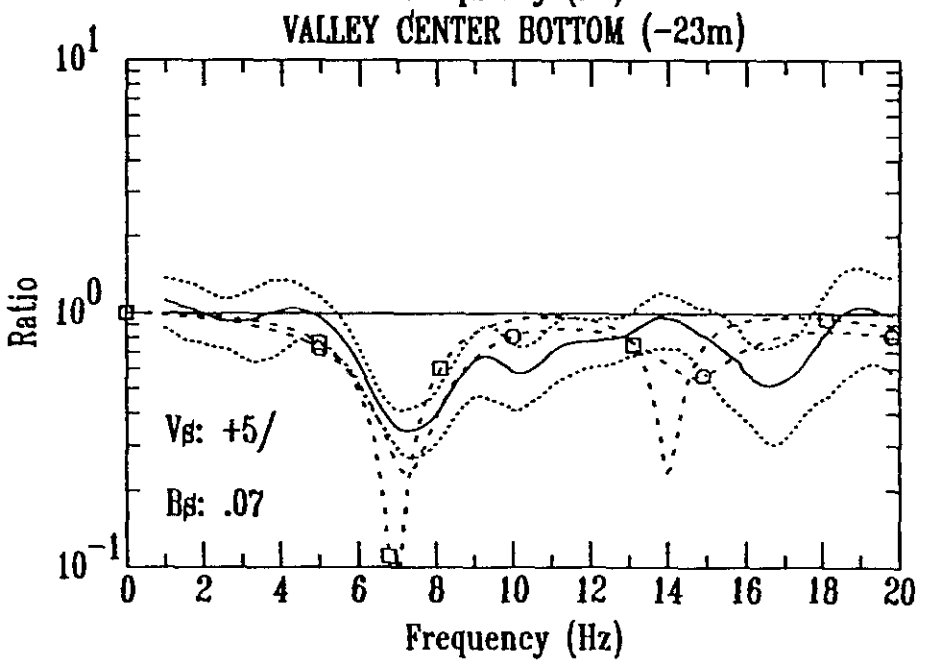

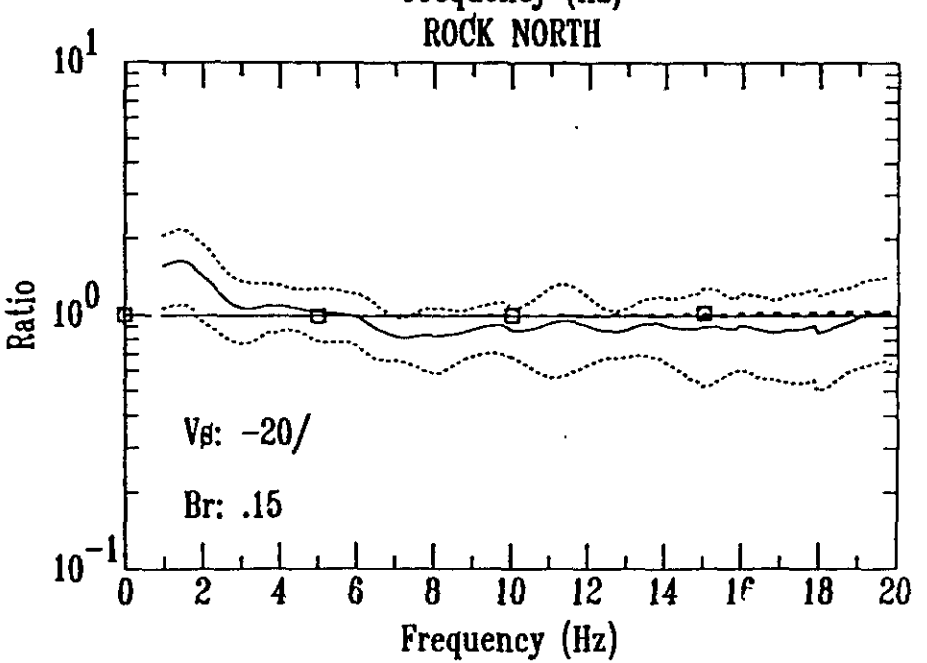

models for downhole measurements in Figure 10. The glaring exception is for the Rock South bottom-hole response (Figure 16a, bottom left plot). Because the Standard Geotechnical Model has a very thin, weathered rock layer at the surface of the Rock South site, velocity and damping can not be adjusted by any reasonable amount to obtain an improved fit to the observed mean spectral ratios. **The slower velocity surface layer for the Rock South site should be thickened in order to obtain a better match to the downhole mean spectral ratio at that site.**

WEAK-MOTION TEST EVENT

This part of the report focuses on the character of the Weak-Motion Test Event (WMTE) in order to address the question of whether or not it is an unusual event. First a general description of the WMTE is provided. Then there is a discussion of windowing effects on Fourier spectral ratios and response spectra, followed by a review of the amount of scatter that can be expected in Fourier spectral ratios. Finally, record sections for P- and S-waves are examined for propagation effects, and waveform covariance/coherence is reviewed.

The following comparison provides the motivation for this review of the WMTE. Figure 17 compares the east and north component Fourier spectral ratio for the WMTE with the mean and one standard deviation (sd) spectral ratios for all 33 weak-motion events. Clearly there is considerable variation of the WMTE spectral ratios from the mean spectral ratios as well as variation between the east on north component spectral ratios for the WMTE. This raises the question of whether there is anything unusual about the WMTE that might have contributed to these variations.

Figure 17a: Weak-Motion Test Event Spectral Ratios:
Spectral Ratios for Rock South Bottom and Valley Center Mid

— Mean and 1 std deviation; Test Event: - - - East Component; ····· North Component

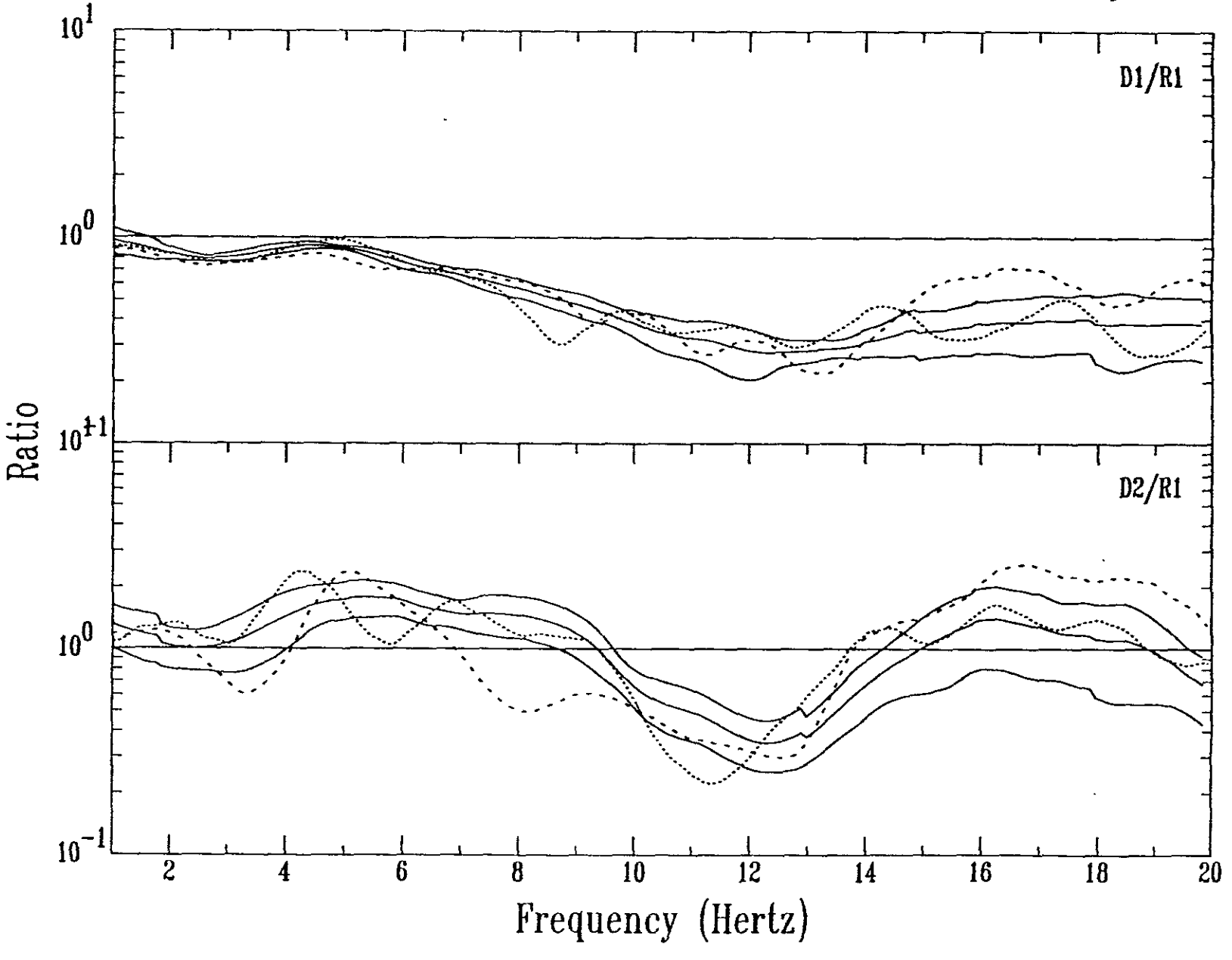

Figure 17b: Weak-Motion Test Event Spectral Ratios:
Spectral Ratios for Valley Center Top and Bottom

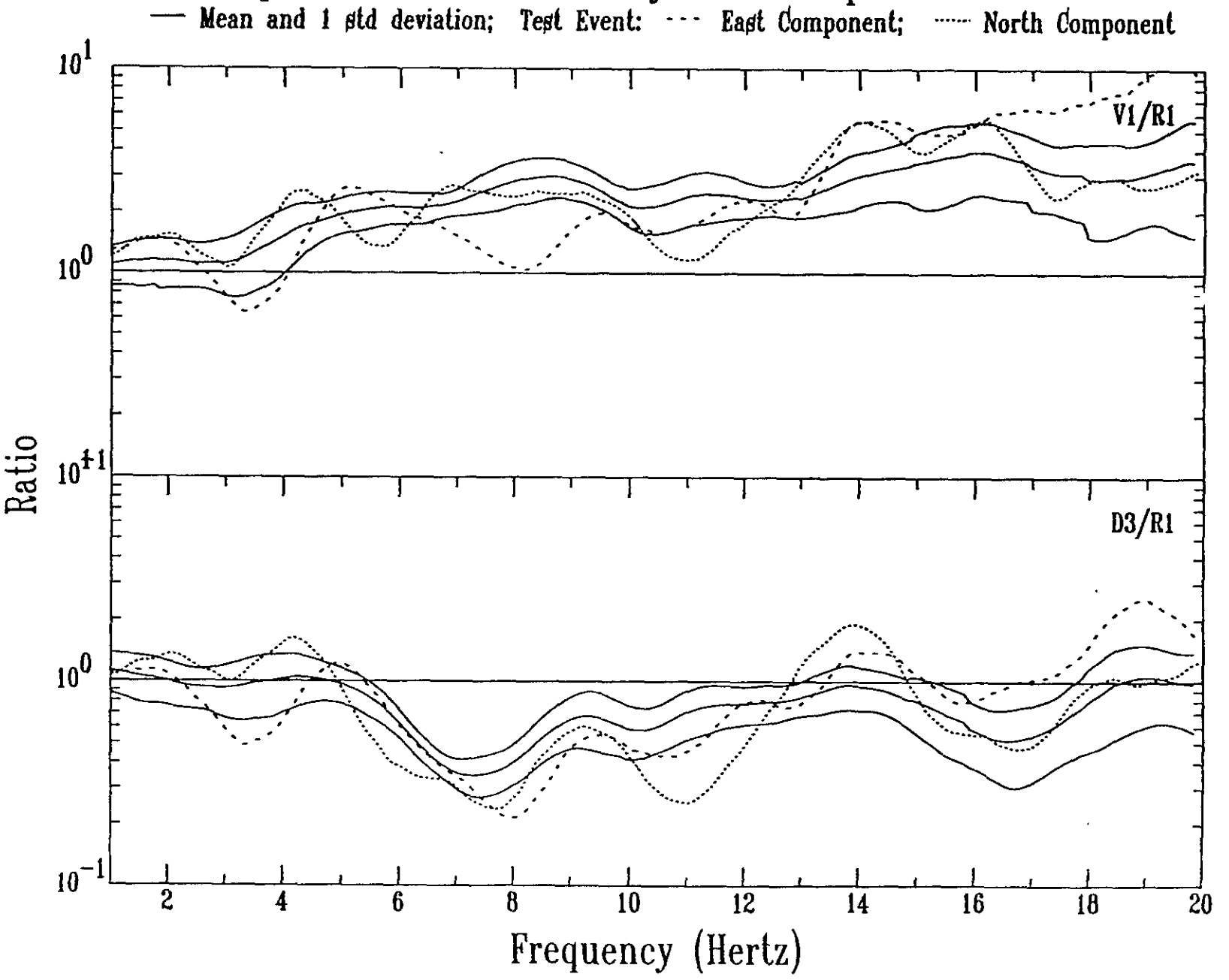

Figure 17c: Weak-Motion Test Event Spectral Ratios:
Spectral Ratios for Valley North and Rock North

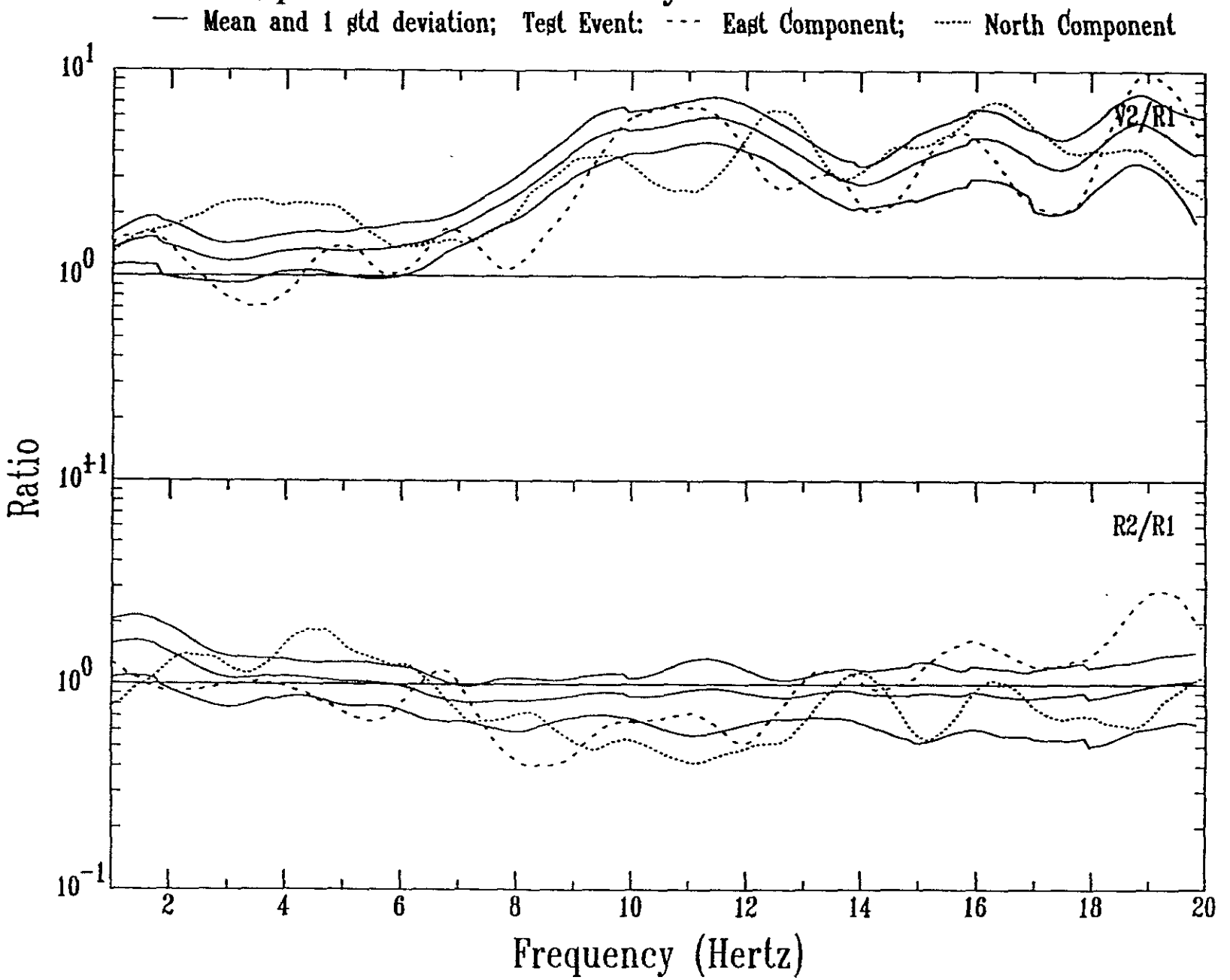

Figure 17d: Weak-Motion Test Event Spectral Ratios:
Spectral Ratios for Valley Center Top and Mid

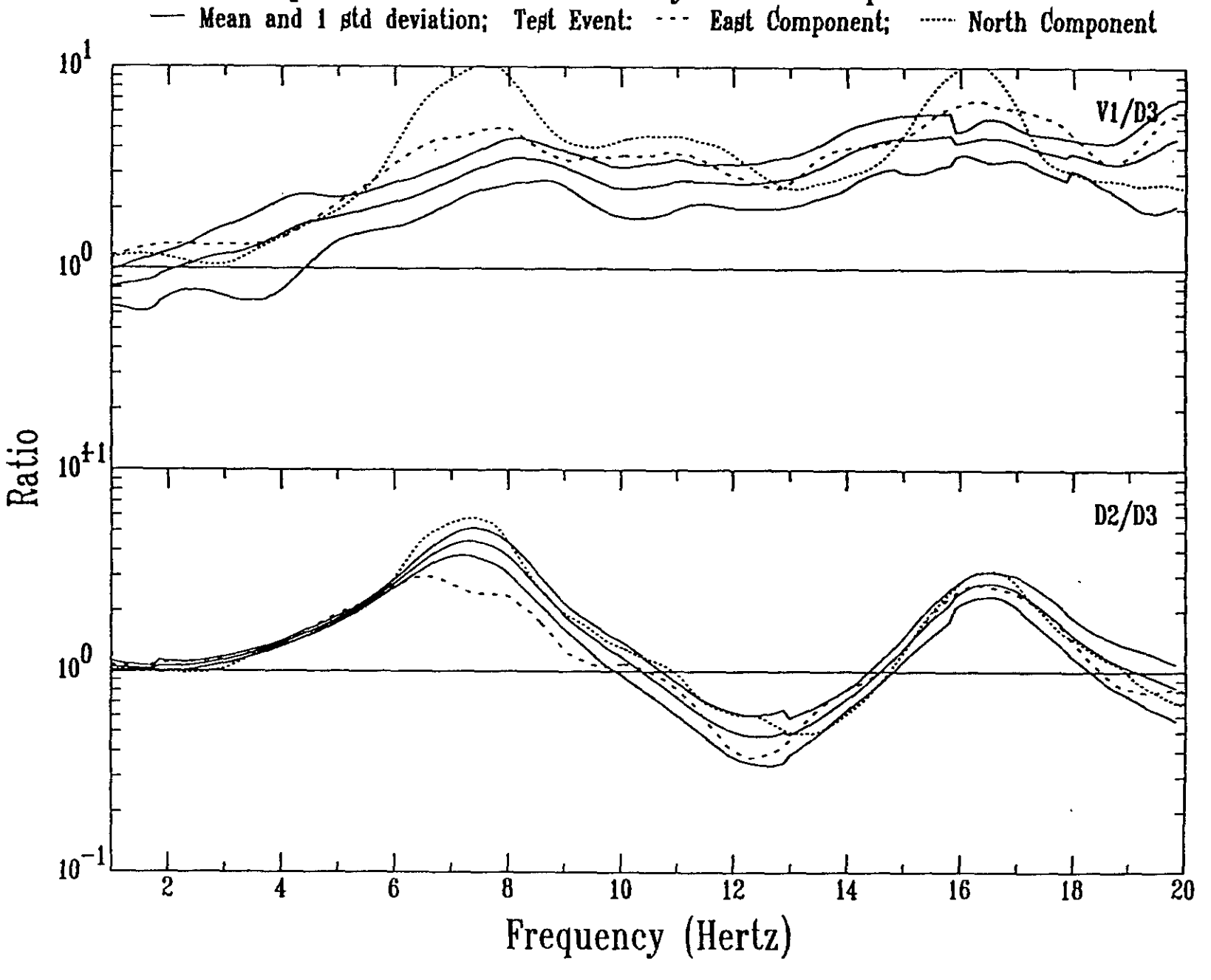

General description

A general description of the WMTE is as follows: The WMTE was selected as the test event because of its high signal-to-noise ratio in the 1-20 Hz band at each of the strong-motion sensor locations (Real and Cramer, 1989, p. 36). Additionally, the horizontal spectral ratios for the WMTE seem typical for the weak-motion events recorded. The WMTE is a shallow M_L = 2.0 earthquake located in the Coalinga area (36.183^{o}N, 120.329^{o}W, 4 km deep according to the USGS). The event occurred 33 km from the center of the recording array. No focal mechanism has been published for this event, but source effects like those observed by Jarpe, et al. (1988) should not be observed at the Turkey Flat Array because of the very small aperture of the array (2 km) compared to the epicentral distance to the source (33 km). The azimuth from the array to the source is 5^{o} and the P-wave first motion pulse at all surface sensors of the weak-motion array is between 185^{o} and 195^{o} in azimuth (Real and Cramer, 1989), essentially along the propagation azimuth.

Other weak-motion events recorded at Turkey Flat have similar magnitudes, epicentral distances, azimuths, and focal depths. Referring back to Figure 5b and Table 1, other weak-motion event magnitudes range between M_L 1.0 and M_L 5.0, with most being between M_L 1.3 and M_L 3.0. Epicentral distances range

between 0 and 300 km, with half falling between 15 and 50 km. Azimuths to source range from -90° to 180° from North, with most falling between -75° to 76° from North. Focal depths range between 0 and 15 km, with most being between 0 and 10 km. Median values for other weak-motion events are M_L 2.5 for magnitude, 42 km for epicentral distance, 8° from North for azimuth, and 5 km for focal depth. **Compared with other weak-motion events recorded by the Turkey Flat site-specific array, there is nothing unusual about the magnitude (M_L 2.0), epicentral distance (33 km), azimuth (5° from North), or depth (4 km) of the WMTE.**

Spectral ratios

Spectral ratios can show variations due to the choice of time domain window, improper instrumental response corrections, method related random variations from event to event, and systematic variations between horizontal components from effects such as two-dimensional response within a valley. The latter two, in particular, can cause spectral ratio variations larger than a factor of two. For the Turkey Flat WMTE, each of these four sources of spectral ratio variation between horizontal components is examined below.

Sensitivity of Fourier spectral ratios to the choice of time

domain window might be a cause of some of the observed variation in Fourier spectral ratios between components at the same triaxial seismometer. Cramer and Real (1990) showed that time domain window size variation for the same waveform can cause variation in Fourier spectral ratio by up to a factor of two, but no significant variation in response spectra. Figures 18 and 19 show the effect on Fourier spectral ratio and response spectrum of moving the same size time domain window (8 sec) relative to the S-wave onset. Results are shown for time domain windows starting .1, .25, .5, and 1 second before the S-wave onset. Note that moving a fixed-sized time domain window by up to one second relative to the S-wave onset has essentially no effect on the computed Fourier spectral ratio or response spectrum. **Thus, because the same sized time domain window (8 sec.) was used throughout this study, the window starting time was the same on both the east and north components of the same event record, and window starting time was within one second of the S-wave onset for all events, it seems unlikely that the observed variations in the Fourier spectral ratios between components for the WMTE (Figure 17) are due to the sensitivity of Fourier spectral ratios to the time domain window used in this study.**

Instrument response corrections are not a large enough source of spectral ratio scatter to cause the observed variations

Figure 18: Standard Fourier Spectral Ratio Plot:
Spectral Ratio V1/R1 for Four 8-Sec Window Lengths

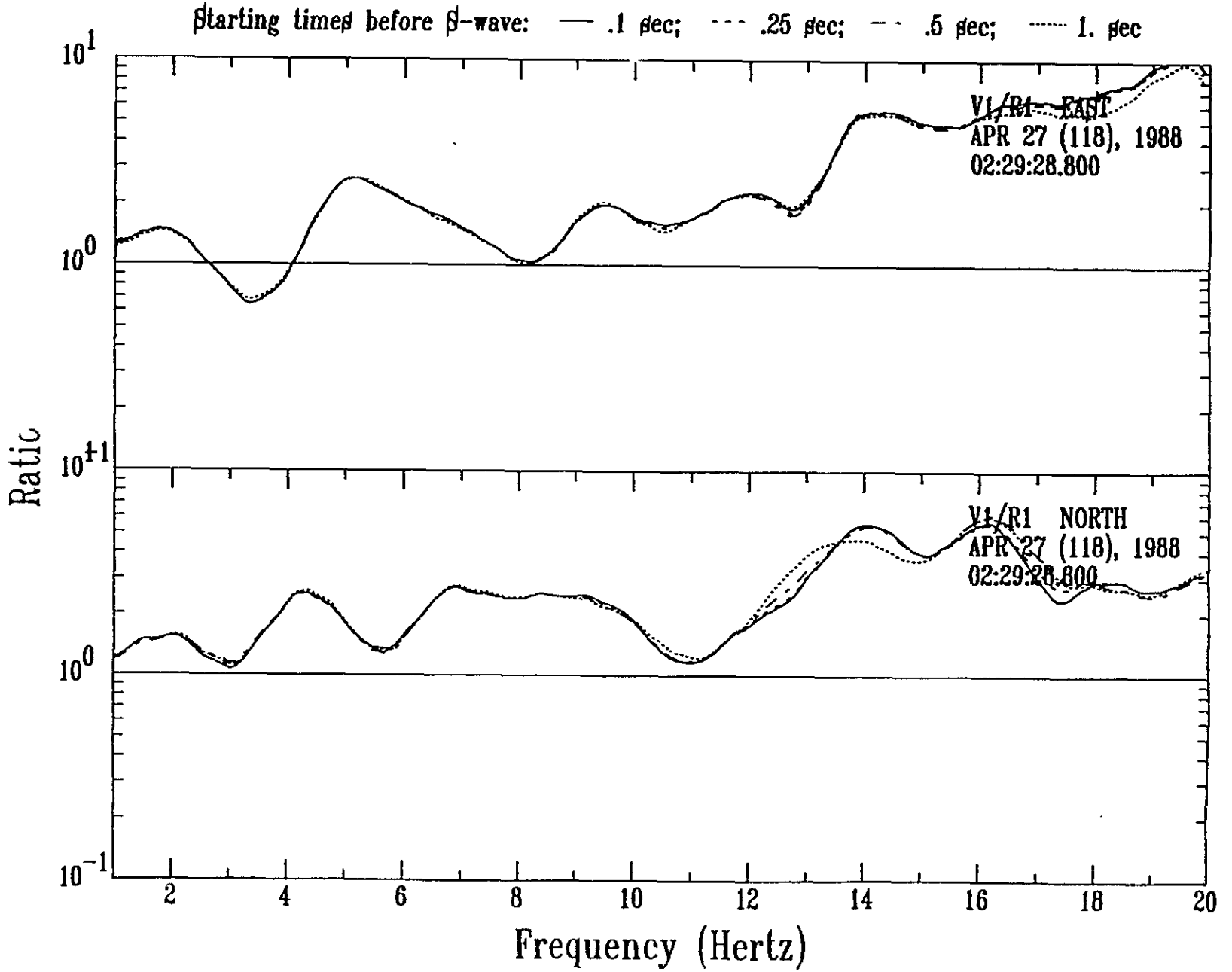

Figure 19: Standard Response Spectra:
Station V1 Valley Center Surface for Four 8-sec Window Lengths
Starting times before S-wave: — .1 sec; - - - .25 sec; — — .5 sec; ····· 1. sec

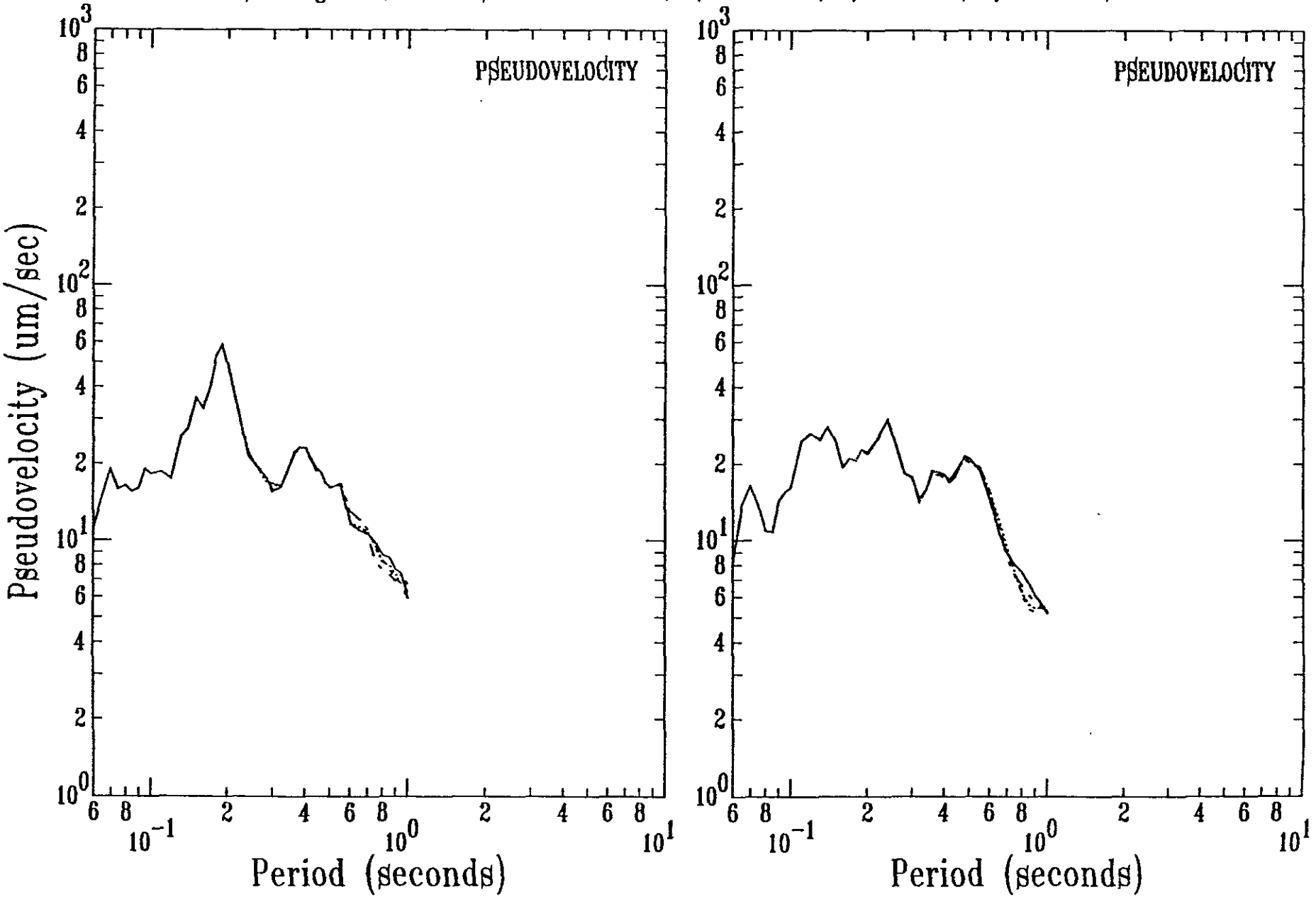

between horizontal components seen in Figure 17. Real and Cramer (1989, Figure 14) show that instrumentation scatter for the site-specific study of this report is 10-20% (factor of 1.1 to 1.2). This is much smaller than the observed factor of two (or more) variation between components of the WMTE in Figure 17.

What is the expected Fourier spectral ratio scatter between horizontal components for the same event? Jarpe, et al. (1988, Figure 4c) show that Fourier spectral ratio scatter between east and north components can be as large as a factor of four for events recorded in the Coalinga area. For Turkey Flat, Figure 20 presents the variation in Fourier spectral ratio between horizontal components for each event at each weak-motion sensor. This is shown as the ratio of the two horizontal component Fourier spectral ratios (i.e., E/N where E and N are the Fourier spectral ratio for the East and North component, respectively). (Data from some events are valid over a frequency band narrower than 1-20 Hz and hence some ratios in Figure 20 end in the middle of the plots.) Variations in Fourier spectral ratio between horizontal components can be up to a factor of four, occasionally higher. In Figure 20, the WMTE's ratio of horizontal spectral ratios for each sensor is indicated as the solid curve (no WMTE ratios are available for CTF1 and CTF9). **The variation in Fourier spectral ratio between horizontal components for the**

Figure 20a: Plots of Ratios of East to North Spectral Ratios for Rock South Top2 and Bottom

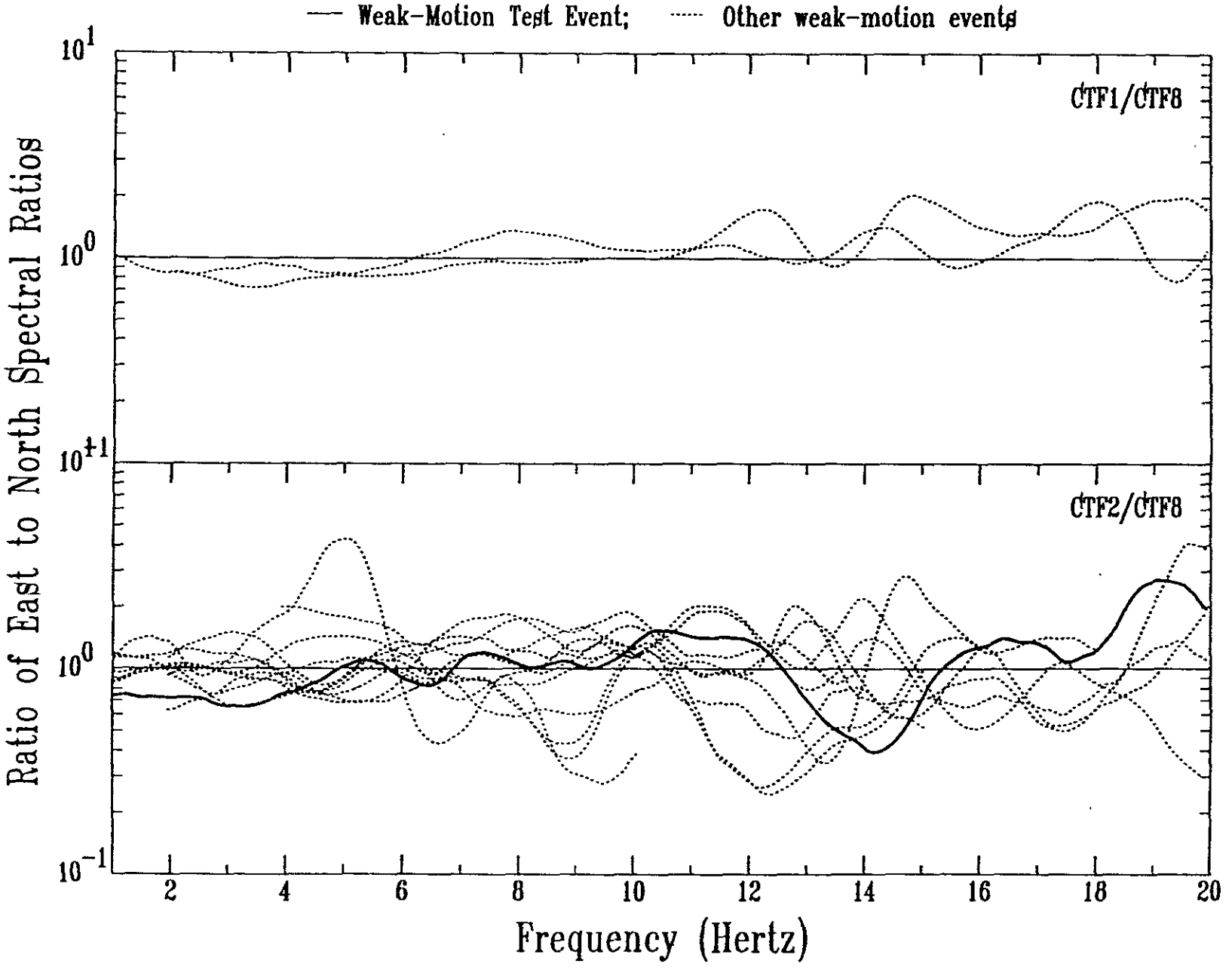

Figure 20b: Plots of Ratios of Horizontal Spectral Ratios for Valley North Top and Bottom

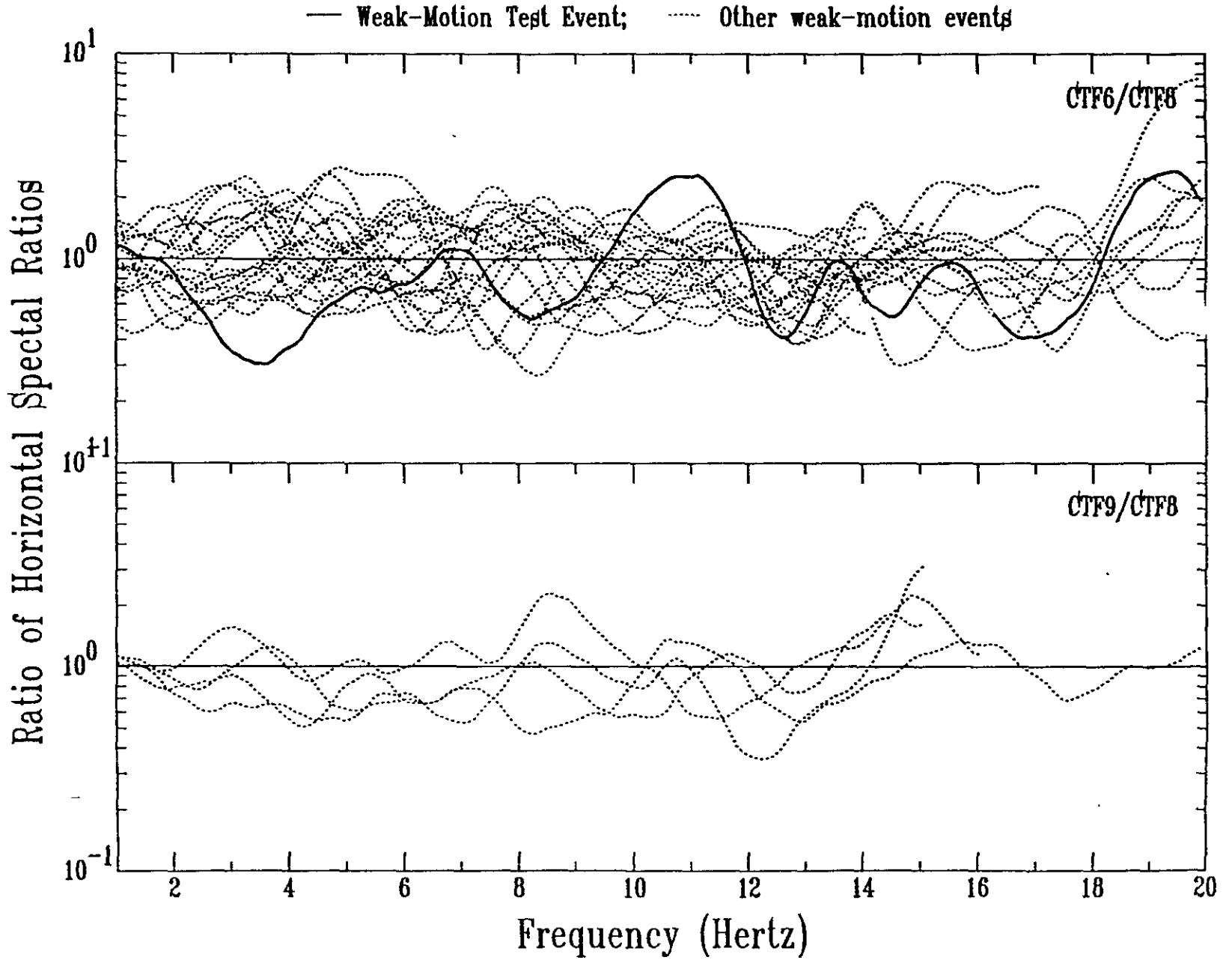

Figure 20c: Plots of Ratios of Horizontal Spectral Ratios for Valley Center Top and Bottom

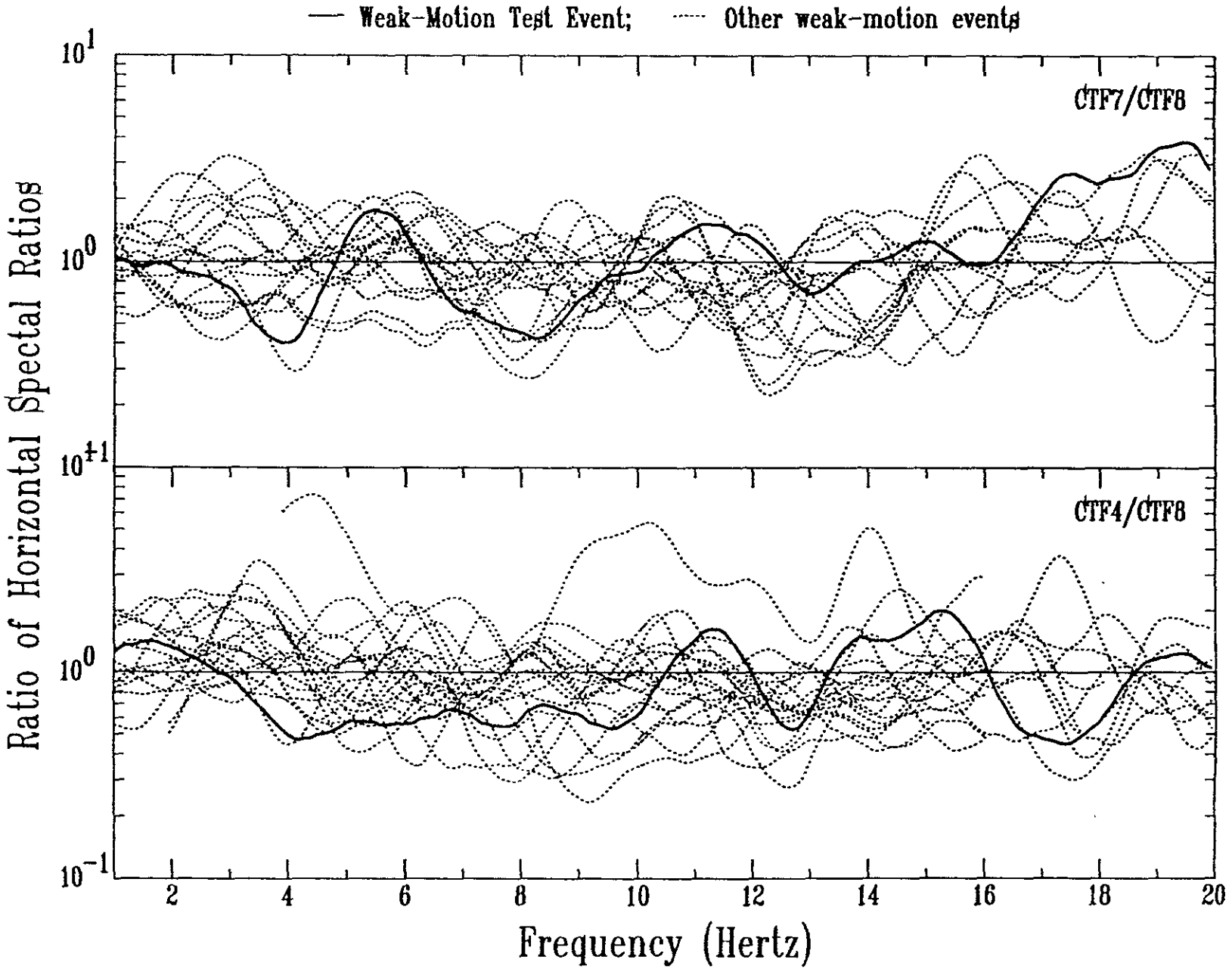

Figure 20d: Plots of Ratios of Horizontal Spectral Ratios for Valley Center Mid and Rock North

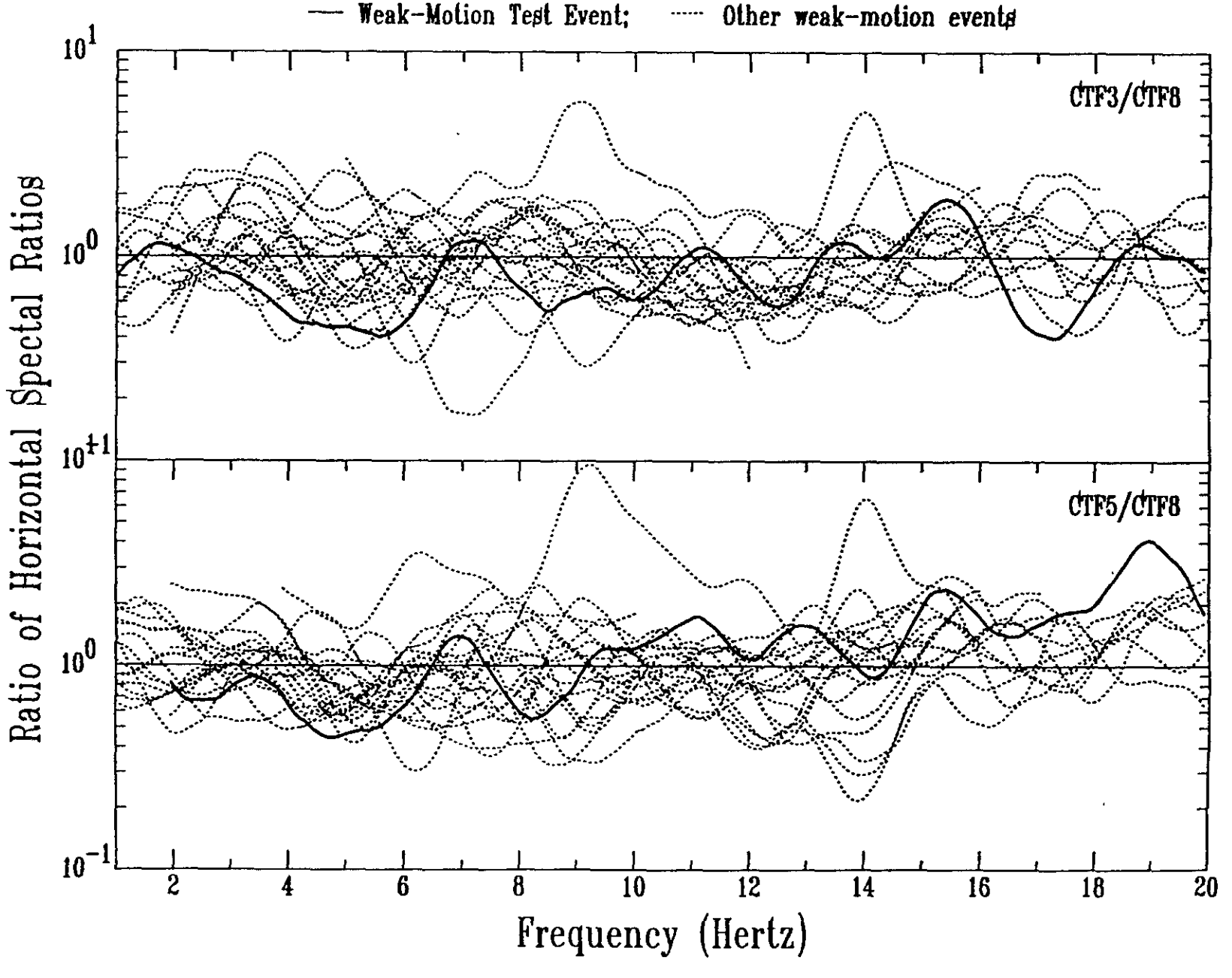

WMTE looks similar to the variation for other weak-motion events.

What about the possibility of a two-dimensional response within the valley causing systematic variations between horizontal components? The east component of the surface triaxial seismometers at each site is essentially parallel to the axis of the valley in the test area while the north component is perpendicular to the valley's axis. (Downhole orientations are less reliably known but should be the same, generally, from event to event.) An examination of Figure 20 shows only random variations between horizontal components and no systematic variations as large as a factor of two. **There is no evidence for systematic variations as large as a factor of two being caused by 2D effects in the valley's response.**

Another possible source of systematic variations between horizontal components is a difference in site response between SV and SH waves. Figure 21 presents the variation in Fourier spectral ratio between radial and transverse components for each event at the surface triaxial seismometers at Rock North, Valley North, and Valley Center sites. Similar to the presentation in Figure 20, Figure 21 shows ratios of radial to transverse component Fourier spectral ratios (i.e., R/T where R and T are the Fourier spectral ratio for the

Figure 21: Plots of Ratios of Radial to Transverse Spectral Ratios for Rock North, Valley North Top and Valley Center Top

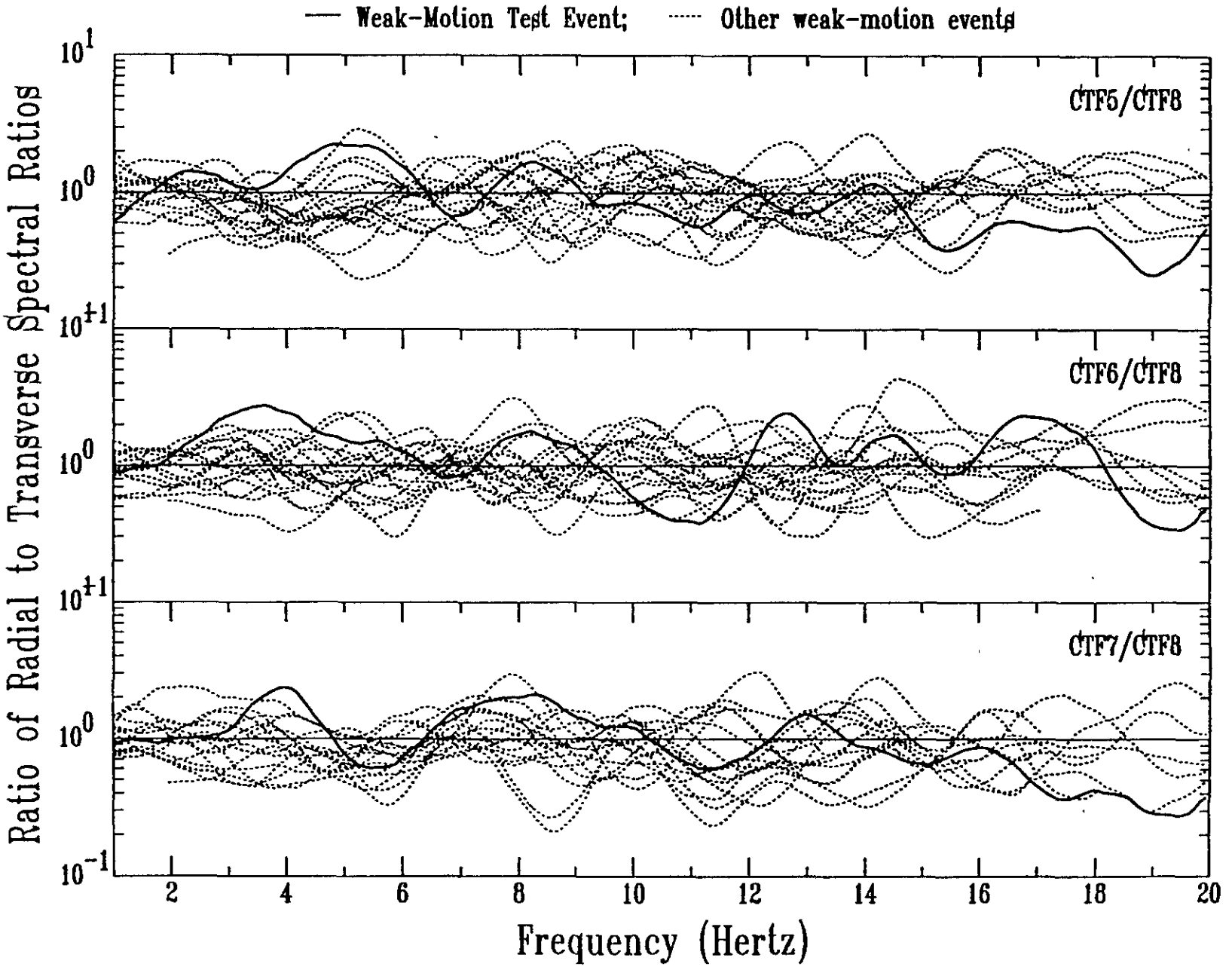

radial (SV) and transverse (SH) component, respectively). As in Figure 20, Figure 21 shows only random variations and no systematic variations as large as a factor of two. **Therefore, the variations between horizontal components in Figure 17 appear to be normal random variations that are observed in other weak-motion events recorded at Turkey Flat.**

Waveforms

Figures 22 - 24 show WMTE record sections for P, SV, and SH velocity waveforms. The WMTE occurred essentially to the north of the Turkey Flat array so that the vertical, north, and east components correspond to P, SV, and SH, respectively. Bedrock surface and downhole sensors were chosen for making these record sections, except for the CTF6 record at Valley North where there was no downhole rock record for the WMTE. The CTF6 record may be slightly delayed by .02 sec for P-waves and .04 sec. for S-waves, which are inconsequential delays for this study.

Figure 22 shows that the P-wave front for the WMTE propagates across the array with an apparent velocity near 6.0 km/sec. The line in Figure 22 labeled 6.0 k/s is a reference line with a slope equivalent to that of seismic waves propagating at 6.0 km/sec across the array along the azimuth from the source to the array (185^{o}). 6.0 km/sec is a reasonable crust-

Figure 22: P-wave Record Section

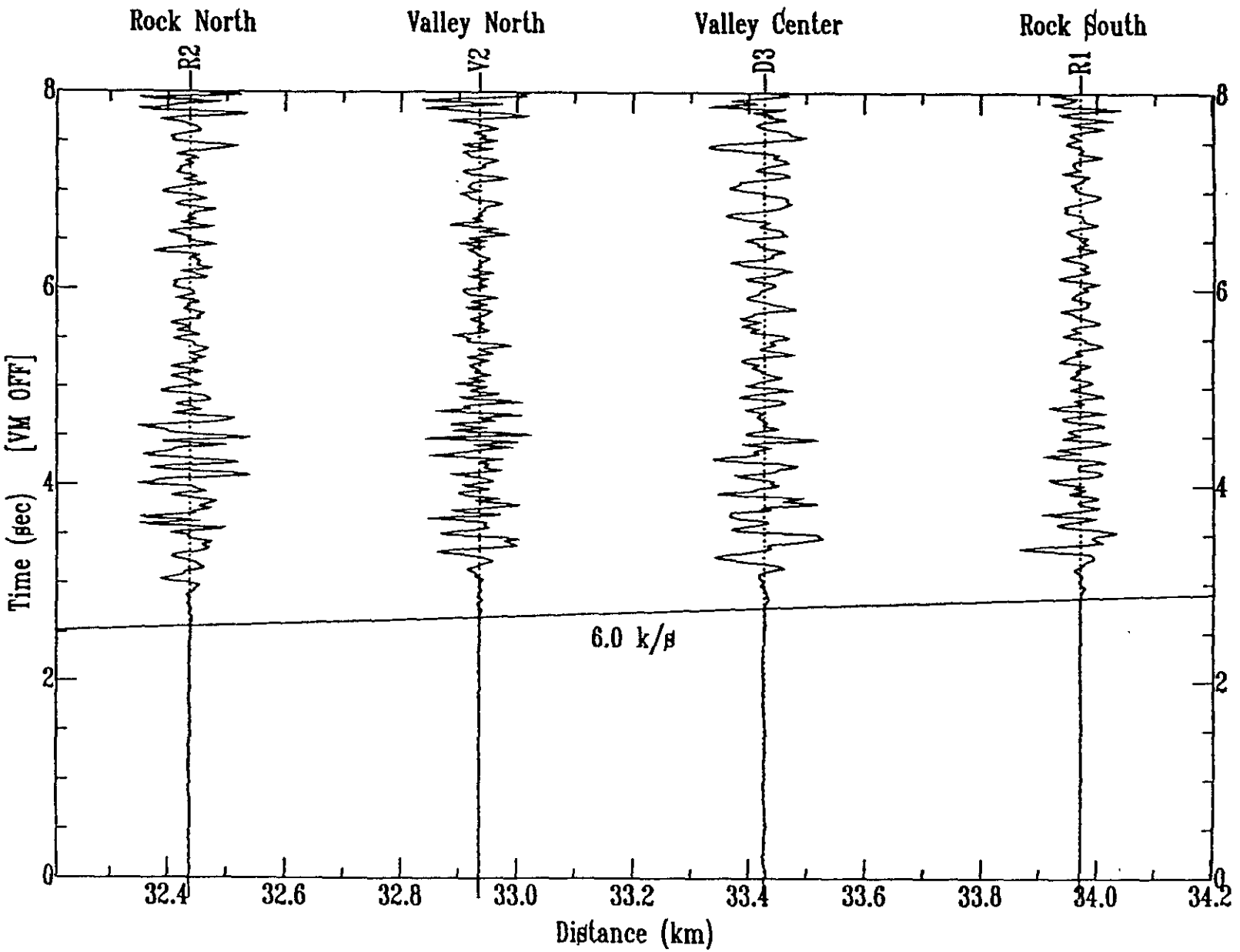

Figure 23: SV-wave Record Section

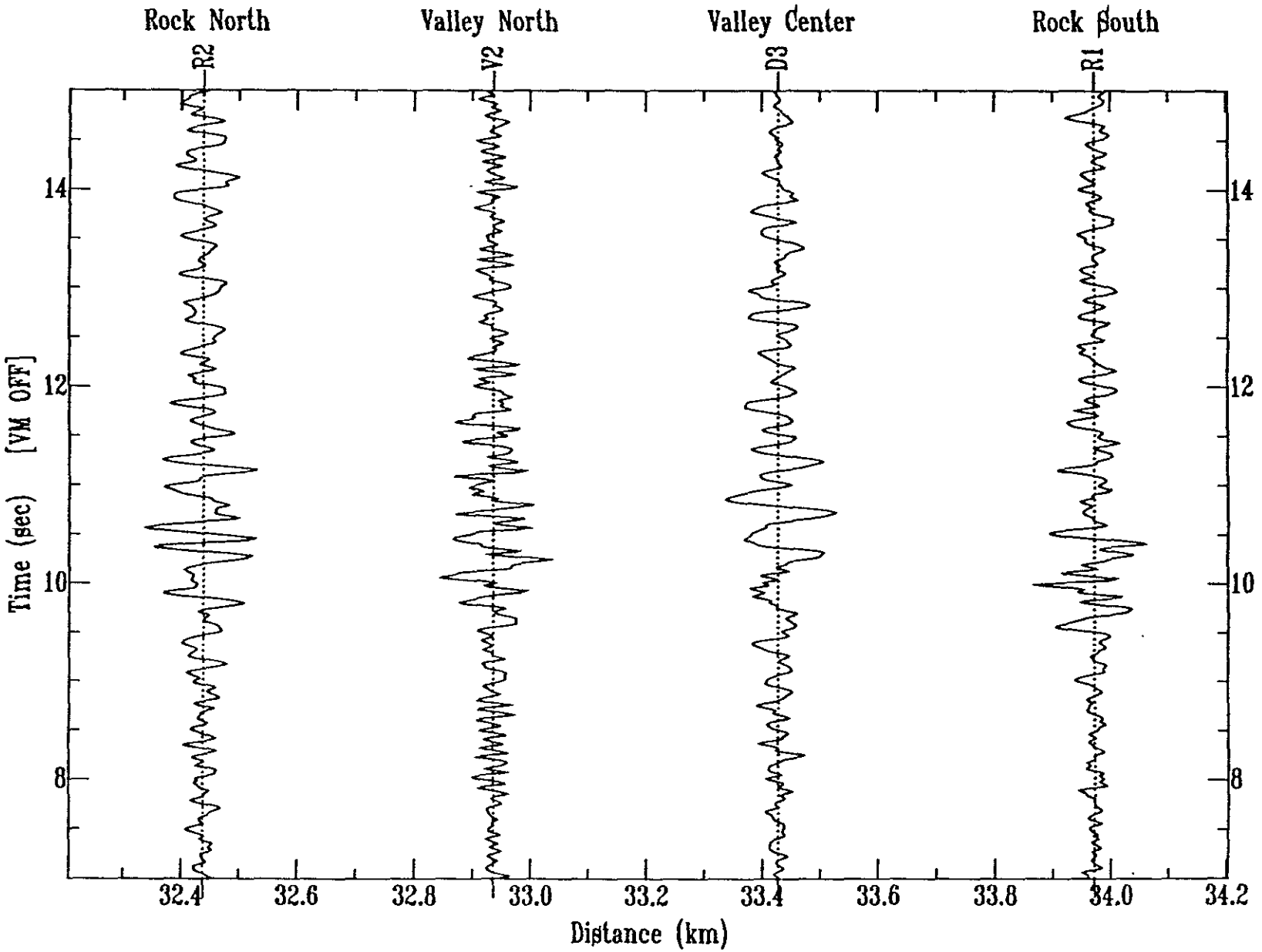

Figure 24: SH-wave Record Section

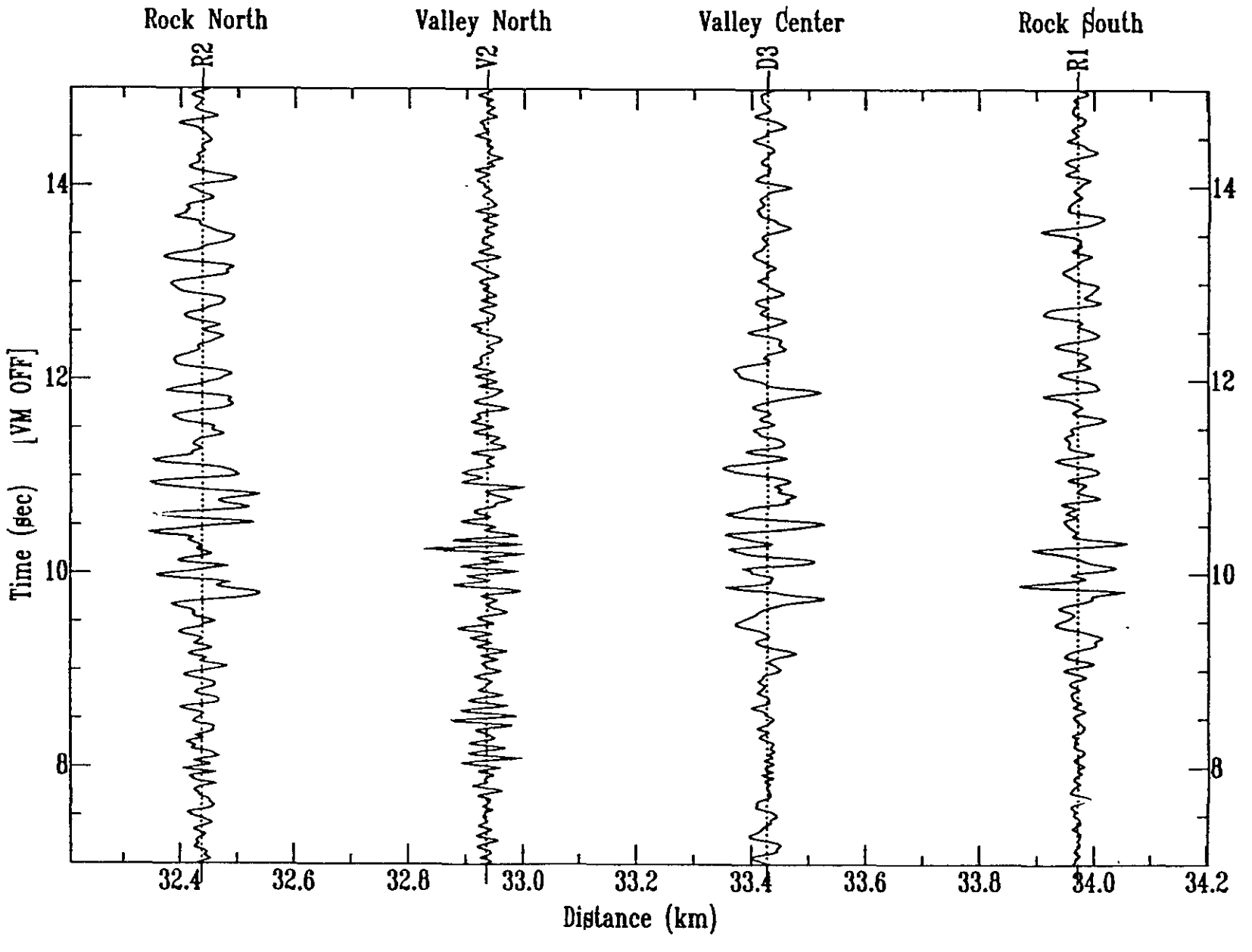

al P-wave velocity in the Central California Coast Ranges.

On the other hand, SV and SH wave fronts (Figures 23 and 24) seem to arrive simultaneously across the array, within the uncertainty caused by the indistinct character of the S-wave arrivals. This suggests that S-wave fronts are propagating vertically into the array. S-wave fronts would be expected to propagate across the Turkey Flat array in a manner similar to the P-wave arrivals in Figure 22 only with a slower apparent velocity of about 3.5 km/sec. Although the exact cause of the S-wave fronts propagating vertically into Turkey Flat is not known, it suggests a complicated (non-plane layered) S-wave crustal structure between the hypocenter of the WMTE and Turkey Flat. However, actual incident angles of S-wave rays into a specific site at Turkey Flat would be near vertical or vertical in either case.

As shown in Figures 22 - 24, waveforms appear to have dissimilar shapes among sites across the array for both P-waves and S-waves. This can be quantified by looking at covariance and coherence between each seismometer pair of the weak-motion array. Table 5 shows the peak covariance (largest cross-correlation value without regard for its sign) in matrix format for each vertical, north, and east pair of seismometers. Note that only seismometers at the same site (Rock South - CTF2 & CTF8; Valley Center - CTF3, CTF4, & CTF7) have

Table 5:

Peak Covariance Matrix for P-wave Arrivals

	CTF2	CTF3	CTF4	CTF5	CTF6	CTF7	CTF8
CTF2	1.00	-0.39	-0.36	-0.31	0.38	-0.38	**0.98**
CTF3	-0.39	1.00	**0.68**	-0.40	-0.30	**0.94**	-0.38
CTF4	-0.36	**0.68**	1.00	-0.37	-0.33	**0.54**	0.35
CTF5	-0.31	-0.40	-0.37	1.00	0.38	-0.38	-0.29
CTF6	0.38	-0.30	-0.33	0.33	1.00	-0.28	0.42
CTF7	-0.38	**0.94**	**0.54**	-0.38	-0.28	1.00	-0.38
CTF8	**0.98**	-0.38	0.35	-0.29	0.42	-0.38	1.00

Peak Covariance Matrix for SV-wave Arrivals

	CTF2	CTF3	CTF4	CTF5	CTF6	CTF7	CTF8
CTF2	1.00	-0.34	-0.38	-0.26	-0.34	-0.32	**0.91**
CTF3	-0.34	1.00	**0.87**	0.27	-0.32	**0.92**	-0.35
CTF4	-0.38	**0.87**	1.00	-0.28	-0.40	**0.71**	-0.35
CTF5	-0.26	0.27	-0.28	1.00	0.35	0.25	0.27
CTF6	-0.34	-0.32	-0.40	0.35	1.00	-0.28	-0.37
CTF7	-0.32	**0.92**	**0.71**	0.25	-0.28	1.00	-0.32
CTF8	**0.91**	-0.35	-0.35	0.27	-0.37	-0.32	1.00

Peak Covariance Matrix for SH-wave Arrivals

	CTF2	CTF3	CTF4	CTF5	CTF6	CTF7	CTF8
CTF2	1.00	-0.28	-0.29	-0.33	-0.19	-0.25	**0.96**
CTF3	-0.28	1.00	**0.89**	-0.29	-0.29	**0.93**	-0.29
CTF4	-0.29	**0.89**	1.00	-0.33	-0.26	**0.77**	-0.30
CTF5	-0.33	-0.29	-0.33	1.00	-0.19	-0.27	0.31
CTF6	-0.19	-0.29	-0.26	-0.19	1.00	-0.28	-0.18
CTF7	-0.25	**0.93**	**0.77**	-0.27	-0.28	1.00	-0.27
CTF8	**0.96**	-0.29	-0.30	0.31	-0.18	-0.27	1.00

peak covariances exceeding 0.5. Similarly Figures 25 - 27 show P, SV, and SH (Z, N, & E) normalized coherence functions (Abrahamson, et al., 1989) in matrix format for corresponding pairs of seismometers. The normalized coherence functions shown are determined from 5 sec time domain S-wave windows using an 11 point Hamming filter for smoothing in the frequency domain. Only seismometers at the same site show coherence exceeding 0.8 below 10 Hz. With site separations of 500-2000m, poor coherence among Rock South, Valley Central, Valley North, and Rock North sites is expected based on studies at Lotung, Taiwan (Abrahamson, et al., 1990) and Parkfield, Ca. (Schneider, et al., 1990). Good coherence below 10 Hz for seismometer separations of 10-24m is also expected based on Abrahamson, et al. (1990) and Schneider, et al. (1990). **This confirms that waveform coherence among the strong-motion recording sites at Turkey Flat is poor, which prevents the use of frequency-wavenumber analysis to determine both P-wave and S-wave propagation velocity and azimuth across the weak-motion array.**

Figure 25: Normalized P-Wave Coherence Matrix

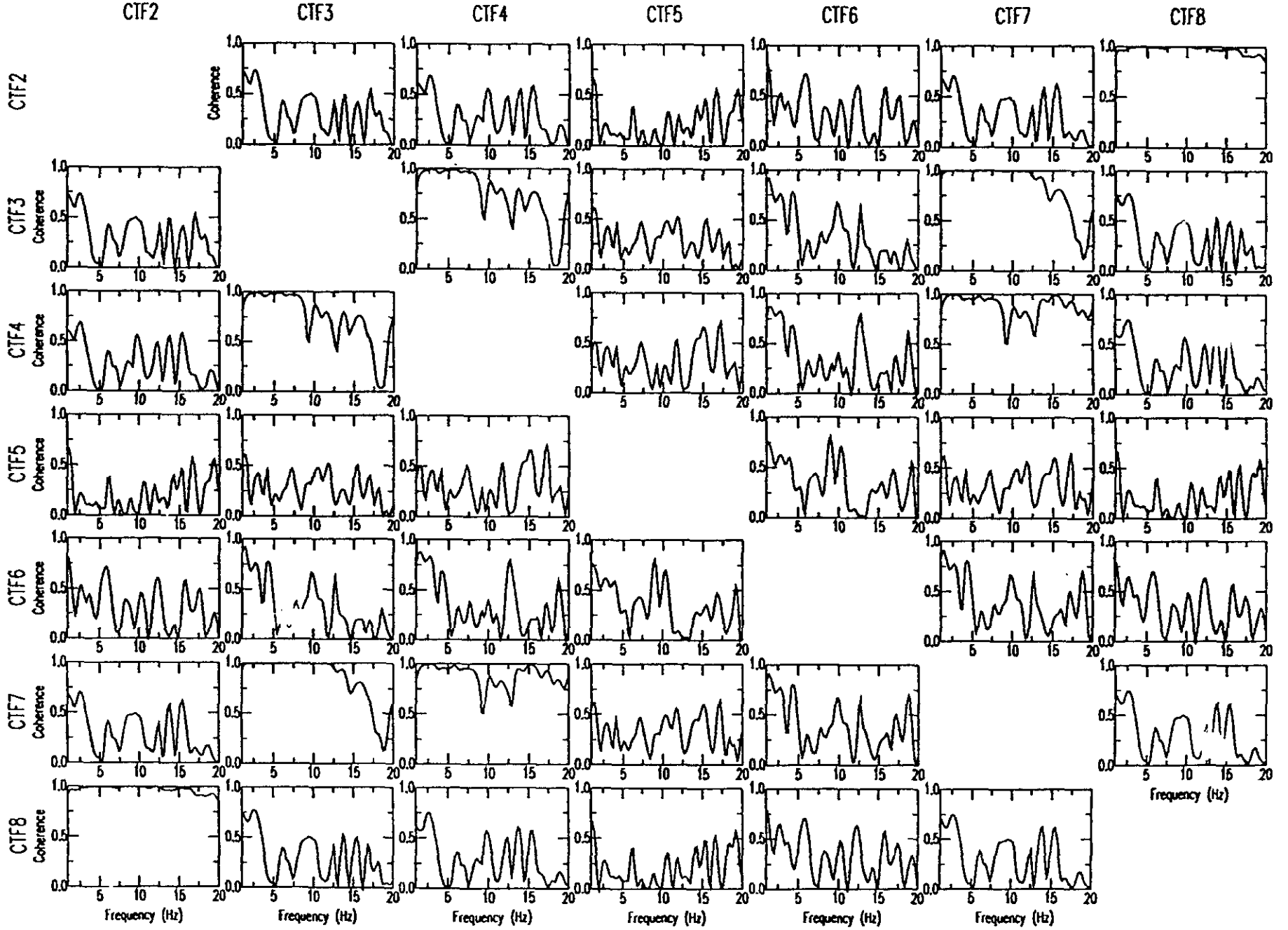

Figure 26: Normalized SV-Wave Coherence Matrix

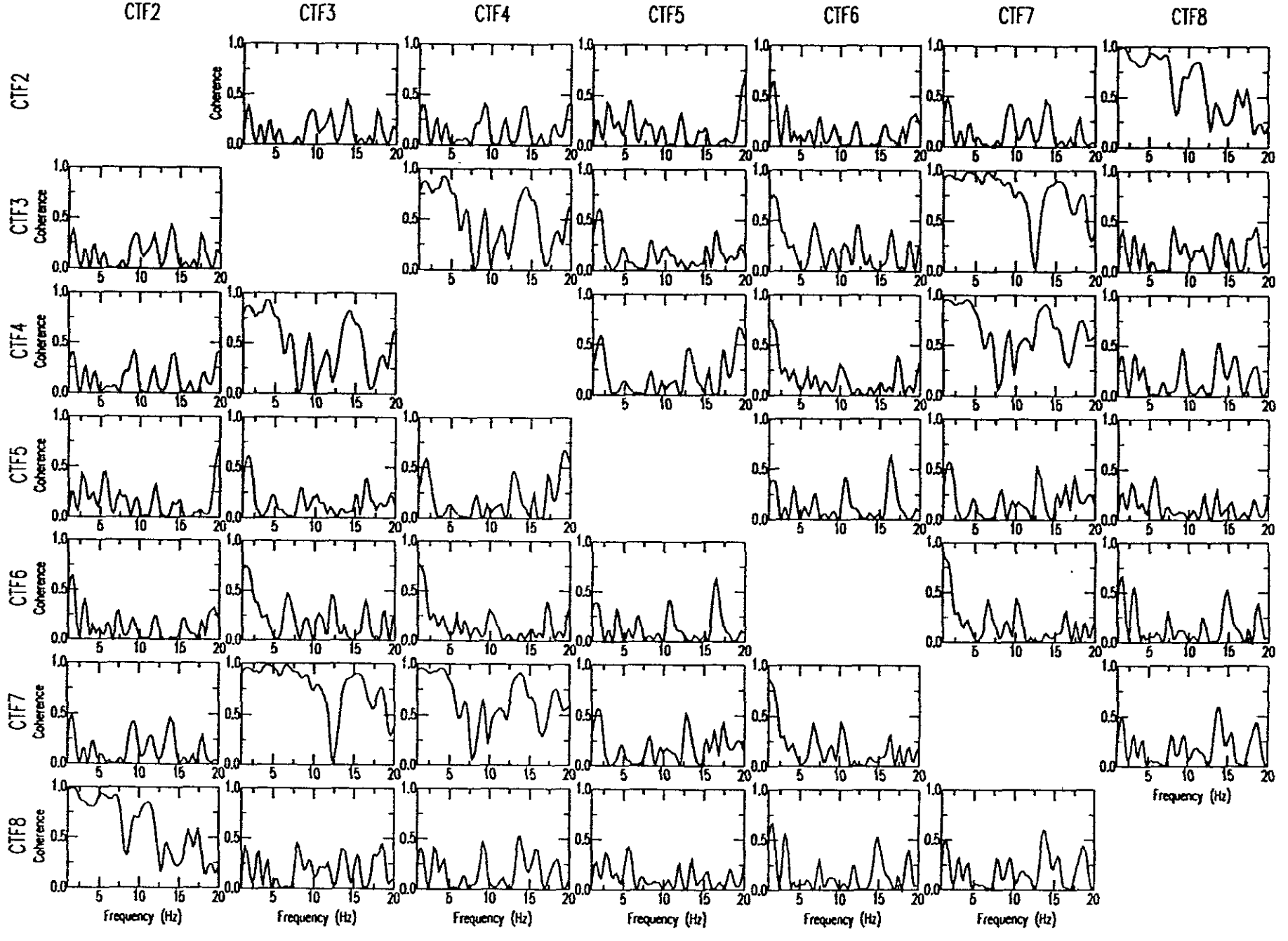

Figure 27: Normalized SH-Wave Coherence Matrix

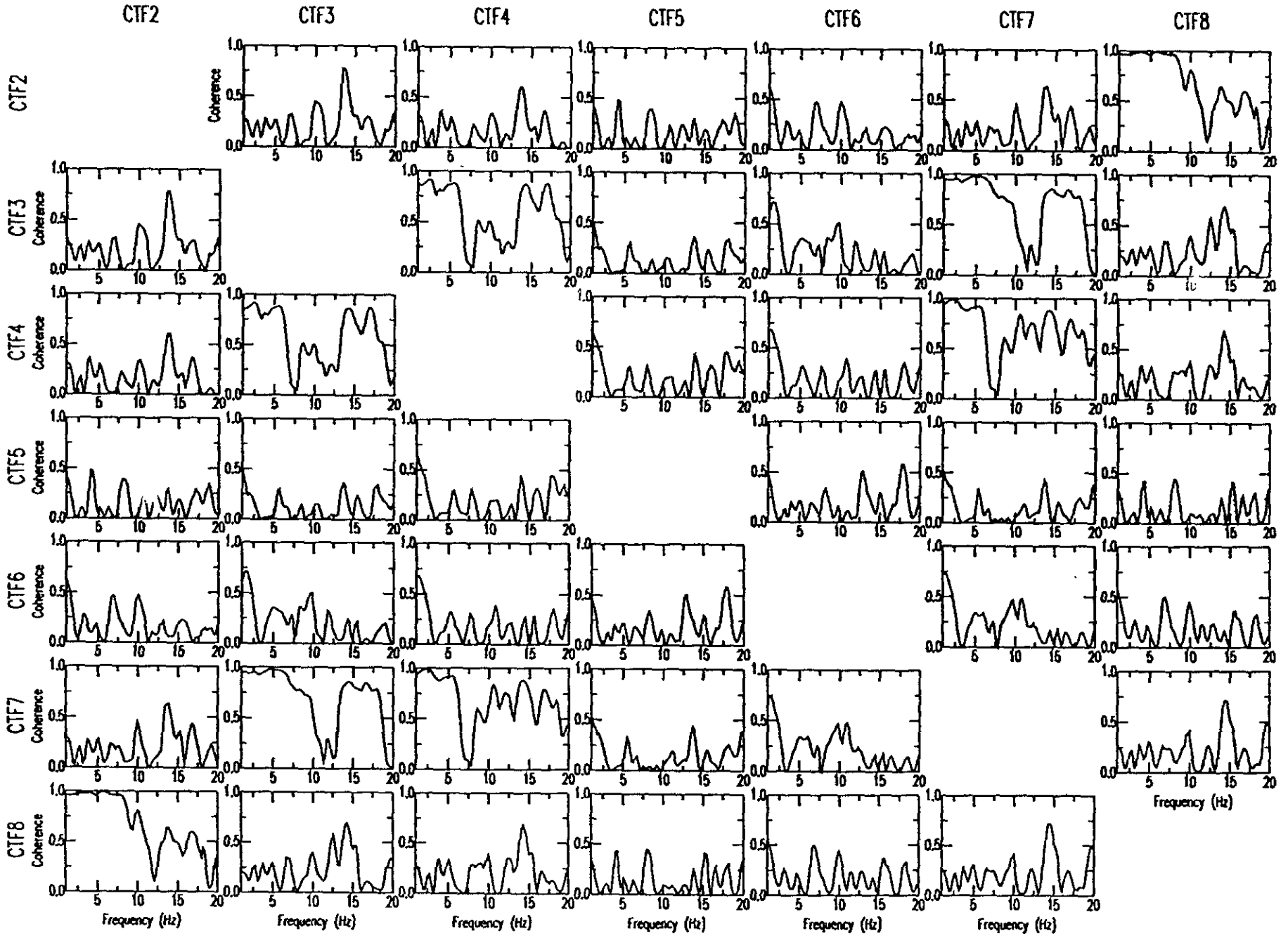

CONCLUSIONS

Based on the observed weak-motion mean spectral ratios at Turkey Flat and the simple modeling presented in this report, five principal conclusions can be drawn concerning the repeatability, the nature, and the predictability of relative site transfer functions at the Turkey Flat, USA, Site Effects Test Area:

1) Site transfer functions are repeatable at a given site to within a factor of 1.3 and variations between sites are suitable for a site effects prediction test. At Turkey Flat there are some rapid spatial variations in site transfer functions over distances as short as 20m.

2) As expected at Turkey Flat, weak-motion empirical transfer functions (mean spectral ratios) can be modeled by linear, one-dimensional, viscoelastic techniques, but the modeling results are sensitive to changes in S-velocity/layer-thickness that are greater than 5%. Modeling results from downhole measurements provide a better fit to the observations than modeling results from P-wave refraction profiles converted to S-wave profiles by using Vp/Vs ratios.

3) Calculated transfer functions may not predict empirical transfer functions because current downhole S-velocity/layer-thickness measurements are subject to 10-20% errors, while model fits to observations are sensitive to 5% changes in S-wave velocity.

4) S-velocities in the Standard Geotechnical Model for Turkey Flat appear too high by 20% for weak-motion site responses observed at the Rock South site. For Valley Center and Valley North sites, S-velocities in the Standard Model seem low by only 5% when compared to values obtained by modeling the observations of site response.

5) Damping in the Standard Geotechnical Model for Turkey Flat is too low for weak-motion site responses observed at the Valley Center and Rock South sites. For the Valley North site, damping values in the Standard Model are much closer to values obtained by modeling observations of site response and are within the modeling error of +/- .02.

An examination of the character of the Weak-Motion Test Event (WMTE) shows that there is little unusual about the WMTE when compared to the other weak-motion events recorded at the Turkey Flat array. Magnitude, epicentral distance, azimuth from array to source, and hypocentral depth are typical for the weak-motion events recorded at Turkey Flat. Variations in

Fourier spectral ratios of up to a factor of four between East and North components appear to be normal random variations and typical for weak-motion spectral ratios at Turkey Flat and Coalinga. There are no systematic variations between East and North components or between radial and transverse components as large as a factor of two. P-wave arrivals for the WMTE propagate across the Turkey Flat array at an apparent velocity of 6.0 km/sec but S-waves arrive simultaneously across the array. Waveform coherence is poor (<.75) between the four sites of the Turkey Flat array but good (>.75 in the 1-10 Hz band) between seismometers at the same site. This coherence pattern is not unexpected for the Parkfield area. Poor waveform coherence between Rock North and Rock South, coupled with Rock North to Rock South spectral ratios near one for the 1 - 20 Hz band suggest that the waveform incoherence is caused by differences in phase as a function of frequency rather than by differences in amplitude as a function of frequency.

REFERENCES

Abrahamson, N.A., Schneider, J.F., and Stepp, J.C., 1989, Spatial coherence of strong ground motion for application to soil-structure interaction: Electric Power Research Institute, Report 2978-1.

Abrahamson, N.A., Schneider, J.F., and Stepp, J.C., 1990, Spatial variation of strong ground motion for use in soil-structure interaction analysis: Earthquake Engineering Research Institute, Proceedings of the Fourth U.S. National Conference on Earthquake Engineering, v. 1, p. 317-326.

Bard, P.Y., and Bouchon, M., 1985, The two-dimensional resonance of sediment-filled valleys: Bull. Seism. Society of Am., v. 75, n. 2, p. 519-541.

Cramer, C.H., 1987, Downhole velocity measurements at Turkey Flat, California: California Division of Mines and Geology, ESAU Internal Report No. 87-1, 17 p.

Cramer, C.H., and Real, C.R., 1990, Turkey Flat, USA, site effects test area, report 5, weak-motion test: statistical analysis of submitted predictions and comparisons to observations: California Division of Mines and Geology, ESAU Technical Report No. 90-2.

Jarpe, S.P., Cramer, C.H., Tucker, B.E., and Shakal, A.F., 1988, A comparison of observations of ground response to weak and strong ground motion at Coalinga, California: Bull. Seism. Society of Am., v. 78, no. 2, p. 421-435.

Real, C.R., 1988, Turkey Flat, USA, site effects test area, report 2, site characterization: California Division of Mines and Geology, ESAU Technical Report No. 88-2.

Real, C.R., and Cramer, C.H., 1989, Turkey Flat, USA, site effects test area, report 3, weak-motion test: prediction criteria and input rock motions: California Division of Mines and Geology, ESAU Technical Report No. 89-1.

Schnabel, P.B., Lysmer, J., and Seed, H.B., 1972, SHAKE, a computer program for earthquake response analysis of horizontally layered sites: Earthquake Engineering Research Center, University of California, Berkeley, Report No. EERC 72-12.

Schneider, J.F., Abrahamson, N.A., Somerville, P.G., and Stepp, J.C., 1990, Spatial variation of strong ground motion from EPRI's dense accelerograph array at Parkfield, California: Earthquake Engineering Research Institute, Proceedings of the Fourth U.S. National Conference on Earthquake Engineering, v. 1, p. 375-384.